Biomarker Discovery for Mental Disorders from Neuroimaging Data

A DISSERTATION
SUBMITTED TO THE FACULTY OF THE GRADUATE SCHOOL
OF THE UNIVERSITY OF MINNESOTA
BY

Tingting Xu

IN PARTIAL FULFILLMENT OF THE REQUIREMENTS
FOR THE DEGREE OF
Doctor of Philosophy

Professor Keshab K. Parhi, Adviser

December, 2016

Acknowledgements

First of all, I would like to thank my advisor Professor Keshab K. Parhi for his continued guidance and support throughout my Ph.D. study. I'm very grateful to him for introducing me to this interesting interdisciplinary research area of brain signal processing and pattern discovery, and teaching me valuable skills for conducting scientific research and writing academic papers. I also would like to express my sincere gratitude to my mentors, Professor Kathryn Cullen and Professor Massoud Stephane, for their constant guidance, encouragement and support in my study and career.

I would like to thank Professor Mostafa Kaveh, Professor Emad Ebbini and Professor Kelvin Lim for their support as members of my Ph.D. committee. I would like to thank Professor S. Charles Schulz, Professor Bryon Mueller and Mindy Schreiner for their inputs in the Borderline Personality Disorder research. I would like to thank the Graduate School, the Department of Electrical and Computer Engineering, and the Institute of Engineering in Medicine at the University of Minnesota for their financial support.

My thanks also go to members of our research group and my friends at Minnesota. In particular, Shu-Hsien Chu and Sohini Roy Chowdhury for our discussions on research topics and career development. I'm grateful to Bo Yuan, Yingjie Lao, Zisheng Zhang, Yin Liu, Chuan Zhang, Bhaskar Sen, Manohar Ayinala, Fei Zheng, Sha Shi and Wei Pan, for their friendship and support during my Ph.D.

Finally, and most importantly, I would like to thank my wonderful family for their support and encouragement. I'm forever grateful to my parents for their unconditional love and care. I could never fully express my deepest love to my husband Jieming, who is always there cheering me up and helping me through those hard times. Without the love from them, this work would not have been possible.

Abstract

A mental disorder is a medical condition that disrupts a person's thinking, feeling, mood, ability to relate to others and daily functioning. Despite decades of research, the exact cause of most mental disorders remains unknown and no objective tests are available for their diagnosis. It is crucial to explore quantitative, discriminative and interpretable biomarkers for mental disorders, which could not only assist in clinical diagnosis, but also help in gaining insight into the underlying mechanisms of the illnesses.

In this research, we explore neuroimaging biomarkers for two common mental disorders: schizophrenia and borderline personality disorder (BPD). An interdisciplinary research framework covering feature extraction, selection, classification and validation is presented. Signal processing and graph theory approaches are employed to process and model neuroimaging data, and create meaningful feature sets to characterize brain activity, connectivity and network topologies. Machine learning based feature ranking and classification is performed to select discriminating feature subset and distinguish psychiatric patients from healthy subjects. Statistical analysis is performed to validate the significance of the identified features and control the False Discovery Rate (FDR).

In the first part of the dissertation, we explore spatial-temporal-spectral neural oscillation patterns for schizophrenia using magnetoencephalography (MEG) data. We first extract Event-Related Desynchronization/Synchronization (ERDS) patterns along the space, time and frequency dimensions combined. A two-step feature ranking algorithm combining F-score filtering and Support Vector Machine – Recursive Feature Elimination (SVM-RFE) algorithm is applied to select a small subset of features according to their discriminating power. With top 20 ERDS features, 90% specificity and 91.67% sensitivity is achieved in classifying 12 schizophrenia patients from 10 healthy controls using a linear SVM classifier, following cross validation procedure.

Next, two novel spatial-temporal-spectral feature sets, the Band Power Ratio (BPR) and the Window Power Ratio (WPR) are created, based on the Power Spectral Density of MEG data. Cluster-based nonparametric permutation tests are employed to identify key features with significant between-group difference, which control the FDR while

maintaining low False Negative Rate. The minimum-Redundancy-Maximum-Relevance criteria are then employed to select the optimal feature combinations for classification. Based on only 2 WPR and 1 BPR feature combined, over 95% cross validation classification accuracy is achieved using three different linear classifiers separately, which indicates strong discriminating power of the key Spectral Power Ratio features. Using spectral power features, a computer-aided schizophrenia screening system based on majority voting of single MEG trials is then presented.

In the second part of the dissertation, we explore functional brain network connectivity and topology patterns for BPD using resting-state functional magnetic resonance imaging (fMRI) data. Frequency-specific brain networks are constructed by correlating wavelet-filtered fMRI time series from 82 cortical and subcortical regions. Network-based statistics are employed to identify altered connections using cluster-based thresholding of statistical maps. An interconnected subnetwork in 0.03–0.06Hz frequency band is identified that shows significantly lower connectivity strength in patients. The mean connectivity of the subnetwork shows negative correlation with several key clinical symptom scores, and achieves 90% sensitive and 90% specificity in BPD classification using a simple linear classifier.

We further employ graph theory to investigate the global and local topological structure of the frequency-specific brain connectivity networks. Statistical analysis show that BPD patients have significantly larger measures of global network topology, including the size of largest connected component, clustering coefficient, small-worldness and local efficiency, indicating increased local cliquishness in the functional brain network. These global topology metrics show positive correlations with several clinical symptom scores associated with BPD. Additionally, compared to controls, patients show lower nodal centrality at several hub regions but higher centrality at several non-hub regions in the network. These findings may add to the current understanding of functional brain networks in BPD.

Table of Contents

List of Tables

List of Figures

Chapter 1

Introduction

1.1 Introduction

1.1.1 Background

A mental disorder, also called a mental illness or a psychiatric disorder, is a clinically significant behavioral or psychological syndrome, which is associated with present distress (e.g., a painful symptom) or disability (i.e., impairment in one or more important areas of functioning) or with a significantly increased risk of suffering death, pain, disability, or an important loss of freedom [1]. Examples of mental disorder include anxiety disorders, mood disorders, schizophrenia, personality disorders, eating disorders, and addictive behaviors. Mental disorders affect people's mood, thinking and behavior, and can cause various problems in people's daily life, such as confused thinking or reduced ability to concentrate, detachment from reality (delusions), paranoia or hallucinations, extreme mood changes of highs and lows, withdrawal from friends and activities, alcohol or drug abuse, suicidal thinking, etc. [2].

Mental disorders are common in the United States and internationally. According to the National Institute of Mental Health (NIMH), an estimate of 43 million Americans aged 18 or older suffer from a diagnosable mental disorder in a given year. This number represented nearly 1 in 5 of all U.S. adults [3]. Fully 20 percent of American children ages 13 to 18, either currently or at some point during their life, have had a seriously debilitating mental disorder [4]. In addition, mental disorders were showed as the largest cost drivers in healthcare at $2.5 trillion in global costs in 2010, and projected costs of $6.0 trillion by 2030 [5].

To provide effective prevention, accurate diagnosis, and appropriate treatment for mental disorders, it is crucial to understand the causes and the underlying mechanisms of the illnesses. Current research suggests that mental disorders are caused by a combination of genetic, biological, psychological and environmental factors. However, the exact cause of most mental illnesses remains unknown [6]. Furthermore, current diagnosis of mental illnesses is mainly based on a person's self-reported symptoms, thoughts, feelings and behavior patterns, followed by a clinical assessment by a mental health professional [7]. Such subjective diagnostic process remains uncertain since there is no objective test to support it. Therefore, it is highly desirable to explore quantitative, discriminative, and interpretable biomarkers – objective biological measures that can predict clinical outcomes – for mental illnesses, which could not only assist in validating the clinical diagnosis, but also help in gaining insight into the underlying mechanisms of the illnesses.

A lot of recent research effort has been made to search for "neuroimaging biomarkers" for mental disorders [8]. Modern neuroimaging (also called brain imaging) techniques provide powerful tools for scientists to study the structure and function of human brain. For example, Magnetic Resonance Imaging (MRI) uses magnetic fields and radio waves to produce high quality images of the brain's structure; functional Magnetic Resonance Imaging (fMRI) uses MRI technology to measure brain activity by detecting changes associated with blood flow [9]. Another type of functional neuroimaging technique called Magnetoencephalography (MEG) can map ongoing brain activity on a millisecond-by-millisecond basis, by recording magnetic fields produced by electrical currents occurring naturally in the brain [10]. Figure 1.1 shows how MRI and MEG data are acquired from subjects in a non-invasive manner.

(a)

(b)

Figure 1.1: Acquisition of (a) Magnetoencephalography (MEG) and (b) Magnetic Resonance Imaging (MRI).
[Source: https://www.nimh.nih.gov/health/publications/neuroimaging-and-mental-illness-a-window-into-the-brain/index.shtml]

Various quantitative measures can be extracted from neuroimaging data using advanced signal processing and image processing techniques. If these imaging measures demonstrate sufficient precision and reliability in predicting a clinical diagnosis, they will become objective and tangible "imaging biomarkers" for mental disorders [8]. The discovery of such imaging biomarkers could enable quantitative assessment of the illnesses and bring knowledge to the current understanding of mental disorders, which would benefit a large population of psychiatric patients.

1.1.2 Research Overview

In this research, we focus on exploring discriminative and interpretable imaging biomarkers for two common mental disorders: schizophrenia and borderline personality disorder (BPD). Schizophrenia is a chronic, severe, and disabling mental disorder characterized by deficits in thought processes, perceptions, and emotional responsiveness. It affects about 1.1% of U.S. adult population [11]. BPD is a serious mental disorder characterized by pervasive instability in moods, interpersonal relationships, self-image, and behavior. It affects about 1.6% of U.S. adults [12]. Two neuroimaging modalities:

MEG and fMRI are used to assess brain dysfunctions associated with schizophrenia and BPD, respectively. Various signal processing, graph theory, machine learning and statistical analysis approaches are employed to process the neuroimaging data, extract, select and validate discriminating patterns, and build computer-aided classification systems for diagnosing and understanding the illnesses. Figure 1.2 shows the interdisciplinary research framework of this work.

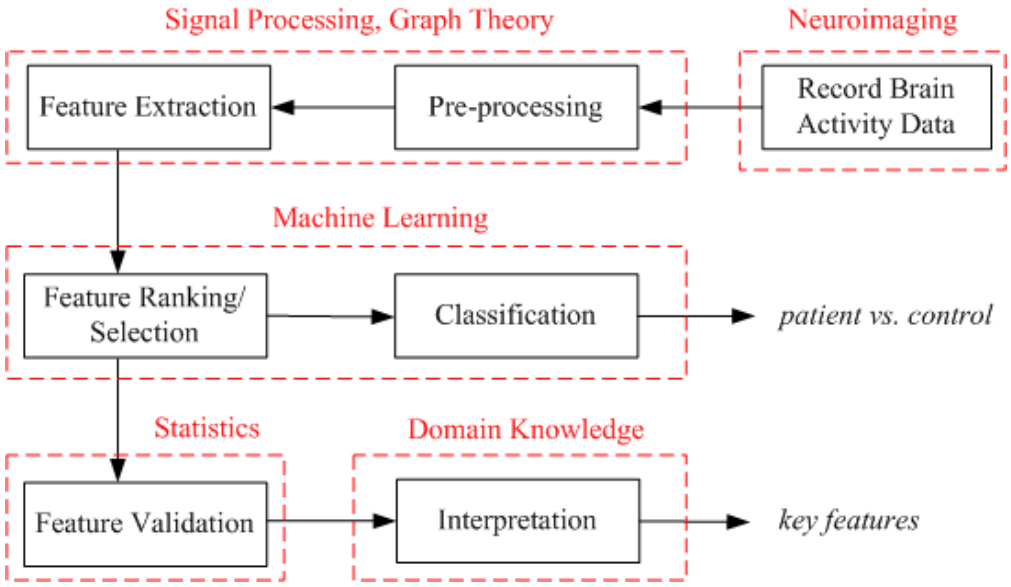

Figure 1.2: Framework of this research

First of all, neuroimaging data are acquired from both psychiatric patients and healthy controls, during either task or resting state. Raw data is preprocessed to remove noise, artifacts and other unwanted components. Advanced signal processing and graph theory approaches are employed to further process and model the preprocessed neuroimaging data, and create meaningful feature sets to characterize brain activity, connectivity and network structure from different perspectives. For the schizophrenia study, we particularly focus on creating spatial-temporal-spectral features, since MEG assesses ongoing neural oscillatory activity at different brain locations with very high temporal resolution. From signal processing perspective, this type of data is a good source for

detailed time-frequency analysis. For the BPD study, we focus on investigating functional brain network connectivity and topology patterns. The main consideration is that fMRI data has relatively low temporal resolution but good spatial resolution, which is suitable for analyzing the interactions among different brain regions.

The original feature sets are extracted from multiple spatial locations, time periods and frequency ranges. Therefore, the dimensionality of the feature space is usually much larger than the sample size, i.e., number of features is much greater than number of subjects. Feature ranking is performed to select a subset of the original feature set that shows high discrimination between psychiatric patients and healthy controls. On the one hand, feature selection process leads to a better understanding of the underlying process that generated the abnormalities in brain functioning that distinguish patients from controls. On the other hand, feature selection improves prediction performance and reduces complexity of a machine learning model by removing irrelevant features and preventing model overfitting [13]. Based on the selected subset of discriminating features, a machine learning classifier can be designed as a computer-aided screening system to assist in clinical diagnosis of mental illnesses.

From statistics point of view, individual features that show high discriminating power may be false discoveries due to multiple comparisons [14], i.e., simultaneous testing of more than one hypothesis. Therefore, appropriate statistical tests are necessary to validate the significance of the identified discriminating features and control the False Discovery Rate (FDR). Traditional multiple comparison correction approach, such as Bonferroni correction [15], is too conservative and does not consider the properties of neuroimaging data. In this work, we employ application-specific statistical analysis methods, such as cluster-based non-parametric tests [16] and Network-based Statistics (NBS) [17], which control the FDR while maintaining a relatively low False Negative Rate (FNR) compared with traditional methods. Finally, the key features will be interpreted using domain knowledge.

1.2 Summary of Contributions

The key contribution of this research is the identification of several discriminating and interpretable neuroimaging patterns, including the spatial-temporal-spectral neural oscillation patterns in schizophrenia, and the functional brain network connectivity and topology patterns in BPD [18]–[21]. These patterns may bring new knowledge into the current understanding of mental disorders, and may have potential to become objective biomarkers for quantitative assessment of the illnesses. Furthermore, the biomarker discovery process follows a rigorous interdisciplinary research framework. Various signal processing, graph theory, machine learning and statistics approaches are presented for neuroimaging data processing, feature extraction, selection, validation and classification. These data analysis methods can be easily applied to other related studies that aim at identifying neuroimaging patterns to distinguish different brain states.

1.2.1 Multidimensional Neural Oscillation Patterns in Schizophrenia

MEG records ongoing brain activity from whole-brain locations with very high temporal resolution. This motivates us to explore spatial-temporal-spectral features in neural oscillatory activity assessed by MEG. We first investigate a traditional neural oscillation feature set called Event-Related Desynchronization/Synchronization (ERDS) [22], which represents power decrease or increase of MEG signals during cognitive functions. ERDS features are computed along the frequency, time, and space dimensions combined. A two-step feature ranking algorithm combining F-score [23] filtering and Support Vector Machine – Recursive Feature Elimination (SVM-RFE) algorithm [24] is applied to select a small subset of features according to their discriminating power. With top 20 ERDS features, 90% specificity and 91.67% sensitivity is achieved in classifying 12 schizophrenia patients from 10 healthy controls, using a linear SVM classifier [25], [26], following leave-one-out cross validation procedure [27]. The space, time and frequency information of the top features is discussed in detail.

1.2.2 MEG Spectral Power Ratio Patterns in Schizophrenia

We next propose two novel spatial-temporal-spectral feature sets: the Band Power Ratio (BPR) and the Window Power Ratio (WPR), based on Power Spectral Density analysis of neural oscillations measured by MEG. Different from traditional spectral power features, the BPR and the WPR reflect the inter-relationships of spectral power between different frequency bands, and between different time periods of neural oscillatory activity, respectively. Cluster-based nonparametric permutation tests are employed to identify key features that show significant between-group difference, which control the FDR while maintaining a low FNR [16]. The minimum-Redundancy-Maximum-Relevance (mRMR) criteria are then employed to select the optimal feature combinations for classification [28]. Based on only two WPR and one BPR features combined, over 95% cross validation classification accuracies are achieved using three different linear classifiers separately, which indicates strong discriminating power of the proposed Spectral Power Ratio (SPR) features.

1.2.3 Functional Brain Connectivity Patterns in BPD

Resting-state fMRI measures intrinsic brain activity with high spatial resolution. This motivates us to explore fMRI patterns that characterize the functional interactions between different brain regions-of-interest (ROI). Frequency-specific functional brain networks are constructed by correlating wavelet-filtered fMRI time series from 82 cortical and subcortical regions. Network-based Statistics (NBS) are employed to identify altered functional connectivity using cluster-based thresholding of statistical maps [17]. An interconnected subnetwork in 0.03–0.06Hz frequency band is identified that shows significantly lower connectivity strength in patient group. The links in the subnetwork are mainly long-distance connections between regions located at different lobes. The mean connectivity in the subnetwork shows negative correlations with several key clinical symptom scores, and achieves 90% sensitive and 90% specificity in classifying 20 BPD patients from 10 healthy controls using a simple linear discriminant classifier.

1.2.4 Functional Brain Network Topology Patterns in BPD

Neuroimaging research on BPD has revealed structural and functional abnormalities in specific brain regions and connections. However, little is known about the topological organizations of functional brain networks in BPD. Based on the bivariate functional connectivity analysis, we further employ graph-theory based complex network analysis to extract several network measures which characterize the global and local topological structure of the functional brain networks. Statistical analysis show that patients with BPD have significantly larger measures of global network topology, including the Size of Largest Connected Graph Component, Clustering Coefficient, Small-Worldness and Local Efficiency, indicating increased local cliquishness of the functional brain network. These global metrics show positive correlations with several clinical symptom scores associated with BPD. Additionally, compared to healthy controls, BPD patients show lower Nodal Centrality at several hub nodes but greater centrality at several non-hub nodes in the network. These novel findings may add new knowledge to the current understanding of functional brain networks in BPD.

1.3 Outline of the Dissertation

The organization of the rest of this dissertation is outlined as follows.

Chapter 2 presents the computation, identification and classification of discriminating ERDS patterns for schizophrenia, using MEG data collected during language processing tasks. The two-step feature ranking scheme combing F-score filtering and SVM-RFE algorithm is described.

Chapter 3 introduces two novel MEG Spectral Power Ratio (SPR) feature sets for schizophrenia: the Band Power Ratio and the Window Power Ratio. We described how SPR features are extracted along space, time and frequency dimensions, and how key features are identified and validated by cluster-based nonparametric permutation tests. Machine learning based feature selection and classification approaches are also presented.

Chapter 4 presents the design of a machine learning based schizophrenia screening system, using majority voting of spectral power features extracted from single-trial MEG. A two-stage feature selection algorithm combining F-score filtering and Adaptive Boosting (Adaboost) model is presented.

Chapter 5 presents the exploration of functional brain connectivity patterns in BPD using resting-state fMRI data. We describe how to construct frequency-specific functional brain networks and apply network-based statistics to identify an interconnected subnetwork with altered connectivity strength in BPD.

Chapter 6 presents the identification of functional brain network topology patterns in BPD, using graph-theory based complex network analysis. The computation of various global and local topological patterns is described in detail. The correlation of key network patterns with BPD clinical symptom scores is also presented.

Finally, Chapter 7 concludes the dissertation with a summary of all the contributions and points out future research directions.

Chapter 2

Multidimensional Neural Oscillation Patterns in Schizophrenia

2.1 Introduction

Schizophrenia is a chronic, severe and complex mental illness which affects about 1.1% of the world population age 18 and older [29]. The key symptoms of the illness include hallucinations, delusions, paranoia, social withdrawal, and disorganization of thought and language [29]. Earlier research in schizophrenia has focused on relating specific cortical regions to the psychotic symptoms. However, recent theory has suggested that the psychotic phenomena and the cognitive dysfunctions that characterize schizophrenia are not simply due to a spatially circumscribed deficit, but rather due to disruptions of coordinated activity in cortical circuits [30]–[32]. Accordingly, neural oscillations, a fundamental mechanism for enabling coordinated activity during normal brain functioning, has become a crucial target for investigating the pathophysiology of schizophrenia, as well as the mechanisms of the cognitive deficits and other symptoms of this disease [32]–[34].

Neural oscillations can be assessed by methods that record dynamic brain activity with high temporal resolution, such as magnetoencephalogram (MEG) and electroencephalogram (EEG). Neural oscillations detected by MEG/EEG correspond to the synchronous firing of the pyramidal neurons. The oscillatory frequency reflects the frequency of neural firing, and the power of a frequency reflects the number of pyramidal neurons firing at that frequency [22]. Previous research has shown that cognitive functions modulate neural oscillations at multiple frequencies simultaneously [22], and

this modulation takes place at the frequency, spatial, and temporal dimensions [35], [36], [18]. This led to the hypothesis that oscillations detected by MEG/EEG are the sum of the activity of neural generators oscillating at different frequencies and distributed in time and space. Consequently, to get a better understanding of the oscillatory activity, the full scale of the frequency, spatial, and temporal dimensions of the brain oscillations needs to be evaluated.

In this chapter, we explore multidimensional neural oscillation patterns in schizophrenia using MEG data recorded during a language processing task [18]. Language disorder is one of the core symptoms in schizophrenia [37]. Linguistic research in schizophrenia has frequently shown abnormalities at multiple levels of language processing (lexical, semantic, syntactic and pragmatic levels) [38], as well as abnormal dynamics between these processing levels [39]. Therefore, the hypothesis here is that neural oscillatory activity during language processing in schizophrenic patients differs from healthy controls at certain frequency ranges, brain locations and time periods. Such frequency, space and time information can be extracted as multidimensional features from MEG data to distinguish schizophrenia patients from healthy subjects.

Cognitive processing, including language processing, results in a change in the ongoing MEG/EEG in form of an Event-Related Desynchronization (ERD) or Event-Related Synchronization (ERS) [40], [41]. The ERD represent frequency-specific power decrease of neural oscillatory activity, due to a decrease in synchrony of the underlying neural populations. On the contrary, the ERS represent power increase in specific frequency bands, due to an increase in synchrony of the neural populations [40]. In this study, we extract ERD/ERS from multiple frequency bands, brain locations and time points of MEG signal, to construct a multidimensional neural oscillation feature set. Machine learning based feature selection and classification algorithms are applied to identify the most discriminating features and distinguish schizophrenia patients from healthy controls. The frequency, time, and space information contained in the top features are analyzed, which may add new knowledge to the current understanding of abnormal neural mechanisms related to language disorder in schizophrenia.

The rest of this chapter is organized as follows. In Section 2.2, the subjects' information and the MEG data acquisition and preprocessing procedures are described. In Section 2.3, the ERDS feature computation and the feature selection and classification methods are presented. Section 2.4 presents the classification results and the analysis of top features. Finally, in Section 2.5, discussions and conclusions are presented.

2.2 Subjects and Data

2.2.1 Subjects

Participants included 12 schizophrenia patients (12 male) and 10 healthy controls (9 male). All the subjects were native English speakers and were right-handed. Handedness was assessed by the Edinburgh Handedness Inventory [42]. None of the control subjects had neurological disease or major medical illness. All the patients met the criteria of the "Diagnostic and Statistical Manual of Mental Disorders, 4th Edition (DSM-IV) [43]" for schizophrenia or schizoaffective disorder. All the subjects gave written informed consent before entering the study. The experimental protocol was approved by the relevant Institutional Review Boards (IRB).

Measures of premorbid intellectual functioning were obtained using the National Adult Reading Test (NART) [44]. The severity of psychopathology was assessed with the Brief Psychiatric Rating Scale (BPRS) [45] and the Positive and Negative Symptoms Scale (PANSS) [46]. The duration of illness was derived from reviews of patient records. Table 2.1 summarizes the demographic and clinical characteristics of the subjects.

Table 2.1: Demographic and clinical characteristics of the subjects.

Characteristics	**Control** mean (std.)	**Patient** mean (std.)
Age, year	49.7 (11.1)	49.5 (7.0)
Education, year	15.0 (2.2)	15.5 (4.7)
Parents education, year	13.6 (2.4)	12.4 (2.7)
NART full score	111.3 (7.3)	106.5 (6.8)
NART performance score	110.5 (3.9)	108.0 (3.6)
NART verbal score	109.3 (8.5)	104.4 (7.8)
BPRS	-	41.4 (9.4)
PANSS, negative symptoms	-	7.5 (4.3)
PANSS, positive symptoms	-	8.8 (5.7)
Duration of illness, year	-	22.1 (10.0)
Chlorpromazine equivalent dose, mg	-	330.3 (118.7)

NART: National Adult Reading Test; BPRS: Brief Psychiatric Rating Scale
PANSS: Positive and Negative Syndrome Scale

2.2.2 Language Processing Task

Subjects were instructed to distinguish between correct and incorrect word stimuli. A correct stimulus is a set of five real English words, e.g., “cabin-fire-roped-big-the”. An incorrect stimulus is a set of five elements with four real English words and one pronounceable non-word, e.g., “cabin-freet-roped-big-the”. The elements in each stimulus were presented visually one at a time in the center of a monitor placed in front of the subjects. Each element appeared for 750 milliseconds followed by a 250 milliseconds blank screen. There was a 10-second interval between consecutive trials. Subjects were instructed to read the stimuli silently and press a button with their right index finger for incorrect stimuli.

Epochs included a baseline period (3 seconds immediately before the first word), and an active period (8.5 seconds after the onset of the first word). The active period included a 5-second ‘‘encoding phase’’ (stimuli presentation) and a 3.5-second ‘‘post-stimuli phase’’ (after stimuli presentation). The timing diagram of the task is shown in Figure 2.1.

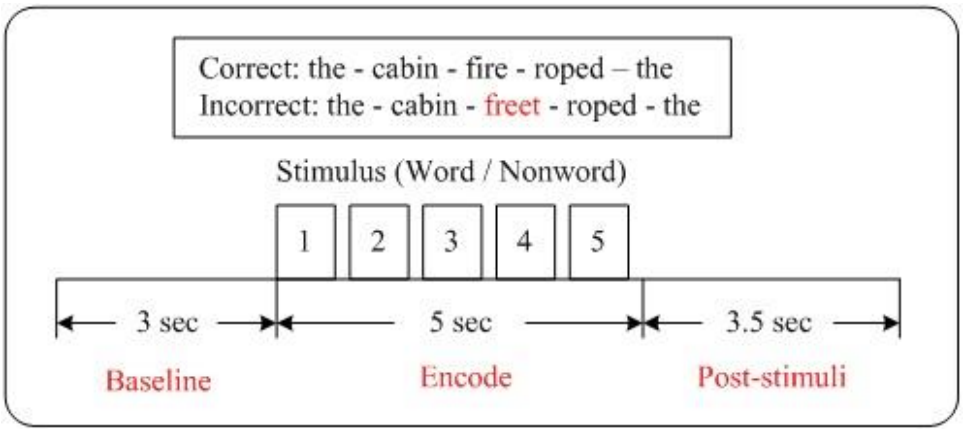

Figure 2.1: Timing diagram of the word processing task

To note, the word processing task was part of a comprehensive procedure for language evaluation described in detail in previous work [38], [39]. The task is based on a standard psycholinguistic procedure - anomaly detection [47]. Here, the detection of a pronounceable non-English word would require the correct identification - and accordingly processing - of English words. To maximize word processing operations, the task was designed in a way that minimize significantly verbal working memory load. That is, subjects were only required to detect the anomaly (non-English word) and were not required to remember the English words. As there was only one possible anomaly per stimulus, there was a working memory load of one item - the lowest working memory load possible.

In the task, each subject performed 60 trials that included 45 correct stimuli and 15 incorrect stimuli. The average correct response rate was 94.17% for the control group and 87.5% for the patient group. In this study, we only analyze trials with correct stimuli, as we are interested in investigating the abnormal neural oscillation patterns in schizophrenia during normal word processing.

2.2.3 MEG Data Acquisition and Preprocessing

During the task, MEG data were recorded from 248 axial gradiometers (Magnes 3600WH, 4-D Neuroimaging, San Diego, CA) in a 2-layer mu-metal magnetically

shielded room (IMEDCO, Hagendorf, Switzerland), with a sampling rate of 1024Hz. Subjects were in a supine position with their heads in the sensor helmet and on a head support to minimize movement. Ambient and distant biological magnetic noises were reduced by using 23 SQUID reference channels, which were situated within the sensor and above the cortical channels. Electrooculogram (EOG) and electrocardiogram (ECG) were recorded to identify and correct epochs contaminated by eye movements and heartbeats.

Artifacts (blinks and heartbeats) correction was carried out according to an algorithm described by Ille et al [48]. Visual inspection was performed to reject trials with residual artifacts. After preprocessing, successful trials were filtered between 1 to 64 Hz and down-sampled to 256Hz. Out of the 45 trials with correct stimuli, the number of artifact free trials did not differ significantly between schizophrenia patients (mean 36, std. 7.2) and healthy controls (mean 41, std. 3.3), *p*-value > 0.05. In addition, successful trials from the same MEG channel were averaged for each subject for further analysis.

2.3 Data Analysis

2.3.1 Feature Extraction

As ERD/ERS has frequency-specific behavior, each MEG channel was filtered into 8 frequency sub-bands: δ (1-4 Hz), θ (4-8 Hz), α (8-12 Hz), β_1 (12-16 Hz), β_2 (16-24 Hz), β_3 (24-32 Hz), γ_1 (32-40 Hz) and γ_2 (40-48 Hz). For each sub-band, the power (square of amplitude) values of MEG signal were computed and smoothed using a 250-millisecond moving window with 125 millisecond overlap, to reduce the variability and the number of data points for the ERD/ERS calculation. For each 11.5-seconds trial, the total number of time points in each channel was reduced to 92, including 24 points in the baseline period (3 seconds) and 68 samples in the active period (8.5 seconds). Finally, the ERD/ERS value was calculated as the percentage power change in each smoothed mean power data relative to the mean power within the baseline period:

$$ERDS = \frac{A(i) - R}{R} * 100\% \tag{2.1}$$

where $A(i)$ is the ith smoothed mean power sample and R is the average power of baseline period, which is calculated as $R = \frac{1}{24} \sum_{i=1}^{24} A(i)$.

The reason for using relative power change is to remove the additive effects like medication, coffee and tobacco consumption, as those effects affect both the baseline and the active period. A positive power change represents ERS while a negative power change represents ERD.

2.3.2 Feature Selection and Classification

Multidimensional evaluation of neural oscillations results in a very large ERD/ERS feature set: 8 frequency sub-bands * 248 MEG channels * 92 time points per channel, leading to a total of 182,528 features per subject. Compared to the small sample size (22 subjects) and small number of groups to discriminate (patient group vs. control group), the features are in an extremely high dimensional space. To avoid spurious group differences, we employed a classification based two-step feature selection algorithm to select a small sub-set of features that have high discriminating power in patient and control classification. These top discriminating features reflect the frequency, brain region and time of oscillations that are abnormal during word processing in schizophrenia, which may help us understand the underlying mechanism of this impairment.

In the two-step feature selection algorithm, we first used F-score filtering to eliminate large number of "garbage" features. F-score is a simple and generally effective technique to measure the discrimination of two sets of real numbers [49]. Consider n training samples: x_k, $k = 1,\ldots,n$ and let the number of positive and negative samples be n_+ and n_- respectively. Each sample is a vector with m features. The F-score of the ith feature is defined as:

$$F(i) = \frac{(\bar{x}_i^{(+)} - \bar{x}_i)^2 + (\bar{x}_i^{(-)} - \bar{x}_i)^2}{\frac{1}{n_+ - 1}\sum_{k=1}^{n_+}(x_{k,i}^{(+)} - \bar{x}_i^{(+)})^2 + \frac{1}{n_- - 1}\sum_{k=1}^{n_-}(x_{k,i}^{(-)} - \bar{x}_i^{(-)})^2} \tag{2.2}$$

where $\bar{x}_i$, $\bar{x}_i^{(+)}$, $\bar{x}_i^{(-)}$ represent the averages of the ith feature of the whole, positive, and negative data samples, respectively; $x_{k,i}^{(+)}$ and $x_{k,i}^{(-)}$ are the ith feature of the kth positive and negative sample, respectively. In short, the numerator indicates the discrimination between the positive and negative sets, and the denominator represents the discrimination within each of the two sets. The higher the F-score is, the more likely this feature is discriminative.

After F-score filtering, large number of irrelevant features were eliminated except the top 150 features with the highest F-score were kept for next step feature ranking by SVM-RFE, a classification based feature selection algorithm [24]. Basically, it is a backward selection strategy using the weights of SVM model [25], [26] to produce a feature ranking. Due to the nature of our dataset (small sample size vs. large number of features) as well as computational consideration, we employed linear SVM, in which the weight vector **w** is obtained by solving the following quadratic optimization problem:

$$\begin{aligned} &\min_{\omega,\xi,b} \quad \frac{1}{2}\mathbf{w}^{\mathbf{T}}\mathbf{w} + C\sum_{k=1}^{n}\xi_k, \\ &\text{s.t.} \quad y_k(\mathbf{w}^T\mathbf{x}_k + b) \geq 1 - \xi_k, \quad \xi_k \geq 0, \quad k = 1,\ldots,n \end{aligned} \tag{2.3}$$

where $\mathbf{x_k}$ is the training vector and $y_k \in \{1, -1\}$ is the corresponding class label; ξ_k is the so called slack variable which allows margin errors and *b* is a bias term. C is a penalty parameter set by the users to control the tradeoff between margin size (generalization ability of the classifier) and the number of samples inside the slab (training error).

To get the optimal *C* value, the training samples were subdivided into learning set and validation set. We used the learning set to build SVM models with different *C* values

($\log_2 C \in \{-1, 0, 1, \ldots, 10\}$) and used these models to classify the validation set. The C value associated with the smallest validation error was used to build the final SVM classifier using all the training samples. Then, the weight values in the classifier were squared and the feature with smallest weight was removed from the ranking list, based on the idea that the smaller the weight is, the less important the feature is. This procedure was repeated after all features were removed from the list, as shown in Figure 2.2. According to the backward elimination characteristic of SVM-RFE algorithm, the later a feature is removed from the list, the higher its ranking is.

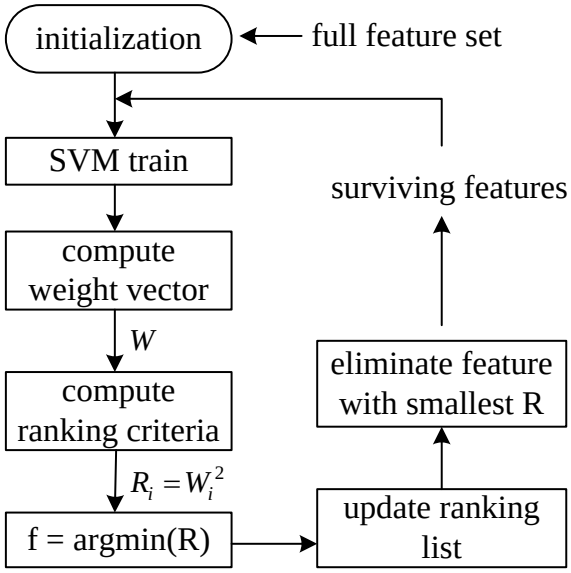

Figure 2.2: Flowchart of the SVM-RFE feature ranking algorithm

To test the robustness and the generalization ability of the selected discriminating features, a leave-one-out double cross validation procedure was performed [27]. Each time, 21 subjects were used for feature selection and training a SVM classifier based on the selected top features, while the other one subject was used for testing the classification result. The testing sample was completely left out before testing and the procedures were repeated until all subjects were classified.

2.4 Experimental Results

2.4.1 Classification Result

We first observed that the group classification accuracy was affected by the number of features used to build the classifier. The prediction accuracy versus the number of features is shown in Figure 2.3. The highest accuracy was achieved with 20 to 40 top features selected by the SVM-RFE algorithm. When the feature number is further increased, the accuracy is degraded due to the negative impact of the less discriminating features. We present the classification result using 20 top features in Table 2.2. A 90.91% overall prediction accuracy is achieved for all the subjects. The classification accuracy for control and patient groups is 90% (True Negative Rate) and 91.67% (True Positive Rate), respectively. The high discriminating power reflects significant oscillation difference between schizophrenia patients and healthy controls at the specific frequencies, brain locations, and time periods indicated by these top features.

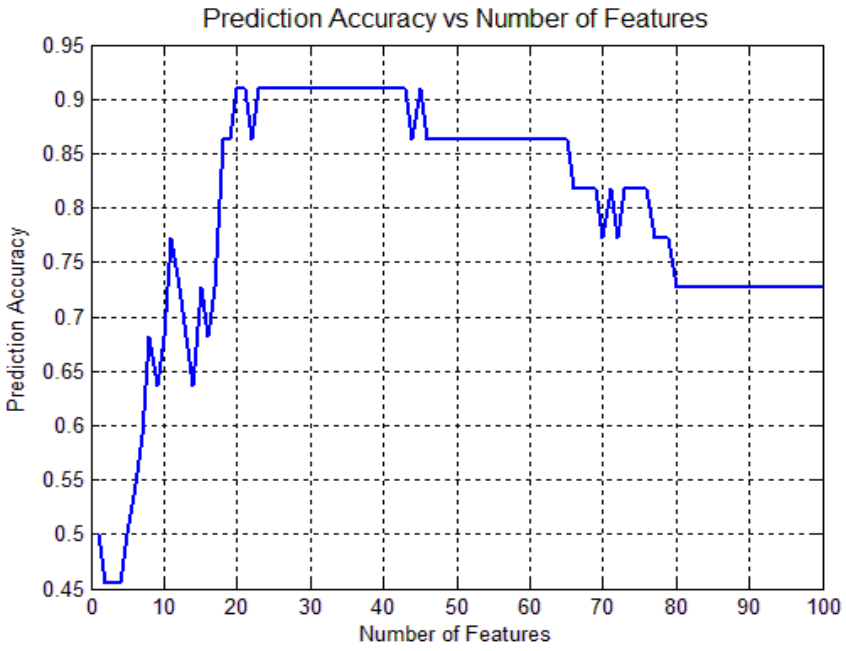

Figure 2.3: Prediction accuracy versus number of features

Table 2.2: Classification results using top 20 ERDS features

Control			Patient			Overall	
Error	TNR	FPR	Error	TPR	FNR	Error	Accuracy
1/10	90%	10%	1/12	91.67%	8.33%	2/22	90.91%

TNR: True Negative Rate; FPR: False Positive Rate; TPR: True Positive Rate; FNR: False Negative Rate.

2.4.2 Feature Analysis

We extract the frequency, space, and time information from the top-ranking features. A general observation is that a variety of frequency bands and cortical areas at different time periods of the language processing need to be selected to get the best discrimination between the patients and the controls. The top-ranked features were located at the occipital and the left frontal-temporal areas, and covered a wide frequency range, including: δ (1-4 Hz), α (8-12 Hz), β (12-32 Hz), and γ (32-48 Hz) bands.

To illustrate the above findings, 5 most frequently selected features (Table 2.3) are analyzed below in detail. The time-varying ERD/ERS waveforms and brain locations of these features are presented in Figure 2.4 to Figure 2.8. The ERD/ERS values shown on the 3D head (plotted by EEGLab [50]) are at the specific time point of the corresponding feature. Red color (positive value) represents ERS, while blue color (negative value) represents ERD.

Table 2.3: List of 5 most frequently selected ERDS features

	Channel	**Time**	**Frequency**
f1	181, occipital lobe	70, post-stimuli	1-4 Hz
f2	239, occipital lobe	50, encoding	16-24 Hz
f3	241, occipital lobe	44, encoding	32-40 Hz
f4	129, left-temporal lobe	40, encoding	8-12 Hz
f5	123, left-frontal lobe	68, post-stimuli	32-40 Hz

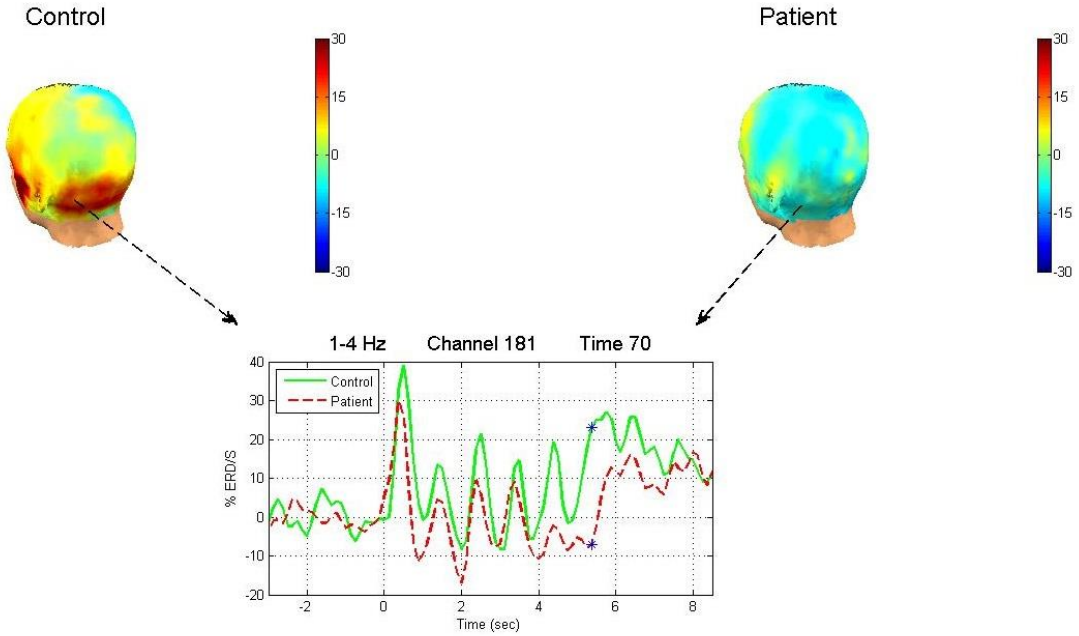

Figure 2.4: Top feature f1 (1-4Hz, occipital lobe, post-stimuli phase)

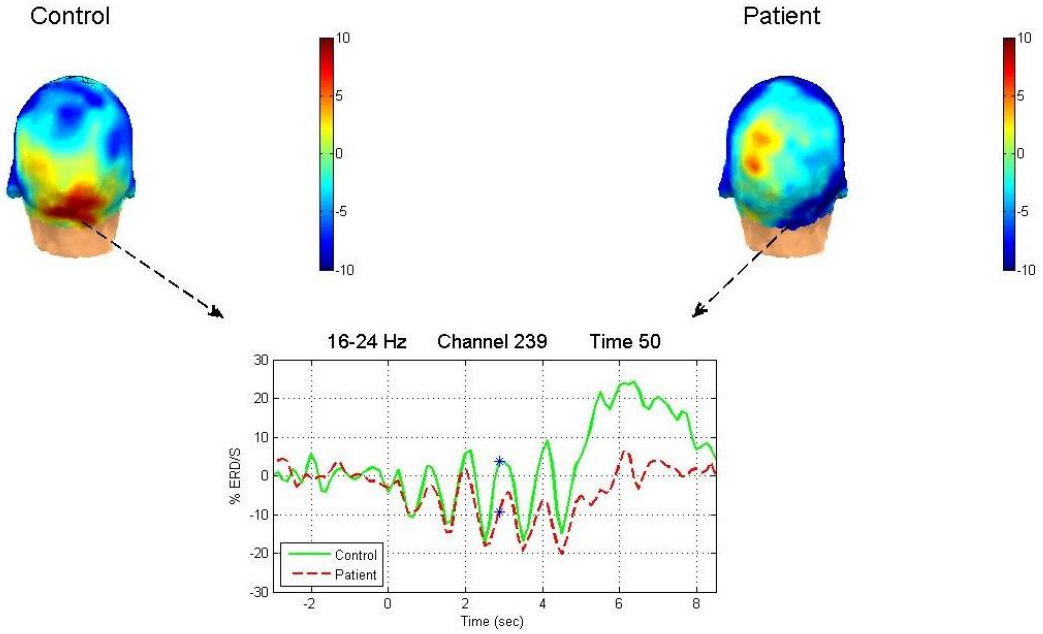

Figure 2.5: Top feature f2 (16-24Hz, occipital lobe, encoding phase)

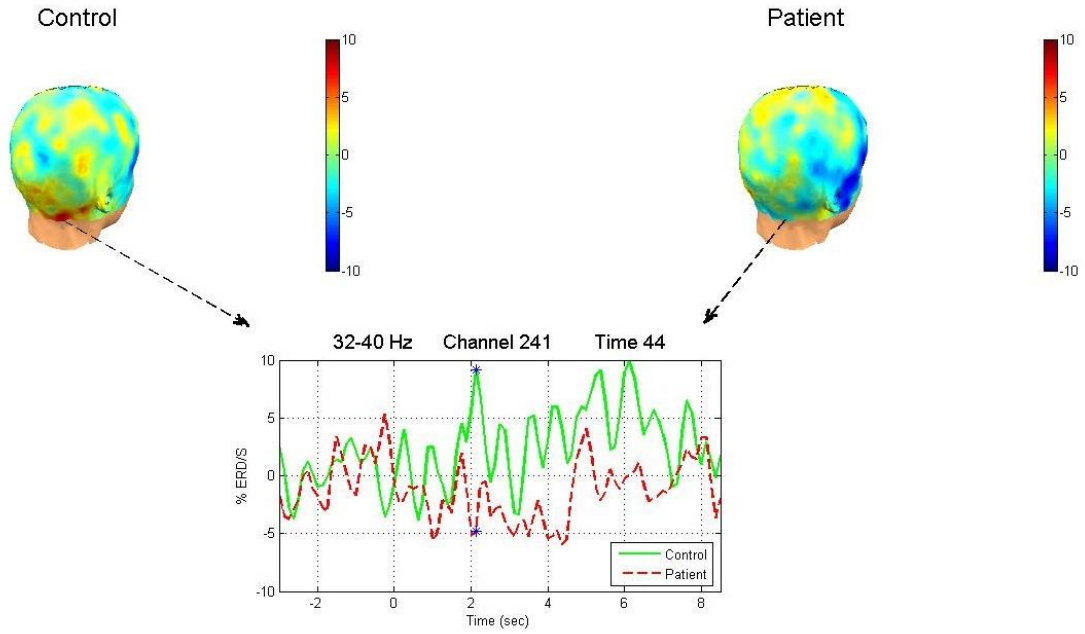

Figure 2.6: Top feature f3 (32-40Hz, occipital lobe, encoding phase)

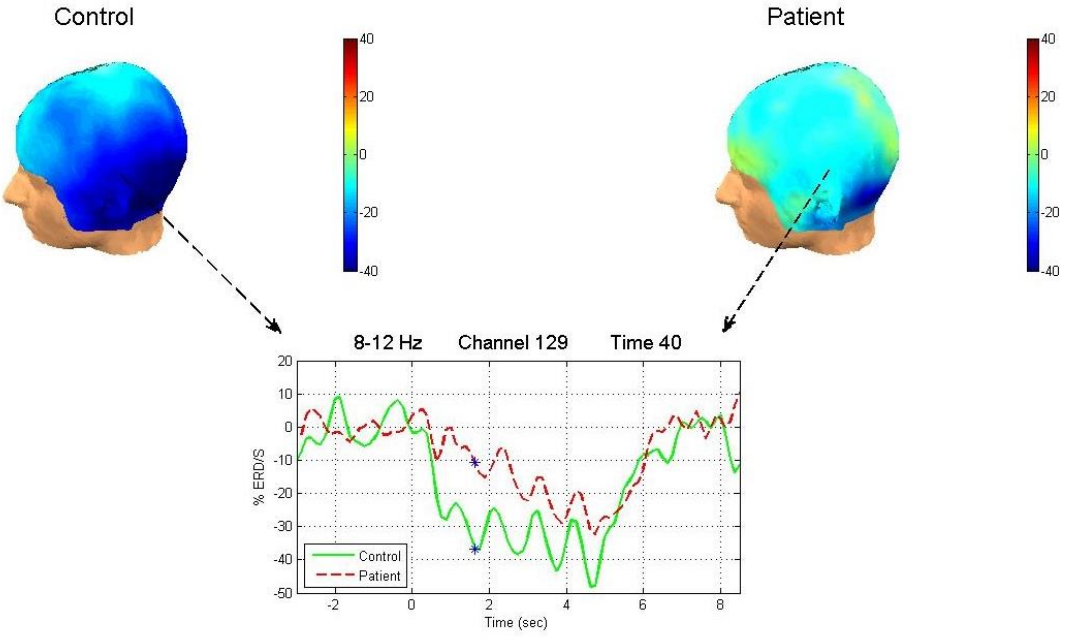

Figure 2.7: Top feature f4 (8-12Hz, left-temporal lobe, encoding phase)

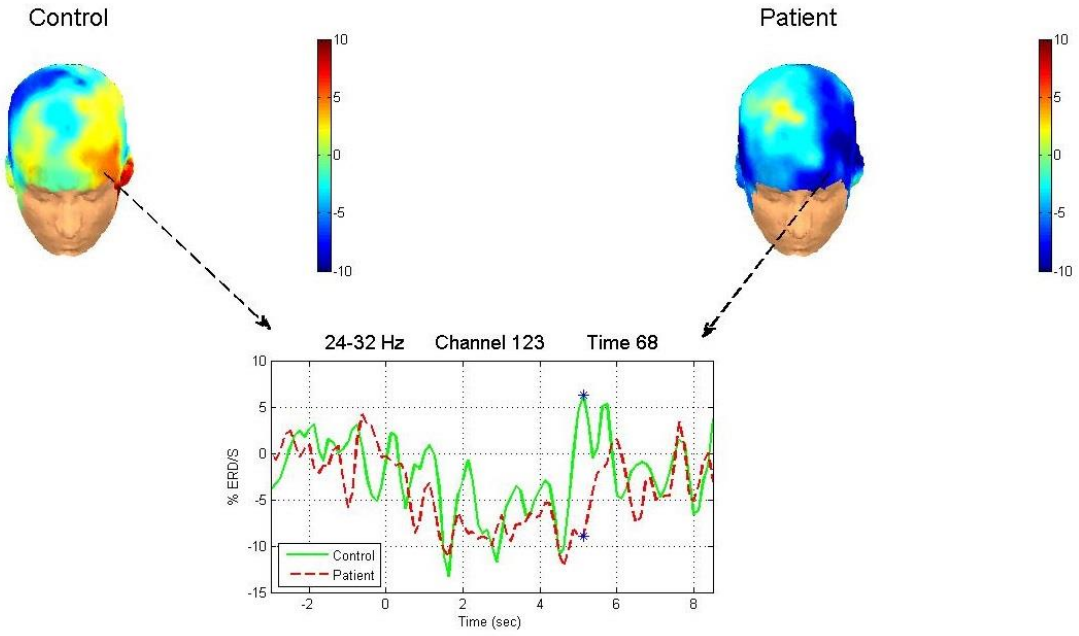

Figure 2.8: Top feature f5 (24-32Hz, left-frontal lobe, post-stimuli phase)

Features f1, f2, and f3 were selected from the visual cortex at the occipital lobe, which is related to the visual modality of the stimuli. Feature f1 was selected from 1-4Hz at the beginning of the post-stimuli stage. Controls exhibited an increased power (high δ band ERS) while patients were still showing ERD, which reflects a difficult recovery from the active state in lower band at the occipital lobe for patients with schizophrenia.

Features f2 and f3 were also located at the occipital lobe but were selected from higher frequency range. Feature f2 was selected from 16-24Hz β band. Its time course showed reduced power in patients with schizophrenia after each word presentation and in the post-stimuli phase. Feature f3 was selected from 32-40Hz γ band. The two groups showed opposite modulation (ERS in controls while ERD in patients), during the encoding and post-stimuli stages. Therefore, processing visual lexical stimuli in schizophrenia was associated with abnormal oscillatory activity in the visual cortex. This abnormality covered a wide range of oscillation frequencies and was characterized by power reduction after each word and in the post-stimulus period. The first indicates

abnormal lexical encoding activity, and the second indicates abnormal recovery from the activity of encoding.

In contrast to these features, the spatial location of feature f4 was near the Wernicke area at the left temporal lobe, a well-known area involved in the understanding of written and spoken language. During lexical encoding, both groups showed an 8-12Hz ERD, but the ERD level for the patients was significantly lower than the controls. The ERD is associated with the activation of cortical areas [40]. This result suggested that the activation of neural circuits in the temporal lobe was less active in patients with schizophrenia than in healthy controls during lexical processing.

Finally, feature f5 showed smaller 24-32Hz β band modulation in the patient group than in the control group at the left frontal lobe. At the end of stimuli encoding, controls showed a pronounced power increase (change from ERD to ERS), while patients showed persistent ERD. This insufficient β modulation reveals dysfunction of this area in patients with schizophrenia during lexical processing.

2.5 Discussions and Conclusions

In this chapter, we investigated discriminating biomarkers in schizophrenia from MEG data recorded during language processing task. We specifically investigated neural oscillation patterns, given their important functional significance as measures of the synchrony of neural populations and their important role in cognition and language. The MEG recordings provide information in the frequency, space, and time dimensions. It was previously shown that an evaluation of oscillations along these dimensions combined is informative and is necessary to fully understand the oscillatory activity associated with cognitive functions [51]. Multidimensional evaluation of the oscillations results in a dauntingly large amount of data, and machine learning methods have been successfully used previously to address this problem. Using machine learning techniques, we found the top features of oscillatory activity that discriminate between patients and controls. Following the leave-one-out cross-validation procedure, we obtained a 90.91% overall

prediction accuracy using the top 20 features of oscillatory activity that demonstrated the robustness of these top features.

The most discriminating features were selected from the active phase (encoding and post-stimuli), and no feature was selected from the baseline period. This result is consistent with the findings that functional brain state provides better classification accuracy for patients and control discrimination than resting state [52]. More importantly, the discriminating features provide information about the electrophysiology of the functional state and word processing in the current context. The spatial locations of the top features were not restricted to one specific cortical area but rather involved several different brain regions. These findings combined the support of many recent theories that emphasize the role of a dysconnection syndrome and disturbed coordination in the pathophysiology of schizophrenia [32]. According to our results, the main impaired areas are the occipital and the left frontal-temporal lobes.

Furthermore, the dysfunctional regions mentioned above were associated with specific oscillation frequencies. Because of conduction delays in the brain, slow oscillations, such as δ, are considered necessary to link remote areas of the brain. Fast oscillations, such as γ, are considered necessary for the synchrony of local circuits [32], [53]. Consistent with the above, our results showed that ERD/ERS patterns selected from low-frequency bands (δ, α) represent similar behavior of a relatively large region, while the features selected from γ band seem more localized.

First, the time evolution of feature f1 showed that the presentation of the visual stimuli excited δ ERS at the occipital lobe during lexical processing. This is consistent with other studies that reported low-frequency ERS during stimuli encoding in healthy control subjects [52], [54]. However, at the end of the encoding stage to the beginning of the post-stimuli stage, controls showed further power increase (higher ERS) while patients were still showing ERD. This reduced δ band power indicates failure of the neural systems to resume idle state in patients with schizophrenia [51].

Second, feature f4 showed higher level of α ERD (8-12 Hz) in healthy controls than in patients with schizophrenia, at the left temporal lobe near the Wernicke area. The α activity is associated with attention demands or modulated by stimulus-related aspects or semantic memory process [55]. Significant α ERD was reported in healthy control subjects during a lexical decision task using both visual and auditory stimuli [54], and an auditory lexical processing task [56]. As higher level of ERD reflects a higher level of attention and alertness during encoding, as well as the activation of cortical areas involved in the cognitive information processing [40], reduced α ERD in schizophrenia reflects that the left temporal lobe was hypoactive during lexical processing. Abnormal α oscillation in schizophrenia was also reported in several recent oscillation studies [53], [57].

The time evolution of features f2(16-24 Hz) and f5(24-32Hz) showed somewhat similar β band behavior in the occipital and frontal areas, respectively. The ERD/ERS after each word presentation was followed by a pronounced ERS (transient in f5) at the end of the encoding phase in the control group. This result is consistent with another lexical decision task using visual stimuli in healthy control subjects [54]; however, the late β ERS was not found in the patient group. Abnormal β oscillation in schizophrenia has been widely reported [32], [53], [57]. The timing of the reduced β ERS suggests similar difficulty of the neural system to resume idle state in schizophrenia.

Finally, feature f3(32-40 Hz) exhibited localized γ ERS during lexical encoding at the occipital lobe for healthy control subjects, while patients with schizophrenia showed opposite modulation (ERD). The γ oscillation reflects a stage of active information processing [40] and is often the first component in response to a sensory stimulus, including visual stimuli [53]. It was proposed that neurons in different parts of the visual cortex fire at nearly the same time during a cycle of γ oscillations to convey different attributes of the scenery and to help form a unified representation [58]. The γ band ERS has been found in many cortical areas and is induced by different stimuli or tasks [59]. In the domain of language, γ oscillations have been associated with lexical processing [60];

and in a recent MEG study, γ ERS was reported in healthy control subjects during lexical processing [56]. In schizophrenia, γ oscillation has become a major research focus because of its role in cognition [61]. A series of studies have examined γ band activity in patients with schizophrenia, providing consistent evidence for the presence of abnormal γ band oscillations. Overall, reductions in power or synchrony of evoked γ oscillations have been reported in chronic, first episode as well as early-onset schizophrenia [58].

In summary, this chapter investigated abnormal neural oscillation patterns in patients with schizophrenia during lexical processing. As neural oscillation abnormality may be due to the mechanisms of the disease [53], the spectral, spatial and temporal content of the discriminating features may offer useful information to help us understand the physiological basis of language disorder in schizophrenia, as well as the underlying mechanism of the illness itself.

Chapter 3

MEG Spectral Power Ratio Patterns in Schizophrenia

3.1 Introduction

As introduced in Chapter 2, cognitive dysfunctions in schizophrenia, such as language disorder, is not simply due to a spatially circumscribed deficit, but rather represents a distributed impairment involving many cortical areas and their connectivity (disconnection hypothesis) [32]. Based on these findings, neural oscillations and their synchronization have become a crucial research area, due to their role in realizing flexible communication within and between cortical areas; abnormal brain oscillations have been frequently reported in schizophrenia (see [32] for review).

MEG/EEG studies that examined neural oscillations in schizophrenia at different temporal and spatial scales have reported decreased or increased oscillation power in all frequency bands, including *delta* (< 4Hz), *theta* (4-8Hz), *alpha* (8-12Hz), *beta* (12-30Hz) and *gamma* (> 30Hz) bands (see [53] for review). The specificity of frequency abnormalities may provide key biological markers linking disease mechanism to the clinical dysfunctions in schizophrenia [53]. Furthermore, some recent MEG/EEG studies showed that band power of neural oscillations during both cognitive tasks and resting state could be used as quantitative features to distinguish schizophrenia patients from healthy controls with machine learning classifiers [20], [18], [52], [62]–[65].

In this chapter, we specifically investigate the Power Spectral Density (PSD) of neural oscillatory activity during word processing measured by MEG. The central

hypothesis here is that the spectral power of neural oscillations in schizophrenic patients differs from healthy controls at certain frequency ranges, brain locations and time periods of word processing. Such spectral-spatial-temporal information can be extracted as quantitative features from MEG recordings to distinguish schizophrenia patients from healthy subjects. Note that in Chapter 2, the ERD/ERS features were obtained by computing power of MEG sample points in time-domain, while in this chapter, the spectral power features are extracted from the PSD of MEG signal in frequency domain.

The key contribution of this chapter is three-fold. First, we extracted two novel Spectral Power Ratio (SPR) feature sets: the Band Power Ratio (BPR) and the Window Power Ratio (WPR), to assess neural oscillatory activity in schizophrenia. Spectral power has been employed in previous studies to delineate oscillatory abnormalities in schizophrenia, mostly in the form of Absolute Band Power (ABP) [65]–[68] or Relative Band Power (RBP), i.e., ABP normalized by the total power [63], [69]. Unlike ABP and RBP, which characterize oscillation power in different frequency bands and in different time windows separately, the BPR and the WPR reflect the inter-relationships of spectral power between different frequency bands, and between different time periods of word processing, respectively.

On the one hand, the ratio of band power (BPR) amplifies the increase of power in one band and the decrease of power in another band, which has been shown to be effective in epileptic seizure prediction [70], [71], seizure detection [72], and stroke diagnosis [73]. Previous work has also shown the discriminating power of BPR in schizophrenia classification, using single-trial MEG data during sentence processing [20]. On the other hand, the ratio of power in two consecutive time windows (WPR) for a specific spectral band captures the power change across different time periods of word processing, which could not be assessed by single window based analysis. As such, the BPR and WPR provide information about the frequency and temporal dynamics of neural oscillations, respectively. To the best of our knowledge, BPR and WPR have not been employed together before to analyze MEG data collected from schizophrenia patients during word processing.

Second, we employed cluster-based non-parametric permutation test [16] to identify statistically significant SPR features. SPR features are extracted from hundreds of brain locations measured by MEG. Discriminating features identified by sample-wise uncorrected *p*-values or other univariate feature ranking methods that measure the between-group difference at single feature level may be false discoveries due to multiple comparisons [14]. Some previous studies employed traditional Bonferroni correction [63], [69] or False Discovery Rate (FDR) control procedures [67] for multiple comparison correction. These methods are not optimized for MEG data, and may lead to high False Negative Rate (FNR), i.e., low sensitivity for detecting significant features, due to the small sample size compared with the large feature size. The cluster-based non-parametric permutation tests [16] we employed in this study control the FDR while maintaining a low FNR, which results in high specificity and sensitivity of the discriminating features. It may be noted that cluster-based non-parametric permutation test has rarely been employed as a feature selection procedure in the context of schizophrenia classification.

Third, after identifying statistically significant SPR features, we applied machine learning based feature selection algorithm to select optimal feature combinations for classifying schizophrenia patients from healthy controls. We achieved over 95% classification accuracy using three different linear classifiers separately, following cross validation procedures.

The rest of this chapter is organized as follows. Section 3.2 describes the SPR feature extraction, statistical testing and classification procedures. Sections 3.3 and 3.4 presents the data analysis results and discusses the significance and limitations of the work, respectively. Section 3.5 concludes the current work and points out future directions.

3.2 Materials and Methods

3.2.1 Subjects and Data

In this chapter, we use the same MEG data as described in Chapter 2. See Section 2.2 for details about subjects' information and MEG data acquisition and preprocessing procedures.

3.2.2 Feature Extraction

The BPR and the WPR feature sets are extracted from the PSD of the MEG recordings. Both BPR and WPR are spatial-temporal-spectral feature sets with each single feature containing specific frequency, time and space information. Details of the feature extraction procedures are described below.

Define Spatial Locations:

Unlike most EEG/MEG studies that extract features from each single MEG sensor separately, we averaged MEG signals from 3 adjacent sensors before feature extraction. More specifically, for each MEG sensor, we form 8 triangles from its 8 nearest neighbor sensors which have shortest circumference, as shown in Figure 3.1. This procedure results in 822 averaged MEG signals for each subject. The spatial location of the averaged signal is defined as the geometric center of the 3 averaged MEG sensors.

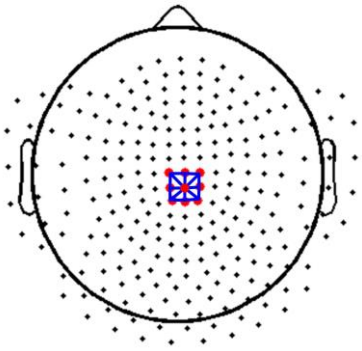

Figure 3.1: Average MEG signals from three adjacent sensors that form a triangle with shortest circumference

The reason for averaging signals from adjacent sensors is that MEG recordings are generally considered "noisy" where the noise level is higher than the signal of interest. To cope with this problem, after averaging trials from same MEG sensor, we average

signals from adjacent sensors to further suppress the random noise components. In addition, due to volume conduction effect, MEG gradiometers tend to show spread activation in sensor space. That is, MEG sensors that are close to each other tend to record similar activities, which makes it reasonable to average signals from a few adjacent sensors. Furthermore, with axial gradiometers, a local brain source is best captured by adjacent sensors, rather than by a sensor just above the source [52].

Define Time Windows:

The averaged MEG signal from each spatial location is further segmented into 5 phases of word processing, using time windows shown in Figure 3.2: 1) *baseline* (BA), three seconds right before the onset of the first word; 2) *transition from baseline to encoding* (BE), one second before and two seconds after the onset of the first word; 3) *encoding* (EN), stimuli presentation, five seconds right after the onset of the first word; 4) *transition from encoding to post-stimuli* (EP), one second before the end of stimuli presentation to two seconds after stimuli presentation; 5) *post-stimuli* (PO), three seconds right after stimuli presentation. After this step, new MEG segments are obtained with each one corresponding to one spatial location and one time window (phase of word processing).

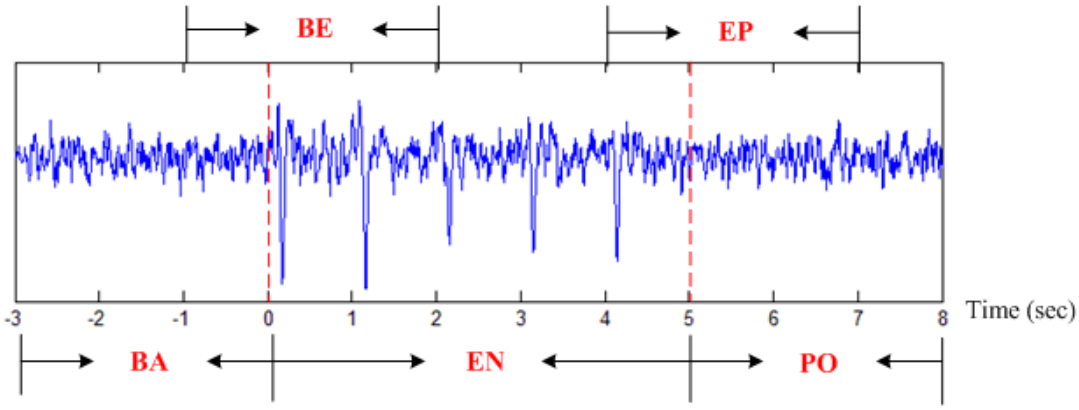

Figure 3.2: Segmentation of the MEG signal into 5 time windows of word processing: *1) baseline* (BA), *2) transition from baseline to encoding* (BE), *3) encoding* (EN), *4) transition from encoding to post-stimuli* (EP), and *5) post-stimuli* (PO).

Define Spectral Power Ratios:

For each MEG segment, the power spectral density (PSD), which describes how the power of a signal is distributed over different frequencies, is estimated using the Welch method [74], which can be computed in an efficient manner with low complexity [75]. Afterwards, the spectral power is computed in 5 frequency bands by integrating the PSD within that frequency band. The frequency ranges of the 5 bands of interests are: *delta* (1-4Hz), *theta* (4-8Hz), *alpha* (8-13 Hz), *beta* (13-30Hz) and *gamma* (30-57 Hz). The spectral power of MEG signal at the i^{th} spatial location, the j^{th} time window, and the k^{th} frequency band is defined as:

$$P_{i,j,k} = \sum_{f \in [f^k_{\min}, f^k_{\max}]} PSD_{i,j,k}(f), \quad i = 1,\ldots,822; \;\; j = 1,\ldots,5; \;\; k = 1,\ldots,5. \tag{3.1}$$

where $f^k_{\min}$ and $f^k_{\max}$ represent the lowest and highest frequency of the k^{th} frequency band, respectively.

The first SPR feature set BPR is defined as the ratio of spectral power between two different frequency bands, at the same spatial location and in the same time window. The BPR between band k_1 and band k_2 at region i and during time window j is defined as:

$$BPR_{i,j,k_1,k_2} = \frac{P_{i,j,k_1}}{P_{i,j,k_2}}, \quad i = 1,\ldots,822; \; j = 2,\ldots,5; \;\; k_1, k_2 = 1,\ldots,5; \;\; k_1 > k_2. \tag{3.2}$$

The second SPR feature set WPR is defined as the percentage power change across two consecutive time windows. The WPR between the j^{th} and the $(j-1)^{th}$ time window at the k^{th} frequency band and the i^{th} region is defined as:

$$WPR_{i,j,k} = \frac{P_{i,j,k} - P_{i,j-1,k}}{P_{i,j-1,k}}, \quad (3.3)$$
$$i = 1,\ldots,822;\ j = 2,\ldots,5;\ k = 1,\ldots,5.$$

The total number of BPR features is 10 BPRs * 4 time windows * 822 spatial locations = 32880 (BA window is not used). The total number of WPR features is: 4 WPRs * 5 frequency bands * 822 spatial locations = 16440. All features are normalized to have zero mean and standard deviation one before further analysis.

3.2.3 Statistical Analysis

Non-parametric Permutation test is employed to determine the statistical significance of the extracted SPR features and control the False Positive Rate (Type I error) caused by multiple comparisons [16]. The test is performed for BPR in each time window and WPR in each frequency bands separately. The permutation test uses a test statistic that is based on clustering of adjacent spatial locations that exhibit a similar SPR difference (in sign and magnitude) between patient group and control group. The calculation of the test statistic involves the following steps:

Step 1: Compute the *t*-score for each SPR feature from all spatial locations: $t = \frac{\bar{X}_c - \bar{X}_p}{\sqrt{s_c^2 / N_c + s_p^2 / N_p}}$, where $\bar{X}_c$ and $\bar{X}_p$ are the sample means, s_c and s_p are the sample standard deviations, and N_c and N_p are the sample sizes of the control group and the patient group, respectively. This *t*-score is called the sample-specific uncorrected *t*-score.

Step 2: Select all SPR features with absolute value of uncorrected *t*-score greater than a threshold, 2.5 in the current study. This step identifies a set of "candidate positives", of which a high proportion is likely to be true.

Step 3: Cluster the selected features in connected sets based on spatial adjacency. In

this study, we define two spatial locations as neighbors if their distance is less than 0.03mm. Note that the clustering is performed for features with positive and negative *t*-scores separately.

Step 4: The cluster-level statistic is defined as the sum of *t*-scores within a cluster.

After getting the cluster-level test statistics for all clusters, the significance of these clusters is obtained by calculating the Monte-Carlo estimate of the *p*-values. The steps are as follows:

Step 1: Randomly reassign the group identity of each subject without replacement.

Step 2: Calculate the cluster-level test statistics on this random partition and record the largest of these statistics.

Step 3: Repeat step 1 and step 2 for a large number of times, 50,000 in this study, and construct a permutation distribution of the test statistics.

Step 4: The Monte Carlo *p*-value of a cluster is defined as the proportion of random partitions that have a larger test statistic than the observed one. An SPR cluster with Monte Carlo *p*-value less than 0.05 is considered statistically significant in this study.

3.2.4 Feature Selection

After identifying statistically significant SPRs, we test whether they could be used as features in machine learning classifiers to distinguish schizophrenia patients from healthy controls (predict diagnosis) with high accuracy. The mean SPR within a significant cluster is used as a scalar feature representing the cluster. A feature ranking algorithm based on the minimum-Redundancy-Maximum-Relevance (mRMR) criteria is employed to select the optimal feature combinations for classification [28]. The mRMR algorithm selects features according to the maximal statistical dependency criterion based on mutual information *I*. Mutual information based feature selection aims at finding a feature set *S* with *m* features $\{x_i\}$, which jointly have the largest dependency on the

target class *c*.

$$\max D(S,c), \quad D = \frac{\sum_{x_i \in S} I(x_i;c)}{|S|}. \tag{3.4}$$

Features selected according to the maximal dependency criterion could have large redundancy. When two features highly depend on each other, the respective class-discriminative power would not change much if one of them was removed. Therefore, the following minimal redundancy condition can be added to select mutually exclusive features:

$$\min R(S), \quad R = \frac{\sum_{x_i, x_j \in S} I(x_i, x_j)}{|S|^2} \tag{3.5}$$

Finally, an operator $\Phi(D,R)$ is defined in terms of dependency *D* and redundancy *R*. The mRMR criterion solves the optimization problem given by:

$$\max \Phi(D,R), \quad \Phi = D - R. \tag{3.6}$$

3.2.5 Classification

Since our sample size is small, to avoid complex classification models overfitting the data, three commonly used linear classifiers are employed to classify patients vs. controls: Linear Discriminant Analysis (LDA) [76], Perceptron [77] and linear Support Vector Machine (SVM) [25], [26]. The basic principle of SVM is described in Section 2.3.2. The basic principles of LDA and perceptron are described below.

Linear Discriminant Analysis (LDA):

Given samples from two classes C_1 and C_2, the goal of LDA is to find out the direction as defined by a vector $\mathbf{w}$, such that when the data are projected onto $\mathbf{w}$, the

samples from the two classes are as well separated as possible. Let $z = \mathbf{w}^{\mathbf{T}}\mathbf{x}$ be the projection of $\mathbf{x}$ onto $\mathbf{w}$. In our two-class case, it is a dimensionality reduction from original *d*-dimensional feature space to a *1*-dimensional line space. Define the within-class scatter matrix $\mathbf{S_w}$ as:

$$\mathbf{S_w} = \sum_{\mathbf{x}\in C_1} (\mathbf{x} - \mathbf{m_1})(\mathbf{x} - \mathbf{m_1})^T + \sum_{\mathbf{x}\in C_2} (\mathbf{x} - \mathbf{m}_2)(\mathbf{x} - \mathbf{m}_2)^T \tag{3.7}$$

where $\mathbf{m_1}$ and $\mathbf{m}_2$ are the means of class C_1 and class C_2, respectively. The LDA solution of the projection direction is:

$$\mathbf{w} = \mathbf{S_w^{-1}}(\mathbf{m_1} - \mathbf{m_2}). \tag{3.8}$$

After obtaining this direction, the data can be easily classified using the following linear classification rule:

$$choose \begin{cases} C_1, & if\ \mathbf{w}^{\mathbf{T}}\mathbf{x} + b \geq 0 \\ C_2, & o.w. \end{cases} \tag{3.9}$$

where the bias term *b* can be calculated as:

$$b = -\frac{1}{2}(\mathbf{w}^{\mathbf{T}}\mathbf{m_1} + \mathbf{w}^{\mathbf{T}}\mathbf{m}_2). \tag{3.10}$$

Perceptron:

Perceptron is a linear classifier aiming at finding a decision hyperplane $g(\mathbf{x}) = \mathbf{w}^{\mathbf{T}}\mathbf{x} + w_0 = 0$ defined by the weight vector $\mathbf{w}$. The weight vector is solved by an optimization problem which tries to minimize the following cost function:

$$J(w) = \sum_{x\in Y} \delta_x w^T x \tag{3.11}$$

where *Y* is the subset of the training data which are misclassified by the hyperplane. The

variable δ_x is chosen so that $\delta_x = -1$ if $x \in w_1$ (class label = +1) and $\delta_x = +1$ if $x \in w_2$ (class label = -1). It is obvious that $J(w) \geq 0$ and the minimum value 0 is achieved when *Y* is empty, i.e., no data is misclassified. To minimize this cost function, an iterative scheme based on gradient descent method is employed to update the weight vector.

$$w(t+1) = w(t) - \rho_t \frac{\partial J(w)}{\partial w} |_{w=w(t)} \tag{3.12}$$

We employed a cross-validation scheme to test the generalization ability of the classification results. Three controls and four patients are randomly chosen from each group to form a testing set. The rest seven controls and eight patients are used as training set to train the classifiers. We construct 1000 such training and testing sets by random sampling and calculate the average classification accuracy, specificity and sensitivity of each classifier over the 1000 test sets.

3.3 Experimental Results

3.3.1 Significant BPR Features

Each BPR feature contains specific frequency, time and space information. In Figure 3.3, we show the frequency-time distribution of the BPR features with absolute value of uncorrected *t*-score greater than 2.5 (candidate positives). Most of the BPR features that show significant between-group difference before the permutation test are: *1)* BPR (*theta/delta*, EN), i.e., the *theta/delta* band power ratio during the *encode* window, *2)* BPR (*alpha/delta*, BE), i.e., the *alpha/delta* band power ratio during the *base-to-encode* window, and *3)* BPR (*beta/delta*, EN), i.e., the *beta/delta* band power ratio during the *encode* window. The spatial locations of these three significant BPRs are shown in Figure 3.4.

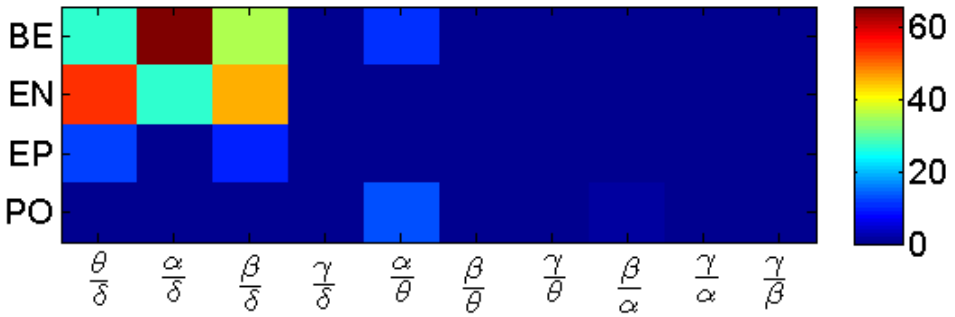

Figure 3.3: Number of occurrences of each BPR that shows significant between-group difference (absolute value of uncorrected *t*-score > 2.5) in each time window

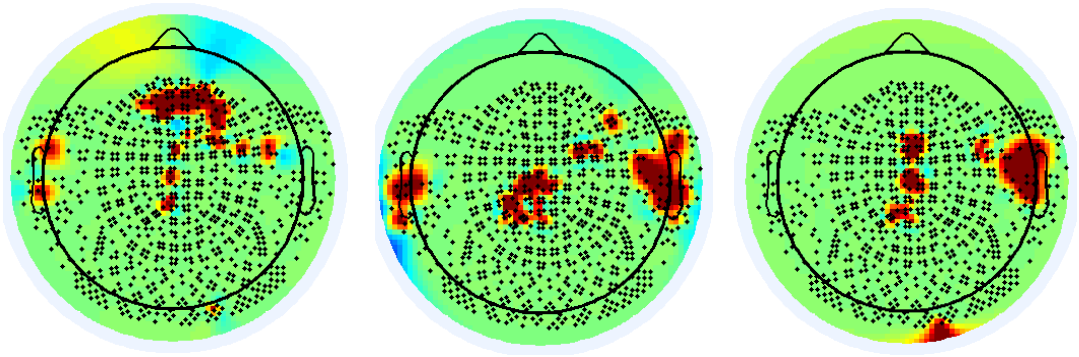

(a) (b) (c)

Figure 3.4: Spatial locations of the BPR features with absolute value of uncorrected *t*-score > 2.5 for (a) BPR (*theta/delta*, EN), (b) BPR (*alpha/delta*, BE), and (c) BPR (*beta/delta*, EN)

From Figure 3.4, we can observe several spatial clusters associate with each of the three significant BPRs. The significant BPR (*theta/delta*, EN) features are located at the middle-to-right frontal, left temporal and middle parietal areas. The significant BPR (*alpha/delta*, BE) features are located at the left temporal, middle parietal, right temporal and right frontal areas. The significant BPR (*beta/delta*, EN) features are located at the middle frontal-parietal, right temporal and occipital areas. However, only three clusters of these candidate BPRs pass the permutation test (corrected *p*-value < 0.05), including *1)* the middle-to-right frontal cluster of BPR (*theta/delta*, EN), average *t*-score = -2.792, corrected *p*-value = 0.024, *2)* the middle parietal cluster of BPR (*alpha/delta*, BE),

average *t*-score = -2.798, corrected *p*-value = 0.047, and *3)* the middle frontal-parietal cluster of BPR (*beta/delta*, EN), average *t*-score = -2.770, corrected *p*-value=0.046. The 3D head plot of the spatial locations, the boxplot of the mean BPR within cluster, and the normalized PSD of a signal in the cluster are shown in Figure 3.5 to Figure 3.7, for the three significant clusters, respectively.

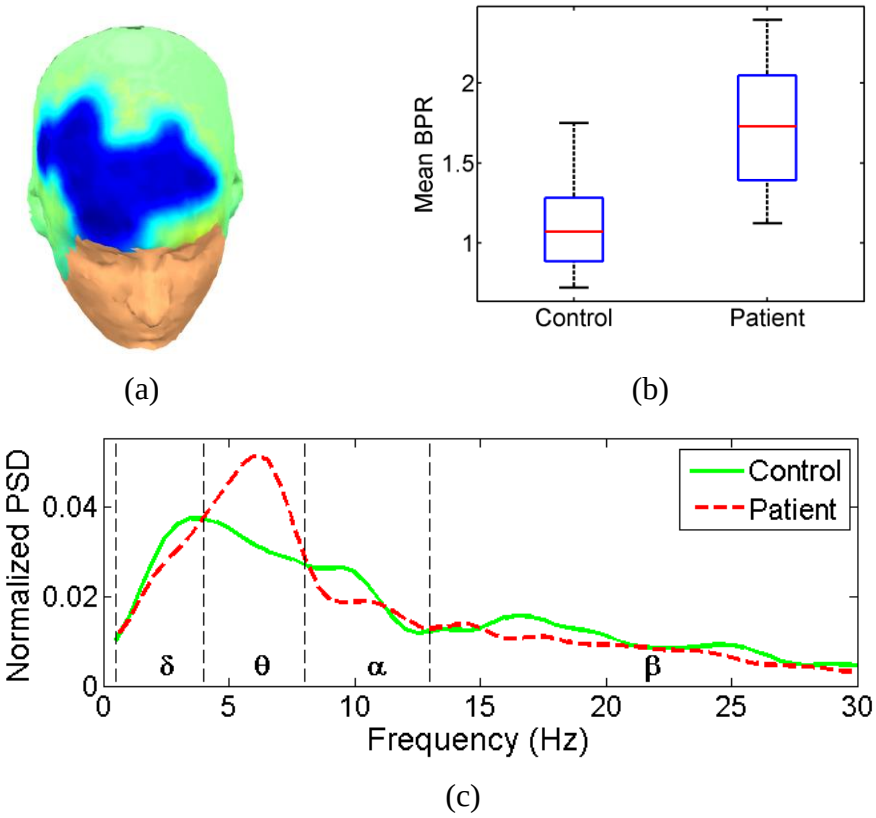

Figure 3.5: (a) Spatial locations (middle-to-right frontal areas) that show significantly increased BPR (*theta/delta*, EN) in schizophrenia patients (average *t*-score = -2.792, corrected *p*-value = 0.024). (b) Boxplot of the mean BPR within cluster. (c) Normalized PSD of MEG signal from a location in the cluster for control group and patient group.

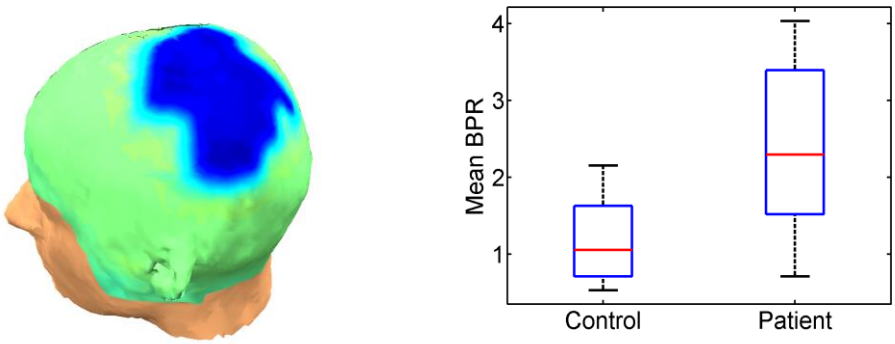

(a) (b)

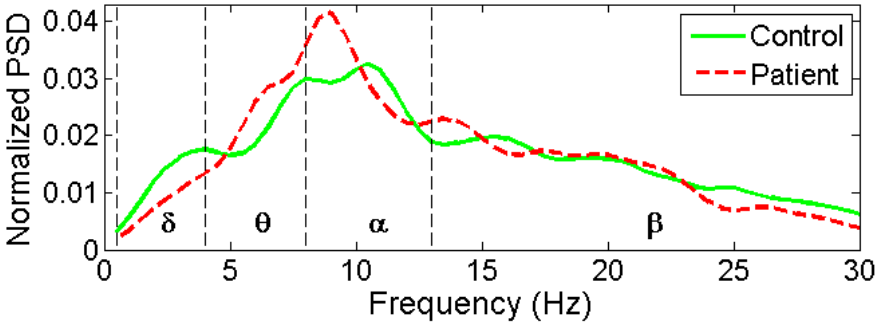

(c)

Figure 3.6: (a) Spatial locations (middle parietal area) that show significantly increased BPR (*alpha/delta*, BE) in schizophrenia patients (average *t*-score = -2.798, corrected *p*-value = 0.047). (b) Boxplot of the mean BPR within cluster. (c) Normalized PSD of MEG signal from a location in the cluster for control group and patient group.

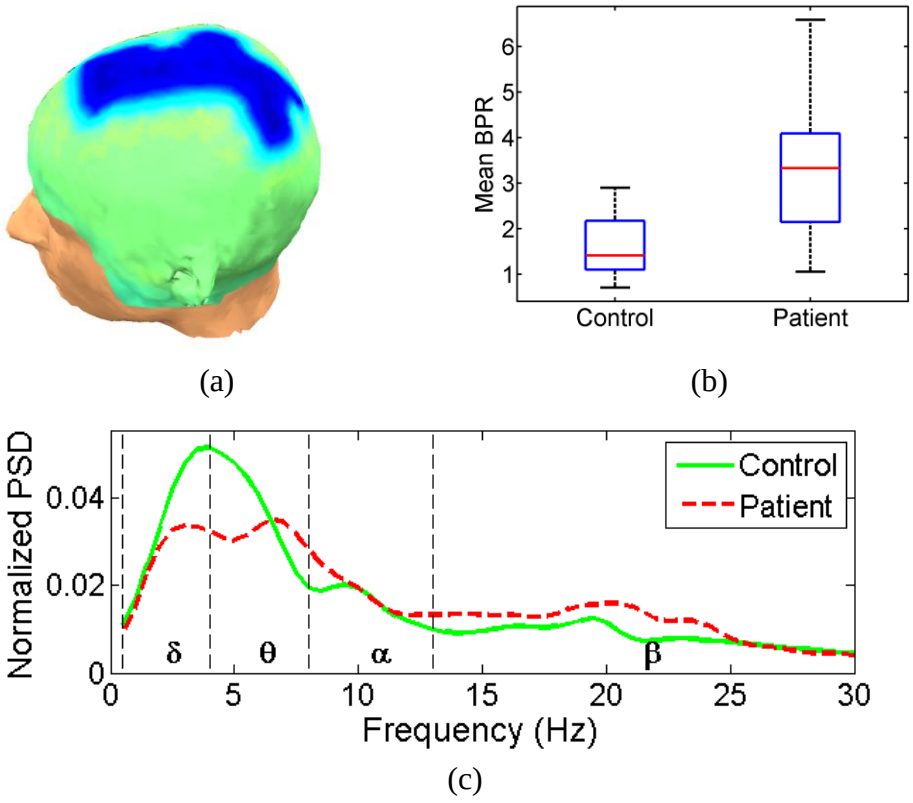

Figure 3.7: (a) Spatial locations (middle frontal-parietal areas) that show significantly increased BPR (*beta/delta*, EN) in schizophrenia patients (average *t*-score = -2.770, corrected *p*-value = 0.046). (b) Boxplot of the mean BPR within cluster. (c) Normalized PSD of MEG signal from a location in the cluster for control group and patient group.

From Figure 3.5, we can observe that patient group shows significantly increased *theta/delta* BPR during encoding period of word processing, at the middle-to-right frontal area. This is due to a decreased proportion of *delta* band power and an increased proportion of *theta* band power in the full spectrum in patient group. In Figure 3.6, we can observe that patients show an increased *alpha/delta* power ratio at the middle parietal area during baseline to encoding period of word processing. The PSD plot shows that the proportion of *delta* power decreases and the proportion of *alpha* power increases in schizophrenia patients compared with healthy controls. Figure 3.7 shows an increased

beta/delta band power ratio at the middle frontal-parietal areas, during encoding phase of word processing. This is due to a decreased portion of *delta* band power and an increased proportion of *beta* band power in the full spectrum of the MEG signal in patient group, as shown in the PSD plot.

3.3.2 Significant WPR Features

Similarly to the BPR features, in Figure 3.8, we show the time-frequency distribution of all WPRs with absolute value of uncorrected *t*-score greater than 2.5 (candidate positives). Most of the WPR features that show significant between-group difference before multiple comparison correction are the WPR (BE/BA, *beta*), i.e., the *beta* band power ratio across *baseline* and *base-to-encode* time windows, and the WPR (PO/EP, *beta*), i.e., the *beta* band power ratio across *encode-to-post* and *post-encoding* time windows. The spatial locations of the two WPRs are shown in Figure 3.9.

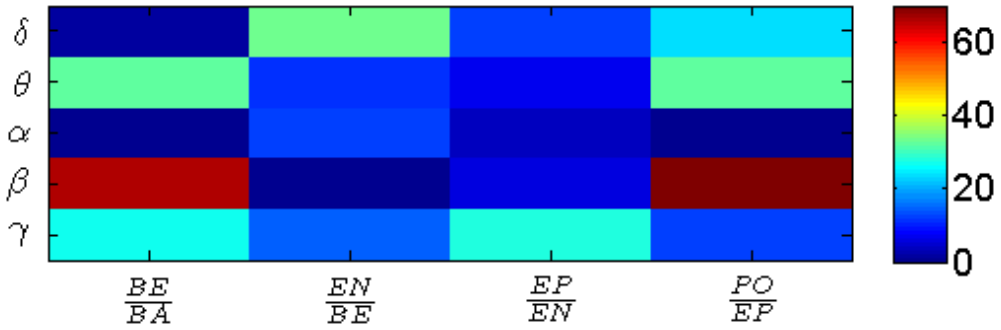

Figure 3.8: Number of occurrence of each WPR in different frequency bands with absolute value of uncorrected *t*-score > 2.5

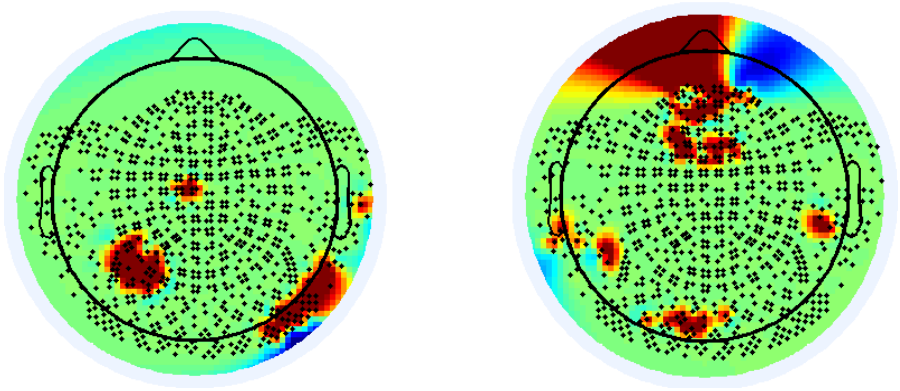

(a) (b)

Figure 3.9: Spatial locations of WPR features with absolute value of uncorrected *t*-score > 2.5 for: (a) WPR (BE/BA, *beta*) and (b) WPR (PO/EP, *beta*)

From Figure 3.9, we can observe that the significant WPR (BE/BA, *beta*) features are mainly located at the left parietal and right occipital areas. The significant WPR (PO/EP, *beta*) features are located at the middle fontal, left parietal, right parietal and occipital areas. Among these candidate WPR features, three spatial clusters pass the permutation tests (corrected *p*-value < 0.05), including *1)* the left parietal cluster of the WPR (BE/BA, *beta*), average *t*-score = 3.015, corrected *p*-value = 0.037, *2)* the right occipital clusters of the WPR (BE/BA, *beta*), average *t*-score = -3.431, corrected *p*-value = 0.037, and *3)* the middle frontal cluster of the WPR (PO/EP, *beta*), average *t*-score = -3.115, corrected *p*-value = 0.013. The 3D head plot of the spatial locations, the boxplot of the mean WPR within cluster, and the *beta* band spectrogram of a signal in the cluster for each group are shown in Figure 3.10 to Figure 3.12, for the three significant WPR clusters, respectively.

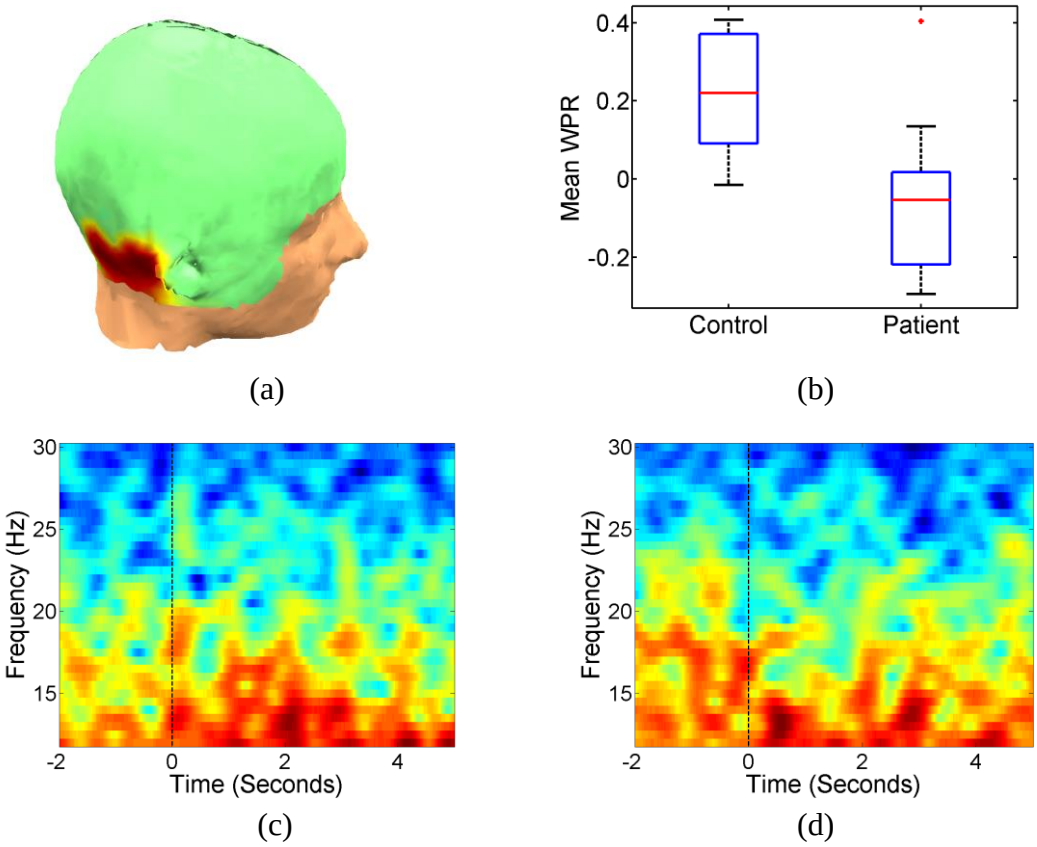

Figure 3.10: (a) Spatial locations (right occipital area) that show significantly decreased WPR (BE/BA, *beta*) in schizophrenia patients (average *t*-score = 3.015, corrected *p*-value = 0.037). (b) Boxplot of the mean WPR within cluster. (c) and (d) *beta* band spectrogram of MEG signal from a location in the cluster for control group and patient group, respectively.

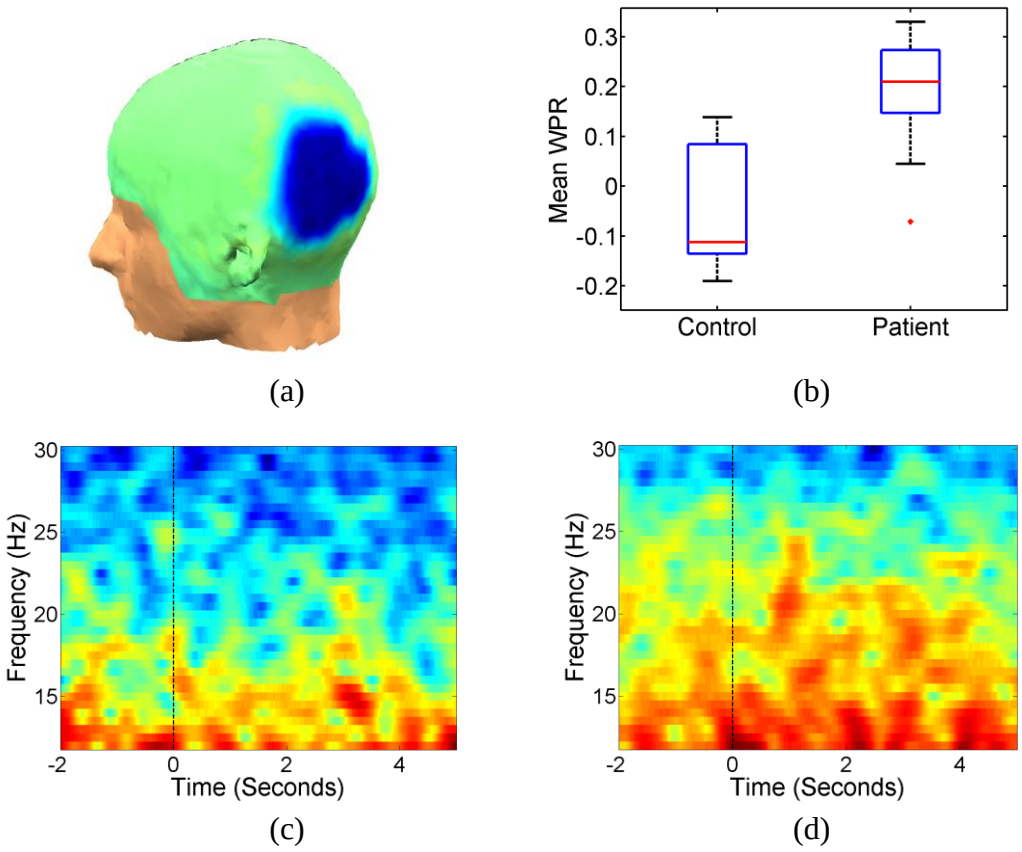

Figure 3.11: (a) Spatial locations (left parietal area) that show significantly increased WPR (BE/BA, *beta*) in schizophrenia patients (average *t*-score = -3.431, corrected *p*-value = 0.037). (b) Boxplot of the mean WPR within cluster. (c) and (d) *beta* band spectrogram of MEG signal from a location in the cluster for control group and patient group, respectively.

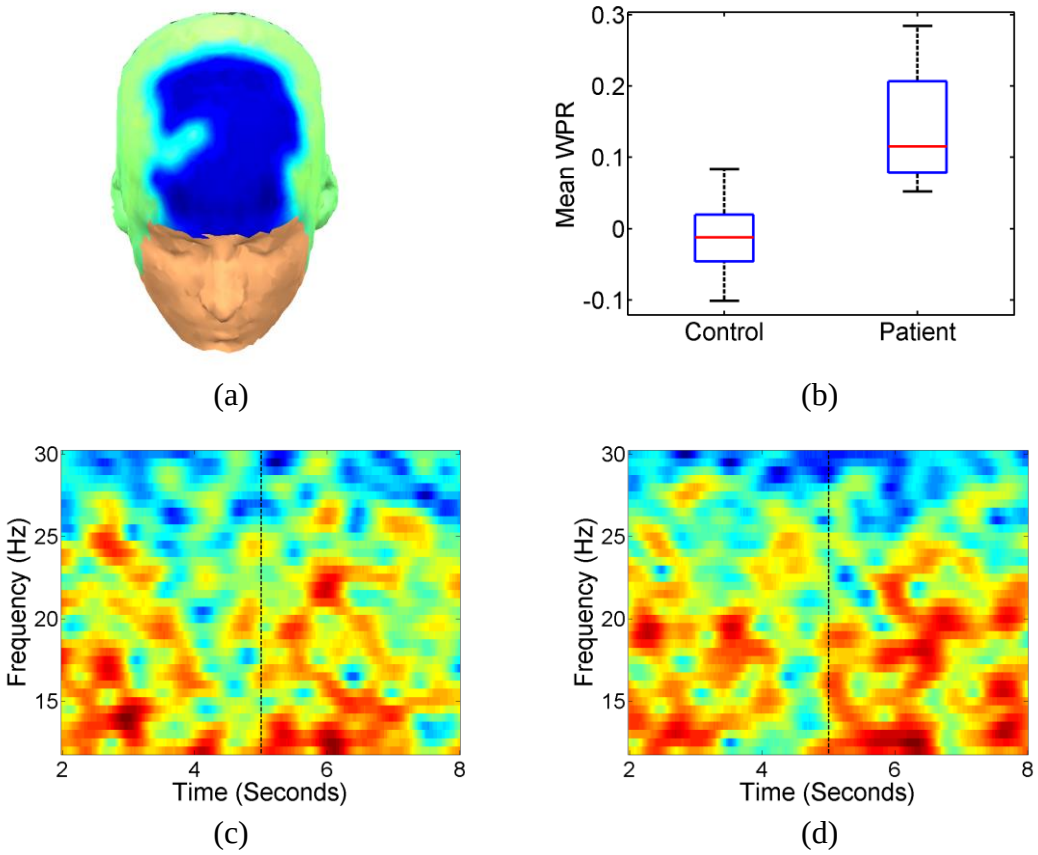

Figure 3.12: (a) Spatial locations (middle frontal area) that show significantly increased WPR (PO/EP, beta) in schizophrenia patients (average t-score = -3.115, corrected p-value = 0.013). (b) Boxplot of the mean WPR within cluster. (c) and (d) *beta* band spectrogram of MEG signal from a location in the cluster for control group and patient group, respectively.

Figure 3.10 shows a decreased WPR (BE/BA, *beta*) at the right occipital area in schizophrenia patients. From the spectrogram, we can observe that from the *baseline* to *base-to encode* phase of word processing, control group shows a significantly increased *beta* band power while opposite change is observed in patient group. Therefore the WPR (BE/BA, *beta*) is lower in patient group compared with that in control group. Figure 3.11 shows a significantly increased WPR (BE/BA, *beta*) at the left parietal area in schizophrenia patients. This is due to an increase of *beta* band power from *baseline* to *base-to encode* window in patient group, which is not shown in the control group. Figure

3.12 shows a significantly increased WPR (PO/PE, *beta*) at the middle frontal area in patient group. This is due to an increase of *beta* band power from *encode-to-post* window to *post-encoding* window in the patient group, as shown in the spectrogram. This increase is not observed in the control group.

3.3.3 Classification Results

Table 3.1 summarizes the 6 significant SPR clusters. The mean SPR within each cluster is used as a scalar feature and the mRMR algorithm is employed to select combinations of 1 to 6 SPR features for classification. Figure 3.13 shows the classification results using combinations of BPR and WPR features, with LDA, perceptron and linear SVM classifiers. The highest classification accuracy is achieved using 2 WPR and 1 BPR features combined for all three classifiers. The three features selected by the mRMR feature ranking algorithm are: F1: WPR (BE/BA, *beta*), F2: BPR (*theta/delta*, EN), and F3: WPR (PO/EP, *beta*)). The detailed classification accuracy, specificity and sensitivity using these three features are listed in Table 3.2. As comparisons, we also list the classification results using 3 BPR features alone and using 3 WPR features alone in Table 3.3 and Table 3.4, respectively. We can see that a combination of BPR and WPR features achieves better classification results than using same number of BPR or WPR features separately.

Table 3.1: List of the 6 Significant SPRs with the corresponding spatial locations, the mean *t*-score within cluster, and the corrected *p*-value

Feature	**Spacial Location**	***t*-score**	***p*-value**
BPR (*theta/delta*, EN)	middle-to-right frontal	-2.792	0.024
BPR (*alpha/delta*, BE)	middle parietal	-2.798	0.047
BPR (*beta/delta*, EN)	middle frontal-parietal	-2.770	0.046
WPR (BE/BA, *beta*)	right occipital	3.015	0.037
WPR (BE/BA, *beta*)	left parietal	-3.431	0.037
WPR (PO/EP, *beta*)	middle frontal	-3.115	0.013

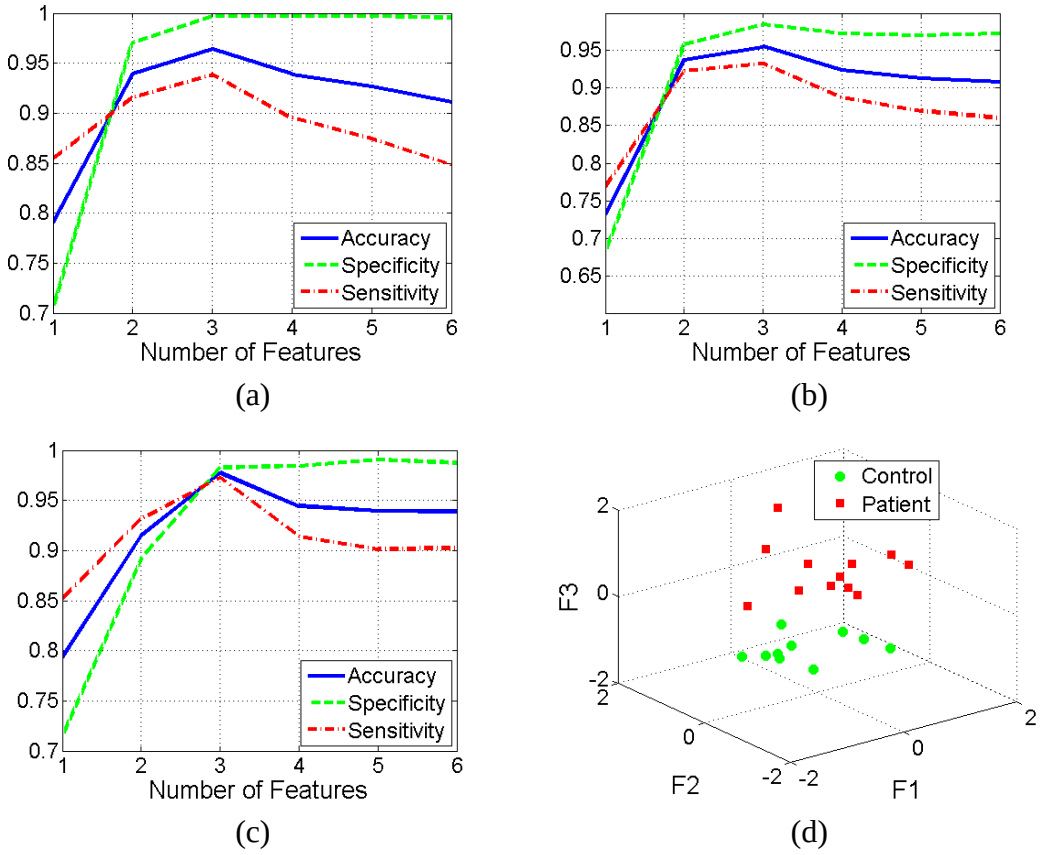

Figure 3.13: Classification results using combinations of BPR and WPR features selected by the mRMR algorithm for (a) LDA, (b) perceptron and (c) linear SVM classifiers. (d) Scatter plot of the 22 subjects in the 3D space formed by top 3 features selected by mRMR algorithm. F1: WPR (BE/BA, *beta*), F2: BPR (*theta/delta*, EN), F3: WPR (PO/EP, *beta*).

Table 3.2: Classification results using 1 BPR and 2 WPR features selected by the mRMR algorithm

Classifier	**Accuracy**	**Specificity**	**Sensitivity**
LDA	0.9637	0.9970	0.9387
Perceptron	0.9550	0.9850	0.9325
Linear SVM	0.9773	0.9830	0.9730

Table 3.3: Classification results using 3 BPR features

Classifier	**Accuracy**	**Specificity**	**Sensitivity**
LDA	0.8097	0.8473	0.7815
Perceptron	0.7354	0.8237	0.6693
Linear SVM	0.7883	0.8060	0.7750

Table 3.4: Classification results using 3 WPR features

Classifier	**Accuracy**	**Specificity**	**Sensitivity**
LDA	0.9251	0.9897	0.8768
Perceptron	0.8920	0.9420	0.8545
Linear SVM	0.9224	0.9883	0.8730

3.4 Discussions

Increasing evidence have suggested that abnormalities in the neural oscillatory activity are related to the impairments in various cognitive functions in schizophrenia [32]. In this chapter, we investigate abnormal neural oscillation patterns in schizophrenia using MEG data from a visual word processing task. Abnormal neural oscillations during cognitive tasks with language stimuli have been reported in both low and high frequency bands, at different brain areas, and during different time periods of language processing [18], [51], [52]. This motivates us to explore spectral-spatial-temporal MEG features to characterize neural oscillations in frequency, space and time dimensions.

Different from commonly used band power features which consider different frequency bands or time windows separately, we created two SPR feature sets which reflect the relationship of oscillation power between two frequency bands (BPR), and the oscillation power changes across two consecutive time windows of word processing (WPR). The reason for taking ratios of spectral power from two frequency bands is that

changes in the power of oscillations occurs at multiple frequencies simultaneously, and patients may show different power changes (increase or decrease) in different frequency bands compared with healthy controls. Taking ratio between one band that has an increased power and a band that has a decreased power, will further amplify the between-group difference, and thus improve the discriminating power of the feature. Similarly, the oscillation power is changing during different time periods of word processing. Taking the relative power changes across consecutive time windows can reveal the changes of oscillation power across different time periods of word processing, which cannot be learned by analyzing the power in one time window at a time.

After extracting the BPR and the WPR feature sets from 822 spatial locations, 5 time windows of word processing and 5 frequency bands, appropriate statistical tests are needed to identify features that show significant differences between groups. Due to large number of statistical comparisons (822 spatial locations) for each SPR feature, it is not possible to control the False Positive Rate (FPR) while maintaining a low False Negative Rate (FNR) by means of traditional Bonferroni correction or FDR control procedures. Therefore, we employed cluster-based non-parametric permutation test to identify significant SPRs, which controls the FPR unconditionally and solve the multiple comparison problem (MCP) in a simple way [16]. The rationale for cluster-based MCP control is based on the idea that MEG signal at a particular location is produced by physiological sources that also affect the MEG from nearby locations. Thus, if a sensor-specific null hypothesis is false for one sensor, then it is also false for the nearby sensors [16].

Note that the cluster-based statistic depends on the threshold that is used to select samples for clustering. It has been shown that the threshold does not affects the false alarm rate of the statistical test but affect the sensitivity of the test [16]. There is no definite criterion about how to choose this threshold to obtain maximum sensitivity for the unknown effect that is present in the data: for a weak and widespread effect, the threshold should be low, and for a strong and localized effect, the threshold should be high [16]. The threshold 2.5 we used in this study is a reasonable sample-specific *t*-value

threshold which corresponds to uncorrected *p*-value of about 0.025. In addition, we need to point out that the sensitivity and the FNR of the cluster-based nonparametric test is less than that of the uncorrected *p*-value approach which does not control the FDR. This is because multiple testing adjustments control false positives at the potential expense of more false negatives. For example, some features within the right-temporal cluster of the BPR (*alpha/delta*, BE) (Figure 3.4b) have very high sample-specific uncorrected *t*-scores. However, the cluster where these features are located did not survive from the MCP correction (marginally, corrected *p*-value = 0.06). The cluster-based nonparametric tests trade in some sensitivity for FPR control to deal with the MCP.

By applying the cluster based permutation test, we identified three BPR clusters which show significantly increased *theta/delta, alpha/delta* and *beta/delta* band power ratios during BE and EN periods of word processing, mainly at the frontal-parietal lobes. We also identified three significant WPR clusters which show altered *beta* band power changes when transferring from BA to BE window at the occipital and parietal lobes, and from EP to PO window at the frontal lobe. The spatial locations of the significant SPRs are not restricted to one specific cortical area but rather involved several different brain regions. This finding supports recent theory that the cognitive dysfunctions that characterize schizophrenia are not due to a circumscribed deficit but rather represent a distributed impairment involving many cortical areas and their connectivity [32].

According to our results, the most impaired regions are the frontal-parietal areas. Dysconnections of the frontal-parietal networks have been shown to contribute to cognitive impairment in schizophrenia [78]. Previous studies have also reported abnormalities in these areas in word processing and verbal working memory tasks [18], [51], [52]. The frequency distribution of the significant SPRs show that abnormal oscillations occur in all frequency bands, which is consistent with previous findings [53]. Furthermore, the time periods when these abnormalities occur include the baseline to encoding phase of word processing, as well as the post-encoding periods. These findings suggest failure of the neural systems to respond to task and problem to resume idle state after task, which is consistent with previous findings using event-related-

desynchronization/synchronization (ERD / ERS) features [18].

Finally, based on combination of two WPR and one BPR features, over 95% cross validation classification accuracy is achieved using three different linear classifiers separately. This result is better than using same number of BPR or WPR features separately, since WPR and BPR offer complementary information to each other. And the mRMR feature selection algorithm selects the optimal feature combinations that maximize the relevant information for classification while minimizing the redundant information among features [28]. A number of recent studies have also reported schizophrenia classification results using various types of EEG/MEG features and classification methods, as listed in Table 3.5. The promising classification result of this study suggests high discriminating power of the identified SPR features, as well as the effectiveness of the feature extraction and selection methods. The reader is, however, cautioned that the present classification results are based on a small sample size (12 patients vs. 10 controls) and have not been fully validated on large samples. Additionally, only linear classifiers are employed in this study in order to avoid overfitting the data with small sample size. More complex classification models can be designed in future studies with a larger sample size.

A limitation of the current study is that the spatial resolution of the significant SPRs is relatively low. This is due to the spatial resolution of the imaging modality as well as the cluster-based statistical testing procedure. Source localization techniques can be used in future studies to obtain better localization of the significant SPR features. Besides, as mentioned above, the results of the study are limited by small sample size. Therefore, the main purpose of the study is to provide new ways of extracting and identifying discriminating neural oscillation patterns. The findings should be viewed as exploratory and need to be validated in future study with larger samples.

Table 3.5: Summary of recent EEG/MEG classification studies for schizophrenia identification

Study	Task	Signal	Feature	Classifier	Nc/Np	Accuracy
Boostani et al. (2009) [62]	rest, eyes open	EEG	AR coefficients, band power, fractal dimension	boosted LDA	18/13	87.51%
Sabeti et al. (2009) [152]	rest, eyes open	EEG	entropy, complexity	LDA, Adaboost	20/20	89%, 91%
Sabeti et al. (2011) [65]	rest, eyes open	EEG	AR coefficients, band power, fractal dimension	LDA, Adaboost	20/20	85.9% 91.94%
Escudero et al. (2013) [63]	rest	MEG	frequency spectrum	logistic regression	17/15	71.3%
Ince et al. (2009) [52]	working memory	MEG	ERD/ERS	LDA	23/15	83.8%~ 94.6%
Xu et al. (2013) [18]	word processing	MEG	ERD/ERS	linear SVM	10/12	90.91%
Present work [19]	word processing	MEG	BPR, WPR	LDA perceptron linear SVM	10/12	96.37% 95.50% 97.73%

Nc/Np = number of controls/number of patients; AR = auto-regressive; ERD/ERS = event related desynchronization/synchronization; ANN = artificial neural network; LDA = linear discriminant analysis; SVM = support vector machine; AUC = area under curve

3.5 Conclusions

In summary, this study analyzed abnormal neural oscillatory activity in schizophrenia patients during visual word processing task. Two spectral-spatial-temporal feature sets: the BPR and the WPR were extracted from MEG recordings as quantitative features. Cluster-based nonparametric permutation tests identified 3 BPR clusters and 3 WPR clusters that show significant differences between schizophrenia patients and healthy

controls. Using 2 WPR features and 1 BPR feature combined, over 95% cross validation accuracy was achieved in classifying 12 patients from 10 controls, using LDA, perceptron and linear SVM classifiers separately. Future work will be directed towards exploring more effective features from neural oscillations using neuroimaging, signal processing and machine learning techniques, and to test the robustness of the proposed scheme on other datasets. More detailed feature analysis such as source localization will also be performed to find more accurate spatial locations of the key features.

Chapter 4

A Machine Learning based Schizophrenia Screening System

4.1 Introduction

The importance of biomarker discovery is that a computer-aided screening system can be built based on the quantitative and discriminative patterns to assist in clinical diagnosis of mental disorders. A computer-aided screening system generally contains four major parts: brain signal acquisition, feature extraction, feature selection (dimensionality reduction) and classification. First of all, brain signals are acquired from subjects during either resting or functional state. Different neuroimaging techniques can be applied for recording the brain activity, such as fMRI, EEG and MEG. Next, features are extracted from the recorded brain signals using signal processing approaches. Then, a feature ranking step can be applied to select a small subset of discriminating features. Finally, a machine learning based classifier is trained, which predicts a test subject into the corresponding group, healthy subject or psychiatric patient in the current context.

Recently, much research has been carried out under the above mentioned framework for automated screening of schizophrenia. In [79], independent components of fMRI data obtained during an auditory oddball task are used as features and projection pursuit is used for classification. In [80], the classification is based on resting-state EEG rhythms, with Artificial Neural Network (ANN) as classifier. In [81], high classification accuracy is achieved based on synchronous neural interactions derived from MEG in an eye fixation task, using Genetic Algorithm – Linear Discriminant Analysis (GA-LDA) as classifier. In [18], [52], Event-Related Desynchronization/Synchronization (ERD/ERS) derived from

averaged MEG signals in working memory and word processing tasks has been shown to be effective features for schizophrenia, with classification methods such as LDA and support vector machine (SVM).

In this chapter, we propose a machine learning based system for schizophrenia screening with two major contributions. First, we extract Power Spectral Density Ratio (PSDR) features across 5 frequency bands at 7 different brain locations from single-trial MEG recordings. This is different from the ERDS features described in Chapter 2 and the SPR features described in Chapter 3, which were extracted after averaging MEG signals from the same channel. In addition, the MEG signals we analyze here are acquired during a sentence processing task. Language disorder in schizophrenia has been reported at all levels, including sentence [39]. Compared with some other related works using brain activity during resting state [80] or an eye fixation task [84], the current study not only performs schizophrenia classification, but also looks into an impaired brain function associated with this illness. To the best of our knowledge, this specific feature set has not been previously investigated as biomarkers for schizophrenia diagnosis.

Secondly, we propose a two-stage feature ranking algorithm which combines F-score [23] filtering and Adaptive Boosting (Adaboost) algorithm [82]. This algorithm leads to improved classification accuracy with reduced number of features. A boosted model with linear decision stumps as base classifiers is employed to classify single MEG trials, and a majority voting scheme is followed to combine trial results and make final classification decisions. Experimental results demonstrate the effectiveness of the proposed system.

The organization of this chapter is as follows. Section 4.2 presents the subjects' information, the MEG data acquisition process, as well as the feature extraction, selection and classification methods. Section 4.3 presents the classification results and information about top features. Conclusion of this chapter is presented in Section 4.4.

4.2 Materials and Methods

4.2.1 Subjects and MEG Data Acquisition

13 healthy control subjects (12 male, 1 female) and 10 schizophrenic patients (10 male) participated in the study. The patient group did not differ significantly ($p<0.05$) from the control group with respect to age, personal or parental level of education, and premorbid overall and verbal intelligence. None of the control subjects had psychiatric or neurological disease or major medical illness. All the patients met the DSM-IV criteria [43] for schizophrenia or schizoaffective disorder. All the subjects were native English speakers and were right-handed. The experimental protocol was approved by the relative Institutional Review Boards (IRB). All the subjects gave written informed consent before entering the study.

Subjects were instructed to read silently sentence stimuli visually presented in the center of a monitor in front of the subjects. Each stimulus was a semantically and syntactically correct English sentence composed of 5 words (e.g., the boy ate the apple). Different stimuli were presented in different trials. The five elements in each stimulus were presented one at a time at a rate of one per second and there was a 10 seconds interval between two consecutive trials. This sentence processing task was part of a comprehensive procedure for language evaluation described in detail in previous work [38], [39].

MEG data were recorded during task performance from 248 axial gradiometers (Magnes 3600WH, 4-D Neuroimaging, San Diego, CA) in a 2-layer mu-metal magnetically shielded room (IMEDCO, Hagendorf, Switzerland), with a sampling rate of 1024Hz. Subjects were in a supine position with their head in the sensor helmet and on a head support to minimize movement. Ambient and distant biological magnetic noises were further reduced by using 23 SQUID reference channels, which were situated within the sensor and above the cortical channels. Blinks and heartbeats were removed and the epochs were visually inspected to remove residual artifact activity for each subject. Finally,

30 to 45 artifact corrected trials for each subject were down-sampled to 256Hz for further analysis.

4.2.2 Feature Extraction

We extract Power Spectral Density Ratio (PSDR) as feature to characterize the brain activity during sentence processing. These features are extracted from the MEG signals during stimuli presentation period, i.e., 5 seconds right after the onset of the first word of each sentence stimulus.

First, 4 electrodes are selected from each of the following 7 brain regions: left frontal (LF), right frontal (RF), left temporal (LT), right temporal (RT), left parietal (LP), right parietal (RP) and occipital (OC), as shown in Figure 4.1. The 4 channel MEG signals from the same region are averaged which results in 7 mean signals, one for each region. Next, the Power Spectral Density (PSD) of each mean signal is estimated using the Welch method [74] with Hamming window, length 256 and 50% overlap. Then, the Spectral Power values are extracted from the PSD in 5 frequency sub-bands: θ (4-8Hz), α (8-13Hz), β (13-30Hz), γ_1 (30-57Hz) and γ_2 (63-128Hz). The 60 ± 3Hz frequency components are not included to remove the 60Hz line noise.

$$spectral\ power_k = \sum_{f \in [f_{\min}^k, f_{\max}^k]} PSD(f), \quad k = 1, \ldots, 5 \tag{4.1}$$

where *k* is the index of the frequency band, $f_{\min}^k$ and $f_{\max}^k$ define the frequency range of the *k*th sub-band. Finally, the PSDR is defined as the ratio of the spectral power in two different frequency sub-bands (low band / high band): $\frac{\theta}{\alpha}$, $\frac{\theta}{\beta}$, $\frac{\theta}{\gamma_1}$, $\frac{\theta}{\gamma_2}$, $\frac{\alpha}{\beta}$, $\frac{\alpha}{\gamma_1}$, $\frac{\alpha}{\gamma_2}$, $\frac{\beta}{\gamma_1}$, $\frac{\beta}{\gamma_2}$, $\frac{\gamma_1}{\gamma_2}$. The 7 brain regions and 10 PSDR for each region lead to a total of 70 features for each trial.

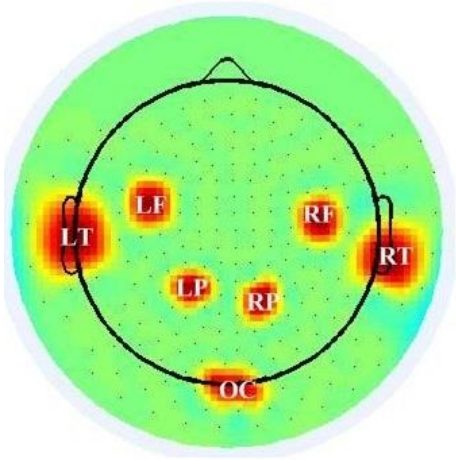

Figure 4.1: MEG sensor locations for the 7 regions: left frontal (LF), right frontal (RF), left temporal (LT), right temporal (RT), left parietal (LP), right parietal (RP) and occipital (OC)

4.2.3 Feature Ranking

The objective of feature selection for a computer-aided schizophrenia screening system is three-fold: 1) a reduced feature dimension can provide faster and more cost-effective predictors for classification; 2) the removal of irrelevant features may improve prediction performance; and 3) the selected top ranked features may inform about the abnormal spatial-spectral characteristics of brain activity in the patient group. In this chapter, a novel two-step feature selection algorithm which combines F-score filtering and Adaboost model [82] based feature ranking is proposed to select the top feature set for classification and analysis.

Step 1: F-score filtering

The basic idea of F-score is that a feature with a large between-group distance and a small within group variance has high F-score value. The higher the F-score, the more discriminating the feature is. The readers may refer to [9] for a detailed definition. We rank the 70 features based on their F-score values and keep top 35 for next-step feature ranking by Adaboost.

Step 2: Adaboost model based feature ranking

Adaboost is a boosting approach which combines *m* base classifiers (classifiers that are only marginally better than guessing) to produce a boosted classification model. A base classifier is called a "decision stump" which is a simple linear classifier based on one single feature. It is defined as:

$$b_j(x) = \begin{cases} -1 & if\ x_d < th \\ +1 & if\ x_d \geq th \end{cases} \tag{4.2}$$

where *d* indicates the feature based on which the split is created and *th* is a threshold value used to differentiate the two classes.

The Adaboost model training process follows an iterative process. Given n training sample $\mathbf{x}_i$ and class label $y_i \in \{-1,1\}$, first initialize the weight assigned to each sample as $\alpha_i = \frac{1}{n}$. Use the base classifier to fit the training samples with weights α_i and produce classification results $b_j(\mathbf{x}_i)$. Then, calculate the classification error err_j for the base classifier and its weight w_j:

$$err_j = \frac{\sum_{i=1}^{n} \alpha_i I(y_i \neq b_j(\mathbf{x}_i))}{\sum_{i=1}^{n} \alpha_i} \tag{4.3}$$

$$w_j = \log \frac{1 - err_j}{err_j} \tag{4.4}$$

Update the weights for each sample where misclassified samples were assigned larger weights.

$$\alpha_i = \alpha_i \exp(w_j I(y_i \neq b_j(\mathbf{x_i}))). \tag{4.5}$$

The above procedures are repeated *m* times with all base classifiers involved. Finally, a testing sample can be classified using the weighted majority vote of all base classifiers:

$$f(\mathbf{x}) = sign(\sum_{j=1}^{m} w_j b_j(\mathbf{x})). \tag{4.6}$$

The classifiers with lower training errors receive greater weight and therefore have more influence on the combination [13].

Adaboost model building process implicitly performs feature selection. During each iteration, the base classifier is built based on one single feature which is chosen to minimize the risk function. Based on this fact, a simple criterion for feature ranking is created: if a feature is selected earlier, we give it a higher ranking. During feature ranking process, we observe that some features are never selected in any of the base classifiers, which implies that they can be discarded when building the final classification model.

4.2.4 Classification

Top ranked features are used to rebuild an Adaboost model for classifying the test subject. For diagnosis purpose, a Leave-One-Out Cross Validation (LOO-CV) procedure [27] is strictly followed. Each time, all trials from one subject are left out for testing while all trials from other 22 subjects are used for feature selection and training the classifier model. This procedure is repeated until every subject has been used as a test subject exactly once.

Within each cross-validation (CV) fold, trials from the test subject are classified separately using the boosted classifier based on the top selected features. After all trials are labeled, a simple majority voting scheme is employed to decide the final class of the test subject. More specifically, if more than half of the trials vote control, the test subject is classified as a control, otherwise classified as a patient. Figure 4.2 shows the flow chart of the feature selection and classification procedures.

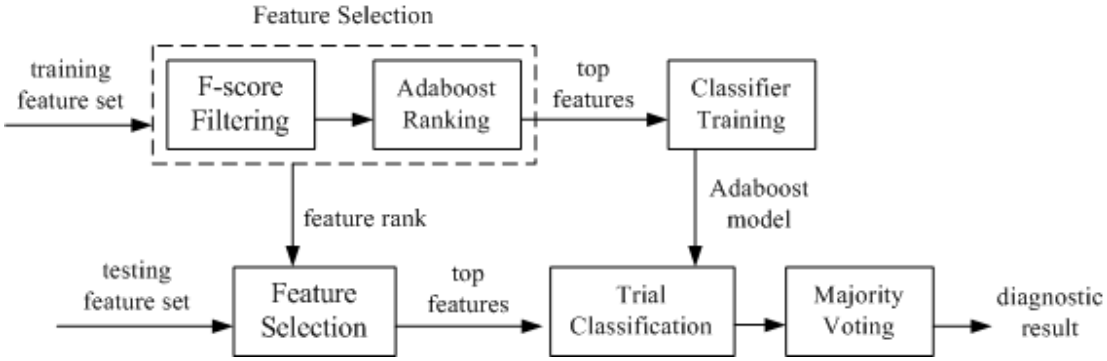

Figure 4.2: Flow chart of the feature selection and classification process

4.3 Experimental Results

4.3.1 Classification Result

In Figure 4.3, we show the LOO-CV classification accuracy (percentage of correctly diagnosed subjects) versus the number of top features. We compare the discriminating power of the top features selected by three feature selection methods: the proposed two-step feature ranking algorithm, ranking using only F-score and ranking using only Adaboost. In addition, the highest classification accuracy, specificity (true negative rate (TNR)) and sensitivity (true positive rate (TPR)) associated with these three feature selection methods and classification using all 70 features without feature selection are shown in Table 4.1.

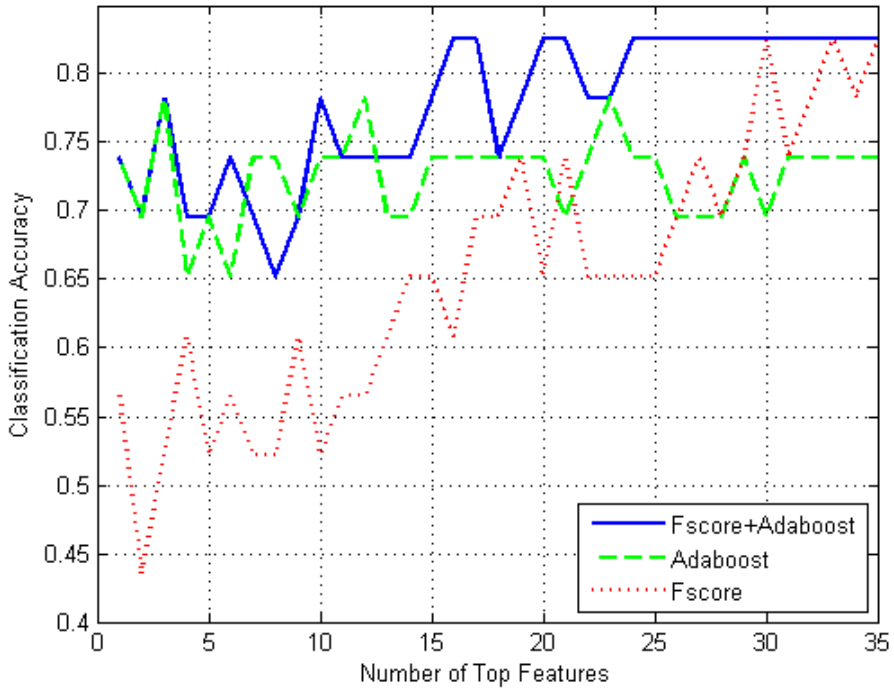

Figure 4.3: Classification accuracy vs. number of top features with 3 different feature section methods

Table 4.1: Classification results with different feature selection

Feature Selection Method	**# of Features**	**Accuracy**	**Specificity**	**Sensitivity**
No feature selection	70	73.91%	76.92%	70%
F-score only	30	82.61%	92.31%	70%
Adaboost only	3	78.26%	84.62%	70%
F-score + Adaboost	16	82.61%	92.31%	70%

82.61% classification accuracy is achieved using 16 top features ranked by the proposed 2-step feature selection algorithm. This result is higher than classification using all 70 features without dimensionality reduction (73.91%), or using features selected by only Adaboost (78.26%). The same accuracy can be achieved using top features ranked by F-score only, but using 30 features. These results demonstrate the effectiveness of the proposed 2-step feature selection algorithm, as well as the whole system for schizophrenia identification.

4.3.2 Feature Analysis

To explore the brain locations and frequency ranges that are most related to the discrimination between controls and patients, we show the region and frequency distributions of top features ranked by the proposed feature ranking algorithm in Figure 4.4. Note that feature selection is performed in each CV fold, which results in 23 different feature sets. We here pick out the top 3 features from each fold which forms a new top feature set containing a total of 12 features. We count the number of occurrences for each of these 12 features in the new set. Then, as each feature is associated with a specific brain region and a PSDR between two frequency sub-bands, we can obtain the number of occurrences of the 7 brain regions and the 10 PSDRs according to the number of occurrences of the 12 top features. From Figure 4.4, we can observe that the most discriminating features are the ratios between *alpha* (8-13Hz) and *beta* (13-30Hz) bands, and are selected from the right parietal, right temporal and right frontal regions.

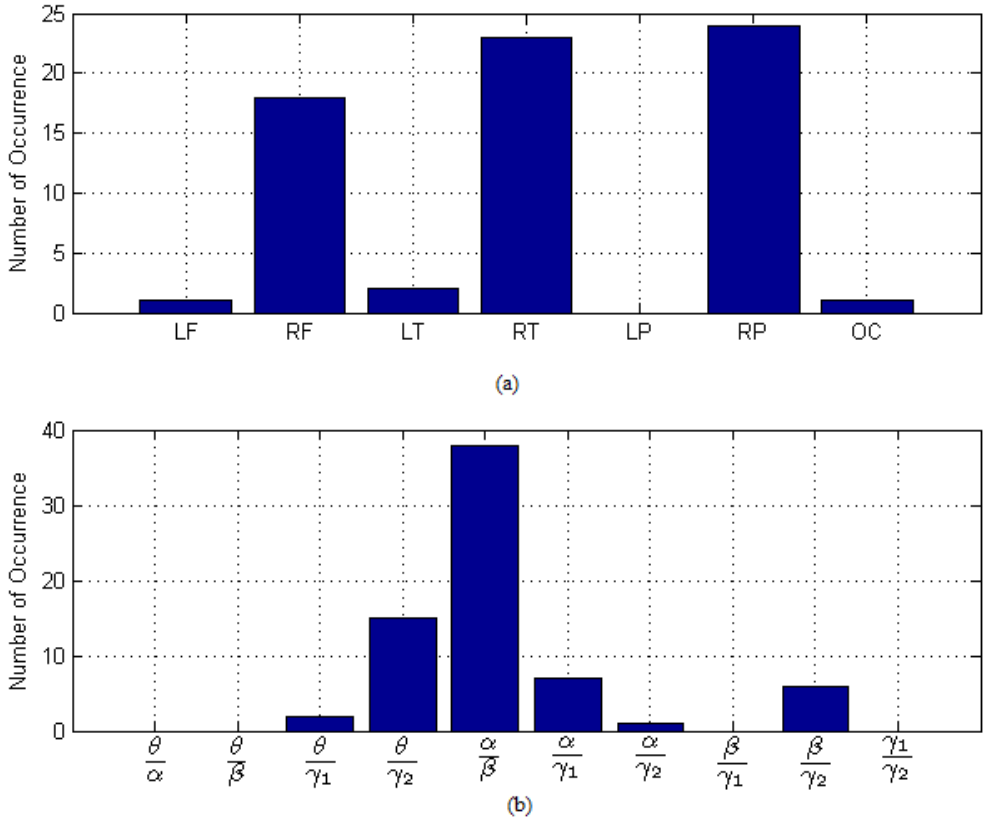

Figure 4.4: Number of occurrences of the 7 brain regions (a) and the 10 PSDRs (b) based on top 3 features selected in each CV fold

In Table 4.2, we list the 3 features with the highest number of occurrences and show their boxplots in Figure 4.5 (a, b, c). Patients show higher PSDR at the specific brain locations and frequency ranges indicated by these top features. At the 3D space formed by these 3 features (Figure 4.5d), we can observe a good separation between samples from the two groups. This indicates the potential of the PSDRs as a functional biomarker for differentiating brain activity of schizophrenia patients from healthy subjects during sentence processing.

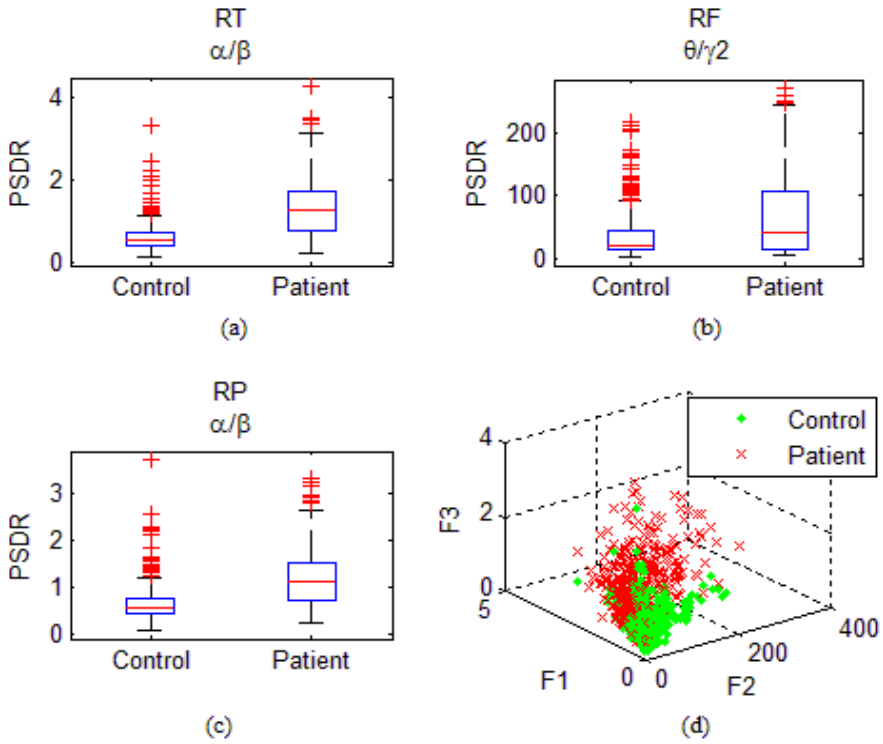

Figure 4.5: Box plot of the top 3 features with highest number of occurrence (a, b, c) and 3D scatter of trial data at the space formed by the 3 features (d)

Table 4.2: Top 3 features with highest number of occurrences

Rank	**Number of occurrence**	**Region**	**PSDR**
1	22	right temporal	α / β
2	13	right frontal	θ / γ_2
3	13	right parietal	α / β

4.4 Conclusions

We have designed a computer-aided system for schizophrenia screening. The graphical user interface of this system is shown in Figure 4.6. First of all, PSDR features in 7 brain regions and 5 frequency sub-bands are extracted from single-trial MEG during sentence

processing. They are explored as features for schizophrenia diagnosis. A two-step feature ranking algorithm is proposed to select the top discriminating features. A boosted classifier is built with linear decision stumps as base classifiers using Adaboost. An 82.61% overall classification accuracy has been achieved among 13 healthy controls and 10 schizophrenia patients following the LOO-CV procedure, which demonstrates the effectiveness of the proposed system. The frequency and space distributions of the top ranked features may provide insight into the abnormal neural activity associated with sentence-level language processing in schizophrenia. Future work will be directed towards improving the sensitivity of current results by employing more effective feature selection and classification approaches.

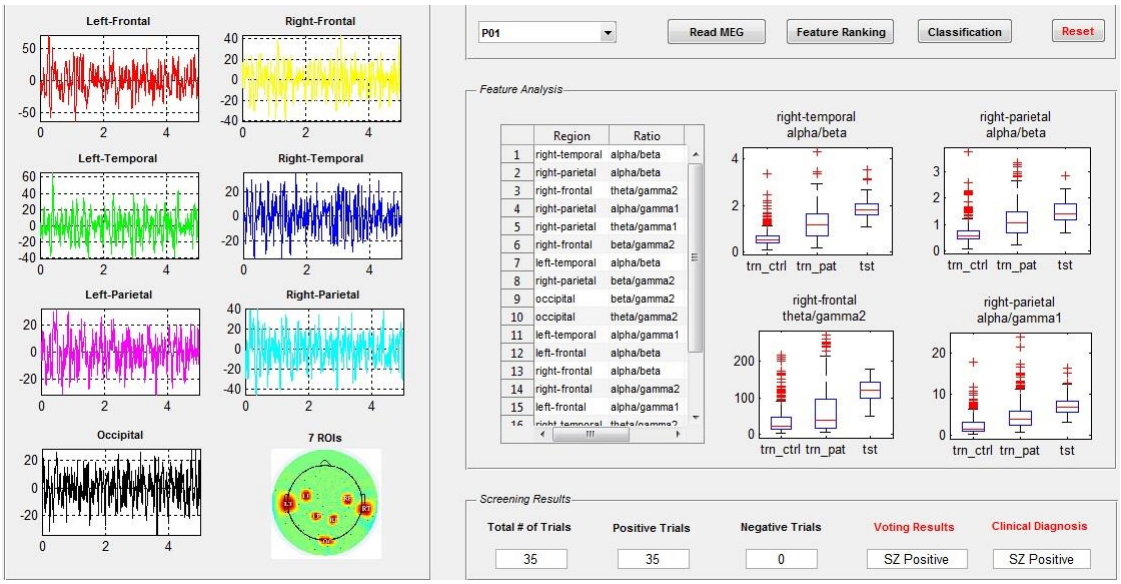

Figure 4.6: Graphical user interface of the computer-aided schizophrenia screening system. The system contains 4 major components: reading MEG data, feature extraction, feature ranking and analysis, and classification.

Chapter 5

Functional Brain Connectivity Patterns in BPD

5.1 Introduction

Borderline Personality Disorder (BPD) is a serious and complex mental illness characterized by a pervasive pattern of instability in affect regulation, interpersonal relationships, impulse control, and self-image. It affects about 1.6 percent of adults in the United States [12]. Currently, BPD is diagnosed by a mental health professional based on a thorough interview and a discussion about symptoms. No single medical test can diagnose the disease, and unfortunately, it is often underdiagnosed or misdiagnosed [83]. Furthermore, the neurobiology of BPD is poorly understood, and this limited knowledge hinders progress in developing novel, neuroscience-based treatments that target specific biological abnormalities. There is now increasing interest in identifying the structural and functional brain abnormalities associated with BPD, which could help in gaining knowledge about the underlying neurophysiological basis of the disease.

Neuroimaging techniques have recently become one of the most influential tools to detect structural and functional brain abnormalities in patients with BPD (See [84], [85] for recent neuroimaging findings in BPD). At the structural level, structural Magnetic Resonance Imaging (sMRI) studies have reported consistent findings of volume reduction in limbic and paralimbic areas [86], [87], prefrontal cortex [88], [89] and various regions of the temporal and parietal lobes [90], in patients with BPD compared with healthy subjects. At the functional level, a number of functional MRI (fMRI) studies have

revealed hyper-reactivity of limbic areas and hypo-activation of frontal brain areas in response to emotional stimuli, in patients with BPD [91].

Furthermore, in addition to examination of regional activation, a few recent fMRI studies have begun to focus on quantifying functional coupling between brain regions, primarily using seed-based correlation [92], [93] or independent component analysis (ICA) [94], [95]. Aberrant functional coupling between limbic and frontal areas during emotional challenge [96], [97], as well as altered resting-state functional connectivity in the default mode network and the executive network were observed in patients with BPD [98], [99]. Together these findings suggest disruptions of functional connectivity between brain regions in BPD.

In this chapter, we employ resting-state fMRI to investigate intrinsic functional brain connectivity patterns in patients with BPD. Resting-state fMRI has become an important tool for understanding the dynamic neural architecture in the absence of task-related activity in psychiatric patients [84]. Different from previous fMRI studies that used seed-based correlation or ICA analysis, a recently-developed Network-based Statistic (NBS) approach [17] is employed to identify altered functional connections in patients with BPD. NBS is a Family-Wise Error Rate (FWER) control approach specifically designed under the framework of a network model. It offers high sensitivity in detecting dysconnections in a network by exploiting the extent to which the abnormal connections are interconnected [17]. After identifying BPD-related abnormalities in functional brain network connectivity, we examine correlations between the connectivity measure and clinical symptom scores, and use the connectivity measure to distinguish BPD patients from healthy controls with a machine learning classifier.

The rest of this chapter is organized as follows. Section 5.2 describes the subjects' information and the fMRI data acquisition and preprocessing procedures. Section 5.3 presents the data analysis methods, including the construction of frequency-specific functional brain networks and the Network-based Statistics. Section 5.4 describes the identified subnetwork that shows significant connectivity difference between BPD patients

and healthy controls. Section 5.5 further discusses the findings and points out limitations of this work. Conclusions of this chapter are presented in Section 5.6.

5.2 Subjects and Data

5.2.1 Subjects

The participants in the current study were a sub-group of a larger, multi-site clinical trial study for adults with BPD [100] (overall PI: Black, site PI: Schulz). A subset of participants in the University of Minnesota site of the larger study were invited to participate in a supplemental neuroimaging study, in which they would undergo neuroimaging before and after the study treatment. A sample of 10 healthy controls was recruited to undergo diagnostic and neuroimaging procedures as a comparison group. The study was approved by the University of Minnesota Institutional Review Board. Interested and eligible participants completed a separate consent form for the neuroimaging portion of the study.

The participants of the present study included 20 patients with BPD aged 20 to 45, and 10 healthy controls aged 19 to 45. The two groups of subjects did not differ significantly in gender (p-value = 0.802) and age (p-value = 0.56). The subjects could not be entered if taking medication within last six weeks, so no subjects were taking any medication at the time of these scans. None of the control subjects met criteria for a psychiatric or neurological disease or had any major medical illnesses, either currently or historically. All the patients met the DSM-IV-TR criteria [43] for BPD diagnosis, and met the criteria for BPD using the Revised Diagnostic Interview for Borderlines [101].

A minimum score of 9 for total score on the Zanarini Rating Scale for Borderline Personality Disorder (ZAN-BPD) was used as a criterion [102]. In order to reduce confounds associated with diagnostic comorbidity, the patients included in this study did not have a history of any psychotic disorder, bipolar disorder, major depressive disorder with psychotic features, obsessive-compulsive disorder, generalized anxiety disorder,

social phobia, or post-traumatic stress disorder. The Structured Clinical Interview for DSM-IV (SCID) [103] was used to screen for the presence of co-morbid Axis I psychiatric disorders. Among the selected patients, five had history of non-psychotic major depressive disorder and four had history of substance abuse. However, these diagnoses were in remission at the time of the current study. Table 5.1 lists the demographic information of the subjects, including three commonly used clinical measures for BPD diagnosis: the ZAN-BPD [102] interview (ZAN-BPD_I) and self-rating (ZAN-BPD_SR), and the symptom checklist 90 (SCL90) [104].

Table 5.1: Demographic information of the subjects

	Control	**BPD**
Gender (male / female)	4 / 6	7 / 13
Age (mean years ± SD)	27 ± 7.5	29 ± 7.3
ZAN-BPD_I total score (mean ± SD)	N/A	18.65 ± 4.32
ZAN-BPD_SR total score (mean ± SD)	N/A	16 ± 6.4
SCL90 total score (mean ± SD)	N/A	113.55 ± 59

SD: standard deviation; SCL90: symptom checklist 90
ZAN-BPD_I: Zanarini Rating Scale for Borderline Personality Disorder, interview score;
ZAN-BPD_SR: Zanarini Rating Scale for Borderline Personality Disorder, self-rating score

5.2.2 fMRI Data Acquisition and Pre-processing

Structural and functional MRI data were acquired at the University of Minnesota's Center for Magnetic Resonance Research, using a Siemens 3T TIM Trio scanner. Whole-brain anatomical images were acquired using a T1-weighted high-resolution magnetization prepared gradient echo (MPRAGE) sequence: TR = 2530ms; TE = 3.65ms; TI = 1100ms; flip angle = 7 degrees; FOV = 256; voxel size 1x1x1 mm; GRAPPA = 2. The 6-minute resting-state fMRI scans were obtained using 180 contiguous echo planar imaging (EPI) whole brain volumes with TR = 2000ms; FOV = 220; voxel size = 3.43x3.43x4 mm; 34 slices. Subjects were instructed to relax, try not to think about anything in particular, and remain awake with their eyes closed. Physiological data, including heart rate and

respiration, were acquired during the fMRI scan. A field map was collected with compatible acquisition parameters as the resting -state fMRI data. The scanning protocol also included diffusion imaging and magnetic resonance spectroscopy (which was collected between the T1 scan and the resting-state fMRI scan) and two task fMRI experiments, which were collected after the resting-state fMRI scan. The current paper focuses only on the baseline resting-state fMRI and T1 data.

FreeSurfer [105] was used to process the T1 data including brain extraction and parcellation of data into a standard set of anatomically-based regions of white and grey matter. FreeSurfer output was visually inspected on a slice-by-slice basis and manually corrected when deemed necessary. The fMRI data was registered to the T1 data using *bbregister*. For the resting fMRI data, a de-noising procedure was applied incorporating RETROICOR [106] to remove the physiological noises caused by cardiac and respiratory cycles as well as any linear trends. The fMRI processing was mainly conducted using tools from the FMRIB software library [107]. Initial processing included brain extraction and motion correction. Correction for magnetic field inhomogeneity-induced geometric distortion was conducted using the field map. FreeSurfer-generated regions of interest (ROIs) for lateral ventricles (cerebrospinal fluid; CSF) and white matter (WM) were aligned to the fMRI data. We performed a regression of each other voxel's time series on eight nuisance variables: WM time series, CSF time series, and the six motion parameters. Data scrubbing was performed following guidelines proposed by previous research [108], excluding any volume with a DVARS value exceeding 8 and/or a framewise dependent value exceeding 0.5, along with the previous volume and the two following volumes. The deleted volumes were then linearly interpolated by averaging previous and following undeleted volumes to make sure all time series have the same number of time points. Finally, mean fMRI time series from 82 cortical and subcortical areas (41 for each hemisphere) were obtained for connectivity analysis. Table 5.2 lists the selected region of interests (ROIs).

Table 5.2: List of FreeSurfer-based regions-of-interest (ROIs)

No.	Region of Interest (ROI)	Abbr.	No.	Region of Interest (ROI)	Abbr.
1	Banks superior temporal sulcus	BANK	22	Posterior-cingulate cortex	PCC
2	Caudal anterior-cingulate cortex	CauACC	23	Precentral gyrus	PreCG
3	Caudal middle frontal gyrus	CauMFG	24	Precuneus cortex	PCUN
4	Cuneus cortex	CUN	25	Rostral anterior cingulate cortex	RosACC
5	Entorhinal cortex	EC	26	Rostral middle frontal gyrus	RosMFG
6	Fusiform gyrus	FFG	27	Superior frontal gyrus	SFG
7	Inferior parietal cortex	IPC	28	Superior parietal cortex	SPC
8	Inferior temporal gyrus	ITG	29	Superior temporal gyrus	STG
9	Isthmus– cingulate cortex	ICC	30	Supramarginal gyrus	SMG
10	Lateral occipital cortex	LatOC	31	Frontal pole	FPO
11	Lateral orbital frontal cortex	LatOFC	32	Temporal pole	TPO
12	Lingual gyrus	LING	33	Transverse temporal cortex	TTC
13	Medial orbital frontal cortex	MedOFC	34	Insula	INS
14	Middle temporal gyrus	MTG	35	Thalamus	THA
15	Parahippocampal gyrus	PHG	36	Caudate	CAU
16	Paracentral lobule	PCL	37	Putamen	PUT
17	Pars opercularis	ParsOPE	38	Pallidum	PAL
18	Pars orbitalis	ParsORB	39	Hippocampus	HIP
19	Pars triangularis	ParsTRI	40	Amygdala	AMYG
20	Pericalcarine cortex	PCAL	41	Accumbens	ACCU
21	Postcentral gyrus	PoCG			

5.3 Data Analysis

5.3.1 Construction of Functional Brain Networks

Observations from previous studies have shown that the strength of functional connectivity between brain regions is not equal at all frequencies [109], and the sensitivity of different frequencies to disease-related alternations of brain connectivity is different [110], [111]. In this study, we applied a 4-level stationary discrete wavelet transform (SDWT) [112], [113] with 'db4' wavelet, to filter the fMRI signal into different frequency bands. The SDWT overcomes the lack of translation-invariance of traditional decimated wavelet transform by removing the down-samplers and up-samplers, and up-sampling the filter coefficients.

The filtered signal at each wavelet scale approximately corresponds to frequency ranges of 0.12~0.25Hz (scale 1), 0.06~0.12Hz (scale 2), 0.03~0.06Hz (scale 3), and 0.015~0.03Hz (scale 4), respectively. We next estimated the functional connectivity by computing the Pearson linear correlation coefficients between all possible pairs of fMRI time series at each wavelet scale separately for each subject. At each wavelet scale, a frequency-specific 82-by-82 undirected connectivity graph was constructed based on the 3321 correlation coefficients. Figure 5.1 shows the mean connectivity matrix in 0.03-0.06Hz frequency range for control group and patients group.

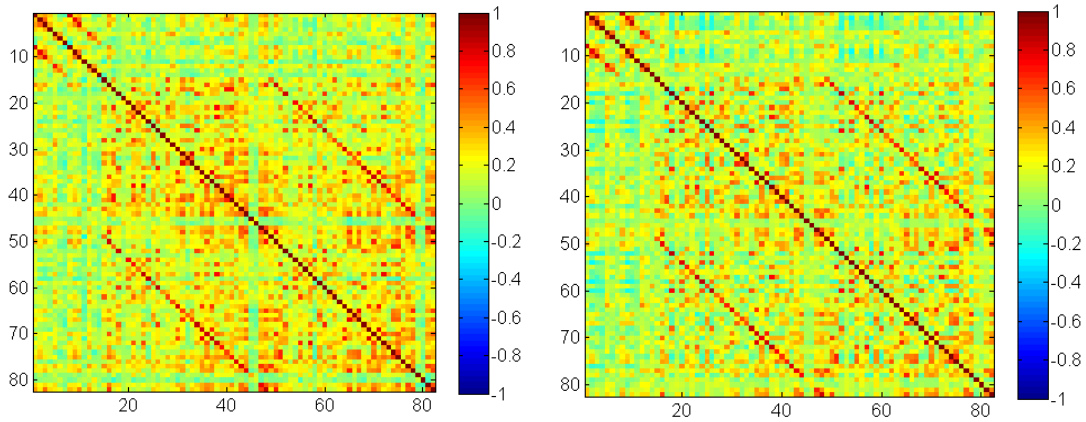

(a) (b)

Figure 5.1: Mean connectivity matrix for control group (a) and patients group (b) based on Pearson correlation of resting-state fMRI signals from 82 brain regions in 0.03~0.06 Hz frequency range.

5.3.2 Network-based Statistics

The functional brain networks consisted of 3321 edges resulting from the pair-wise correlation of the 82 brain regions. To identify altered functional connectivity between nodes in the network, we employed the NBS approach, which is based on the idea of cluster-based thresholding of statistical maps [17]. It is a method of controlling the FWER in the context of a large number of univariate tests are computed at each connection of the network. Specifically, we first computed the *t*-score for each pairwise connection separately. Then, we applied a primary threshold to the *t*-scores to select a set of supra-threshold links with *t*-score exceeding the threshold. The thresholding procedure was performed for links with positive and negative *t*-scores separately to identify connected components where subjects with BPD had either significantly higher or significantly lower connectivity strength compared to healthy controls (directed hypothesis). Connections comprising this set represented potential candidates for which the null hypothesis could be rejected.

Note that the primary threshold is a user-determined parameter in NBS framework, and there is no definite rules guiding how to choose it. Conservative thresholds, e.g., *p*-value < 0.001, characterize strong, topologically focal differences, while liberal thresholds, e.g., *p*-value < 0.05, characterize subtle yet topologically extended differences [17]. Therefore, we tested different primary thresholds in this study. Fortunately, although the choice of primary threshold affects the sensitivity of the method, the control of FWER is guaranteed irrespective of the threshold choice [17].

Next, we identified any connected components in the set of supra-threshold links and stored the size of each component. To determine the significance of each component, we performed non-parametric permutation test. For each permutation, all subjects were randomly reallocated into control group and patient group. The *t*-score was computed independently for each link, and the size of the largest connected component (LCC) within the supra-threshold links was recorded. This procedure was repeated 10,000 times to obtain the null distribution of the pseudo size of the connected component. Finally, the

corrected *p*-value for a true component of size M was determined by the proportion of permutations with size of LCC larger than M.

5.3.3 Classification

The mean connectivity in the significant connected component identified by NBS approach was used as a scalar feature, based on which a linear discriminant analysis (LDA) classifier [76] was trained to distinguish BPD patients from healthy controls. A leave-one-out cross-validation (LOO-CV) procedure was followed during classification. Each time, 29 subjects were used for classifier training, while the other one subject was used for testing the classification accuracy. The procedure was repeated 30 times until each subject has been used as a testing sample. This machine learning based classification scheme provides a framework for evaluating the discriminating power of connectivity measure in BPD identification.

5.3.4 Clinical Correlates of Connectivity Patterns

We examined clinical correlates of the mean connectivity in the significant sub-network identified by NBS approach. The clinical scores include: 1) ZAN-BPD (interview and self-rating) total score and 13 sub-scores (anger, moodiness, chronic emptiness, identity problems, suspiciousness, fear of abandonment, suicidal thoughts and self-injurious behaviors (STSIB), impulsivity, relationship problems, sum affect, sum cognitive, sum impulsivity, and sum relationships) [102]; 2) SCL90 total score and 13 sub-scores: somatization, obsessive-compulsive symptoms (OCS), interpersonal sensitivity, depression, anxiety, hostility, phobic anxiety, paranoid ideation, psychoticism, additional items, general severity index (GSI), positive symptom distress index (PSDI), positive symptom total (PST) [104].

Linear partial correlation coefficient was used to examine the relationships between connectivity measure and the symptoms of the disease, while controlling the gender and age effects. In addition to age and gender, depressive symptoms measured by the

Montgomery–Åsberg Depression Rating Scale (MADRS) [114] were also partialed out, considering the high comorbidity with depression in major depressive disorder.

5.4 Experimental Results

5.4.1 Altered Functional Brain Connectivity in BPD

The NBS approach identified an interconnected subnetwork in 0.03~0.06Hz frequency band, which showed significantly (corrected p-value < 0.05) lower connectivity strength in BPD patients. No connected components showed significantly increased connectivity in patients in this frequency range, and no significant between-group difference were found in other three frequency bands.

The size of the connected subnetwork in 0.03~0.06Hz that showed lower connectivity in BPD is related to the choice of primary threshold in NBS test, as discussed in Section 5.3.2. Table 5.3 lists the number of nodes and links in the subnetwork with different primary thresholds. Generally speaking, the size of the subnetwork increases when the primary threshold is lower, since more candidate links are admitted to the supra-threshold link set. However, significant results cannot always be found with arbitrary choice of primary threshold. If the threshold is chosen too low, e.g., $p = 0.05$, large components can arise in the permuted data as a matter of chance and thereby reduce the sensitivity. In contrast, if the threshold is set too high, e.g., $p = 0.001$, connections comprising the effect of interest may not be admitted to the set of supra-threshold links [17].

Table 5.3: Number of nodes and links, and the corrected *p*-value of the connected subnetwork in 0.03~0.06Hz that shows significantly lower connectivity strength in BPD patients, under different primary threshold in NBS tests.

primary threshold	**No. of nodes**	**No. of links**	**corrected *p*-value**
$t = 1.75$, $p \approx 0.05$	no significant result		
$t = 2.05$, $p \approx 0.025$	68	205	0.048
$t = 2.5$, $p \approx 0.01$	49	87	0.0408
$t = 2.75$, $p \approx 0.005$	40	57	0.0298
$t = 3.05$, $p \approx 0.0025$	26	26	0.0304
$t = 3.4$, $p \approx 0.001$	no significant result		

Figure 5.2 shows the subnetwork obtained with primary threshold *t*-score = 2.75, and the boxplot of the mean connectivity in this subnetwork. The 40 nodes in the subnetwork covered frontal, temporal, parietal, occipital and limbic lobes. The 57 links were mainly long-distance connections that connected brain regions located at different lobes, e.g., between medial occipital lobe and cingulate cortex, between medial occipital lobe and frontal lobe, and between medial occipital lobe and inferior parietal lobe. All the connections within the subnetwork showed lower values of correlation coefficient in BPD patients as compared with in healthy controls.

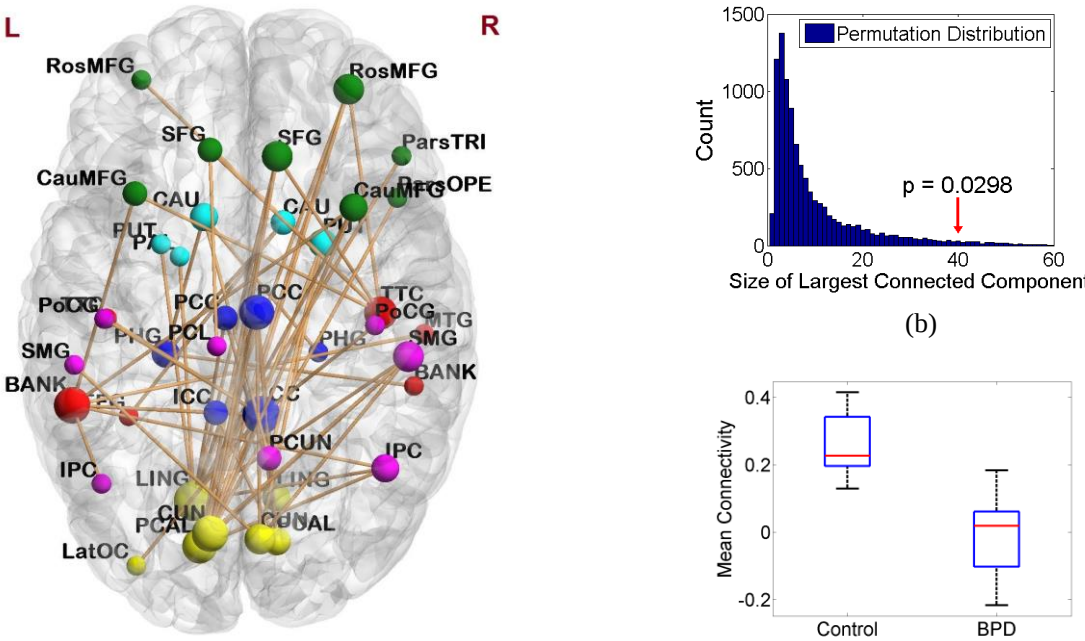

(a) (b) (c)

Figure 5.2: (a) The connected subnetwork in 0.03~0.06Hz frequency band that showed significantly lower connectivity strength in BPD patients identified by NBS approach with primary threshold *t*-score = 2.75. Size of the nodes corresponds to the number of dysconnections to the nodes, and the color of the nodes represents different lobes: yellow: occipital, red: temporal, purple: parietal, green: frontal, blue: limbic, light blue: basal ganglia. (b) Permutation distribution of the size of largest connected component in NBS tests. (c) Boxplot of the mean connectivity strength in the subnetwork.

5.4.2 Classification Result

Given the significant between-group difference of the connectivity strength in the identified subnetwork, we tested whether the mean connectivity in this network could be used as a feature to distinguish BPD patients from healthy controls using a simple LDA classifier. Following cross-validation procedure, the LDA classifier achieves 90% accuracy (90% specificity and 90% sensitivity) in classifying 20 BPD patients from 10 healthy controls. Two patients and one control were misclassified. This promising

classification performance further demonstrates the high between-group difference of the identified connectivity pattern.

5.4.3 Clinical Correlates of the Connectivity Pattern

The mean connectivity in the subnetwork identified by NBS method with primary threshold *t*-score = 2.75 is negatively ($p < 0.05$, uncorrected) correlated with a variety of SCL90 and ZANBPD symptom scores (Table 5.4, Table 5.5, Figure 5.3). As shown in Section 5.4.1, the mean connectivity in the NBS network is significantly lower in patients compared with in controls. The lower the mean connectivity, the higher these correlated clinical scores. These results together suggest that altered functional brain network connectivity may contribute to specific symptoms of the disease.

Table 5.4: Correlations between SCL90 symptom scores and the mean connectivity in the subnetwork that showed significantly lower connectivity strength in BPD identified by NBS method (primary threshold t-score > 2.75). Age, gender and MADRS score were partialed out.

SCL90	**correlation**	**p-value**
Obsessive-Compulsive Symptoms (OCS)	-0.6293	0.0068
Depression	-0.6235	0.0075
Hostility	-0.5164	0.0338
General Severity Index (GSI)	-0.5064	0.0389
Total Score	-0.5024	0.0391

Table 5.5: Correlations of ZAN-BPD Interview and Self-raging scores with the mean connectivity in the subnetwork that showed significantly lower connectivity strength in BPD identified by NBS method (primary threshold t-score > 2.75). Age, gender and MADRS score were partialed out.

ZAN-BPD_I	**correlation**	**p-value**	**ZAN-BPD_SR**	**correlation**	**p-value**
Affect	-0.6218	0.0077	Mood	-0.6238	0.0075
Total	-0.5961	0.0116	Affect	-0.5064	0.0381
Impulsivity	-0.5369	0.0263	Relationships	-0.4951	0.0433
Relationships	-0.4865	0.0477			

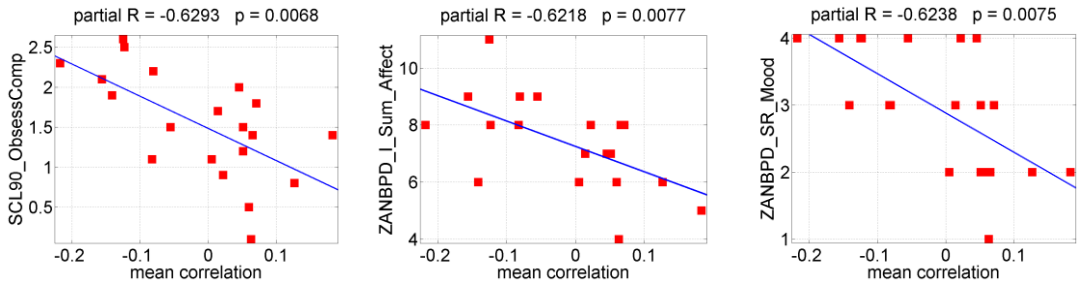

(a) (b) (c)

Figure 5.3: Scatter plot of the mean connectivity of the connected subnetwork that showed lower connectivity in BPD identified by NBS method with primary threshold t-score = 2.75, against several clinical scores. The mean connectivity of NBS network is negatively correlated with: (a) SCL90 obsessive-compulsive symptoms, (b) ZANBPD_I sum affect, and (c) ZANBPD_SR mood scores.

5.5 Discussions

5.5.1 BPD-Related Alteration of Functional Brain Connectivity

Functional brain networks are constructed by pair-wise connections between all nodes in the network. We explore BPD-related functional connectivity patterns in the resting-state networks. By applying the NBS approach, we identified an interconnected subnetwork in the 0.03~0.06 Hz frequency band that showed significantly lower connectivity strength in

patients with BPD compared to healthy controls. The nodes in the subnetwork were mainly located at the medial occipital lobe (lingual gyrus, cuneus cortex and pericalcarine cortex), cingulate cortex (posterior and isthmus divisions), temporal lobe (banks of superior temporal sulcus, transverse temporal cortex), prefrontal lobe (middle frontal gyrus, superior frontal gyrus), inferior parietal lobe (inferior parietal cortex, supramarginal gyrus), and basal ganglia areas (caudate, putamen).

The links in the subnetwork were mainly long-distance connections between regions located at different lobes. The most number of dysconnections existed between the medial occipital lobe and cingulate cortex, medial occipital lobe and prefrontal cortices, medial occipital lobe and inferior parietal lobe, temporal lobe and prefrontal cortices, as well as between temporal lobe and inferior parietal lobe. Note that the posterior cingulate cortex, medial prefrontal cortex, inferior parietal lobe, superior temporal gyrus and cuneus are considered as core regions in the default mode network (DMN) [98], [115], [116]. A recent fMRI study using ICA-based correlation analysis also reported altered resting-state functional connectivity in DMN regions, including decreased connectivity in the cuneus, inferior parietal lobule and middle temporal cortex, in patients with BPD compared with healthy controls [98]. Together these findings suggest alterations in long-distance functional connections between regions associated with self-referential processes in patients with BPD. Previous fMRI study using ICA approach also reported increased resting-state functional connectivity in the left frontal-parietal cortices and left insula in DMN [98], which was not identified in this study. A possible reason is that the NBS approach focuses on dysconnections that form an interconnected structure, rather than isolated links. Therefore, some supra-thresholded links with increased connectivity in patients may not be considered significant if they could not form a connected component with enough size. Nevertheless, the finding of impaired long-distance connectivity in this study may add new insight into previous connectivity analysis for BPD that used ICA or seed-based correlation analysis [98], [99], [117].

5.5.2 Methodological Considerations

To identify functional dysconnections in BPD from more than 3000 links in the whole brain network, it is necessary to control the FWER due to multiple comparisons. In this study, we employed the recently-developed NBS approach, instead of traditional FDR controlling procedure that calculates the test statistic and corresponding *p*-value independently for each link [118]. The main consideration here is two-fold.

On the one hand, NBS approach aims at detecting altered functional connectivity that exists in a connected component, rather than disconnected abnormal links. In our functional brain network analysis, brain regions are defined to be interconnected. Therefore, focal dysconnections can propagate along interconnected pathways, which is suitable for NBS method to detect [17]. Such interconnected structure of dysconnected links was not explored in previous seed-based or ICA-based correlation analysis with traditional FDR controls [98], [99], [117].

On the other hand, compared with traditional FDR control procedure, the NBS approach offers greater sensitivity in network (graph) analysis. Under traditional FDR control, to survive from thousands of multiple comparisons, the link-based *p*-values need to be very small, less than 1e-5 in this study, which leads to high False Negative Rates. However, under the NBS framework, the link-based *p*-value only needs to be significant enough to pass a primary threshold to be admitted into the supra-threshold link set. Connections can be declared significant if they form an interconnected component.

Despite these advantages of NBS in identifying significant connections, there are limitations of this approach. First, when using NBS, a rather arbitrary choice must be made to select the primary threshold used to define the set of supra-threshold links. In Figure 5.4, we show the connected subnetwork in 0.03~0.06Hz frequency band that showed significantly lower connectivity in BPD patients identified by NBS approach with primary threshold t-score = 3.05. This subnetwork contains 26 nodes and 26 links, which is a smaller size compared with the subnetwork with primary threshold *t*-score = 2.75 (Figure 5.2, Table 5.3). Second, the localizing power of NBS is coarser than

traditional link-based approach. Third, only a connected component can be declared significant, but the individual connections comprising the component cannot [17].

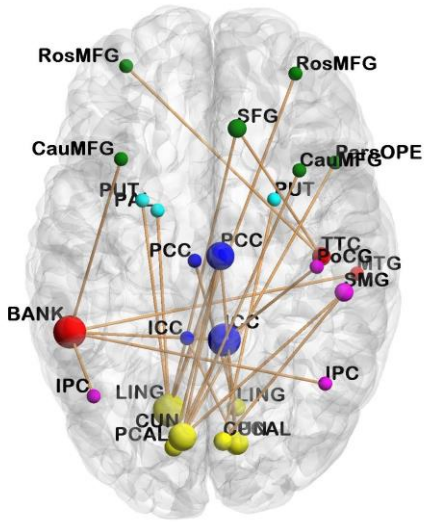

Figure 5.4: The connected subnetwork in 0.03~0.06Hz frequency band that showed significantly lower connectivity in BPD patients identified by NBS approach with primary threshold t-score = 3.05. Size of the nodes corresponds to the number of dysconnections to the nodes, and the color of the nodes represents different lobes: yellow: occipital, red: temporal, purple: parietal, green: frontal, blue: limbic, light blue: basal ganglia.

5.6 Conclusions

In this chapter, we explore functional brain connectivity patterns in BPD, using resting-state fMRI data. Frequency-specific functional brain networks were constructed by correlating filtered fMRI time series from 82 cortical and subcortical areas. A recently developed NBS approach was employed to identify significant connectivity changes in patient group. By applying the NBS approach, we identified an interconnected subnetwork in the 0.03~0.06Hz frequency band that showed significantly lower connectivity strength in patients with BPD compared to controls. The mean connectivity in this subnetwork showed negative correlations with several key clinical symptom scores and achieved 90% prediction accuracy in BPD classification. The high accuracy

indicates the potential of the resting-state functional connectivity pattern as biomarker for BPD identification. A limitation of this study is the small sample size. Therefore, the results of this work need to be viewed as preliminary and need to be tested in future studies. Future work will be directed towards complex network analysis of the topological structure of the functional brain networks in BPD patients.

Chapter 6

Functional Brain Network Topology Patterns in BPD

6.1 Introduction

Although brain dysfunctions have been previously shown in patients with BPD, prior studies have largely been based on specific regions of interest, i.e., regional functional activations and between-area functional connections. However, whether BPD affects the topological organizations in the whole-brain functional networks has not yet been investigated. For example, how different brain areas are integrated and segregated for communication and specialized processing remains unknown. Given the complexity of BPD psychopathology, knowledge about possible disruptions of topological properties in functional brain networks could potentially advance current understanding of brain dysfunctions associated with the disease, and suggest new avenues for developing neuroscience-based treatment. However, to the best of our knowledge, very few studies have reported results on the global and local topological properties of functional brain networks in patients with BPD.

Recent research has shown that graph-theory based complex network analysis provides a powerful framework for examining the topological properties of brain networks, where nodes represent brain regions and edges represent the anatomical or functional connections between brain regions [119]–[122]. Network analysis of structural and functional connectivity data for healthy people have revealed important "*small-world*" properties in the healthy brain, characterized by high *clustering coefficient* and

low mean *path length* [109], [123]–[126]. High clustering is associated with high local efficiency of information transfer for specialized processing (functional segregation); while short mean path length indicates high global efficiency of parallel information transfer for distributed processing (functional integration) [119]. Knowledge about these informative topological properties could advance a comprehensive understanding of how brain networks are organized and how they generate complex dynamics. Furthermore, comparisons of network topology between healthy subjects and psychiatric patients have reported significant abnormalities of brain connectivity networks in patients with schizophrenia [127]–[130], Alzheimer's disease [110], [131]–[133] and depression [134], [135]. These promising results motivate us to explore BPD-related patterns of topological properties in the functional brain networks, which have not been investigated in previous studies.

In this chapter, we perform graph-theory based network analysis on resting-state fMRI data to explore the topological structure in whole-brain functional networks in 20 adults with BPD versus 10 matched healthy controls. The central hypothesis is that BPD disrupts the global and regional topological organizations in functional brain networks. To test this hypothesis, we first constructed frequency-specific connectivity graphs by correlating wavelet filtered fMRI signals from different brain regions. Next, we quantified network topological properties (small-world properties, network efficiency, and nodal centrality) and compared these properties between groups. We computed a variety of global and nodal network measures, including the clustering coefficient, characteristic path length, small-worldness, local efficiency, global efficiency and degree [121]. Non-parametric permutation tests were used for group comparisons. After identifying BPD-related abnormalities in functional brain network topology, we further examined the correlations between the significant network measures and clinical symptom scores, and used the network features to distinguish BPD patients from healthy controls with a machine learning classifier. The correlation between the key topology patterns and the network connectivity pattern we identified in Chapter 5 will also be discussed. The framework of the study design is shown in Figure 6.1.

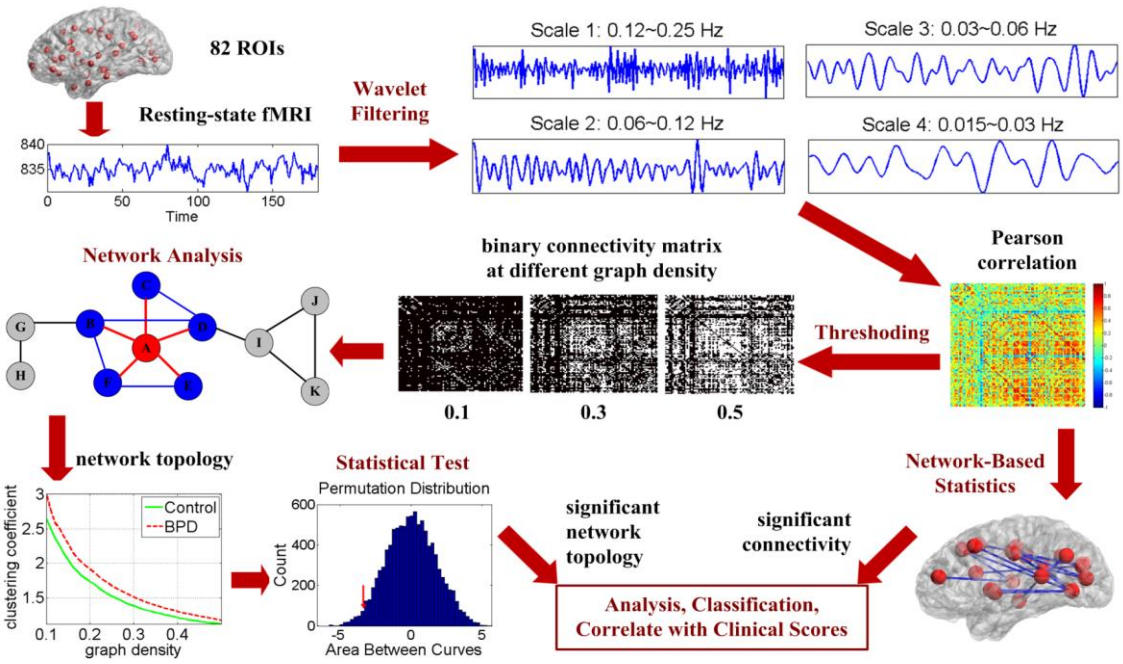

Figure 6.1: Framework of the study design

The rest of this chapter is organized as follows. In Section 6.2, the graph-based functional brain network analysis procedures are presented, including details of computing network topology measures. Section 6.3 presents the data analysis results, which describes altered network topology patterns in BPD. Discussions and conclusions are presented in Section 6.4 and Section 6.5, respectively.

6.2 Graph Analysis of Brain Network Topology

6.2.1 Subjects and Data

In this study, we use the same resting-state fMRI data as described in Chapter 5. See Section 5.2 for details about subjects' information and fMRI data acquisition and pre-processing steps.

6.2.2 Thresholding

First of all, as described in Section 5.3.1, we construct frequency-specific functional brain networks by computing the Pearson linear correlation coefficients between all possible pairs of fMRI time series at each wavelet scale separately for each subject. At each wavelet scale, a frequency-specific 82-by-82 undirected connectivity graph is constructed based on the 3321 correlation coefficients.

To analyze the topological properties of brain networks using graph measures, the original weighted connectivity matrices were first converted to binary matrices by applying a set of thresholds to the correlation coefficients, such that if the correlation coefficient between two ROIs exceeded a threshold, a connection was defined between the two ROIs. To ensure that the graph measures were mathematically comparable across subjects, subject-specific thresholds were used so that the connectivity graphs from different subjects had the same graph density, i.e., the ratio of the number of existing links over the number of all possible links in the graph. Instead of studying network properties at a single graph density, we thresholded the connectivity matrices repeatedly over a wide range of graph densities between 0.1 and 0.5, with an increment of 0.01. A graph density of 0.1, for example, means keeping the top 10% of the highest correlation coefficients. This specific graph density range is chosen to ensure that the graph is sparse and the small-world properties are estimable [136].

6.2.3 Network Topology Measures

The thresholding procedure reduced the weighted connectivity matrix to a set of binary graphs, each of which we characterized using a variety of graph-based measures. See [121] for review of complex network measures of brain connectivity. In this study, we specifically investigated the small-world properties [136], network efficiency [137], and nodal centrality.

Small-World Properties

Prior functional neuroimaging studies have shown that functional connectivity networks in a healthy brain can be modeled as a "small-world" system [109], [125], [126]. A small-world system has the ability for specialized processing to occur within densely interconnected groups of brain regions (highly segregated), and also has the ability to combine specialized information from distributed brain regions (highly integrated) [121].

The small-world properties of a network are mainly quantified by the *clustering coefficient* and the *characteristic path length* of the network. The clustering coefficient c_i of a node i is defined as the ratio of the number of existing links and the number of all possible links among the direct neighbors of the node. High value of c_i implies that most of the neighbors of the node are also neighbors of each other. The clustering coefficient of the entire network C_{net} is the mean c_i of all nodes in the network. This global measure quantifies the cliquishness of a network.

The characteristic path length L_{net} quantifies the integration ability of a network. The original definition of L_{net} is the average distance between any two nodes in the network. To avoid the disconnection problem, i.e., the distance between some nodes is infinity, the harmonic mean version of the original definition is used in this study: $L_{net} = \frac{N(N-1)}{\sum_{i \neq j \in G} d_{ij}^{-1}}$, where G is the set of all nodes in the network, N is the total number of nodes in the network, and d_{ij} is the shortest path length between node i and node j [138].

To diagnose the small-world properties, C_{net} and L_{net} are normalized by the same metrics estimated from random networks with same number of nodes, edges and degree distribution. The normalized network clustering coefficient is defined as

$C_{norm} = \frac{C_{net}}{C_{rand}}$, while the normalized characteristic path length is defined as $L_{norm} = \frac{L_{net}}{L_{rand}}$. A small-world network is expected to have high local clustering and low mean path length, i.e., $C_{norm} > 1$ and $L_{norm} \approx 1$. Finally, a scalar summary of the *small-worldness* of the network is defined as: $S = \frac{C_{norm}}{L_{norm}}$ [139]. A small-world network has $S > 1$.

Network Efficiency

Network efficiency measures how efficiently information is exchanged over the network. Small-world networks are seen as systems that are both globally and locally efficient [137]. The global efficiency of the network is defined as the mean inverse shortest path length between all node pairs in the network: $E_{glob} = \frac{\sum_{i \neq j \in G} d_{ij}^{-1}}{N(N-1)}$. The local efficiency of node i is defined in the subgraph of the direct neighbors of node i: $e_{loc,i} = \frac{\Sigma_{j,h \in G_i} [d_{jh}(G_i)]^{-1}}{k_i(k_i - 1)}$, where G_i is the set of nodes that are directly connected to node i, $d_{jh}(G_i)$ is the shortest path length between node j and node h that contains only direct neighbors of node i, and k_i is the number of direct neighbors of node i. The local efficiency of the whole network is the mean $e_{loc,i}$ of all nodes in the network: $E_{loc} = \frac{1}{N} \sum_{i \in G} e_{loc,i}$. This metric plays a similar role to the clustering coefficient, and it shows how efficient the communication is between the direct neighbors of node i when node i is removed [137].

Nodal Centrality

Degree k_i was used to measure the centrality of a node. It is defined as the number of links connected to the node. Hub regions often interact with many other regions in the network and thus have high centrality.

6.2.4 Statistical Testing

The set of graph metric values computed at each single graph density form a functional curve, where the x-axis represents the graph density and the y-axis represents the graph metric value. To determine whether there exists significant between-group difference in the graph measures, we performed non-parametric permutation tests on the area under the graph-metric-versus-graph-density curve of each graph metric. The area under curve (AUC) is computed by integrating the curve over specified density range, which serves as a scalar feature for the topological property of the network. We first calculated the difference D between the mean AUC of control group and patient group. To test the null hypothesis that the observed group difference (BPD > control or BPD < control, directed hypothesis) could occur by chance, we then randomly reassigned the group identity (healthy control or BPD patient) for each subject without replacement. The difference D' between the mean AUC of the two pseudo groups were recorded for each permutation. This procedure was repeated 10,000 times, and the *p*-value of the group difference was defined as the number of times that D' is greater or less than D, divided by 10,000, depending on the sign of D.

In addition to the *p*-value, the effect size and the power for each significant graph measure (*p*-value < 0.05) were also analyzed. The effect size of the group mean difference is measured using Cohen's *d* with pooled standard deviation [140]. The statistical power of the test with significance level 0.05 is calculated based on the group means, standard deviations and sample sizes, using online power calculator [141]. To note, before group comparison of each graph measure using permutation tests, the confounding factors of gender and age were removed by multiple linear regression

(independent variables: gender and age; dependent variables: the AUC of each graph measure).

6.2.5 Clinical Correlates and Classification

We examined clinical correlates of the AUC of the significant network topology measures. In addition, the AUC of the significant topology measures was used as a scalar feature to distinguish BPD patients from healthy controls using a linear discriminant analysis (LDA) classifier [76]. Detailed descriptions of the clinical symptom scores and the cross validation classification procedures are described in Section 5.3.3 and Section 5.3.4, respectively.

6.3 Experimental Results

6.3.1 Altered Small-World Properties and Network Efficiency

Figure 6.2 shows the group mean curve of 6 global network measures versus graph densities in 4 frequency bands. Figure 6.2a-c show the 3 small-world measures, including the normalized characteristic path, normalized clustering coefficient, and small-worldness. The functional brain networks of both healthy controls and BPD patients showed small-world properties within density range 0.1 to 0.5: $C_{norm} > 1$, $L_{norm} \approx 1$, and $S > 1$. Furthermore, the small-worldness and the clustered structure were more salient in low frequency bands compared to in high frequency bands: scale 4 (0.015~0.3Hz) ≈ scale 3 (0.03~0.6Hz) > scale 2 (0.06~0.12Hz) > scale 1 (0.12~0.25Hz), for S and C_{norm}. This finding is consistent with previous fMRI study that examined the small-world properties in multiple wavelet scales in healthy brain [109].

Figure 6.2d-e shows the normalized global and local network efficiency across graph densities. From Figure 6.2d, we can observe that the E_{glob} is slightly lower than one, and it approaches one as graph density increases. This is consistent with the findings that the

L_{norm} is slightly greater than one but approaches one as graph density increases, since both the characteristic path length and the global efficiency are based on the average distance between nodes in the network. The shorter the characteristic path length is, the higher the global efficiency. The values of L_{norm} and E_{glob} together show that resting-state functional brain networks have slightly longer but almost equal path length as degree-preserved random networks with same number of nodes and edges. From Figure 6.2e, we can observe that the values of E_{loc} in scale 4 $\approx$ E_{loc} in scale 3 > E_{loc} in scale 2 > E_{loc} in scale 1 >1 across graph densities. This is consistent with the C_{norm} measure, since both C_{norm} and E_{loc} measure the local cliquishness, i.e., clustered structure, in a network.

Besides the small-world properties and network efficiency, another simple but important graph measure, the size of largest connected component (LCC) is shown in Figure 6.2f. We can observe that as the graph density decreases, a few nodes become disconnected, and that the number of disconnected nodes is larger in high frequency bands compared with in low frequency bands.

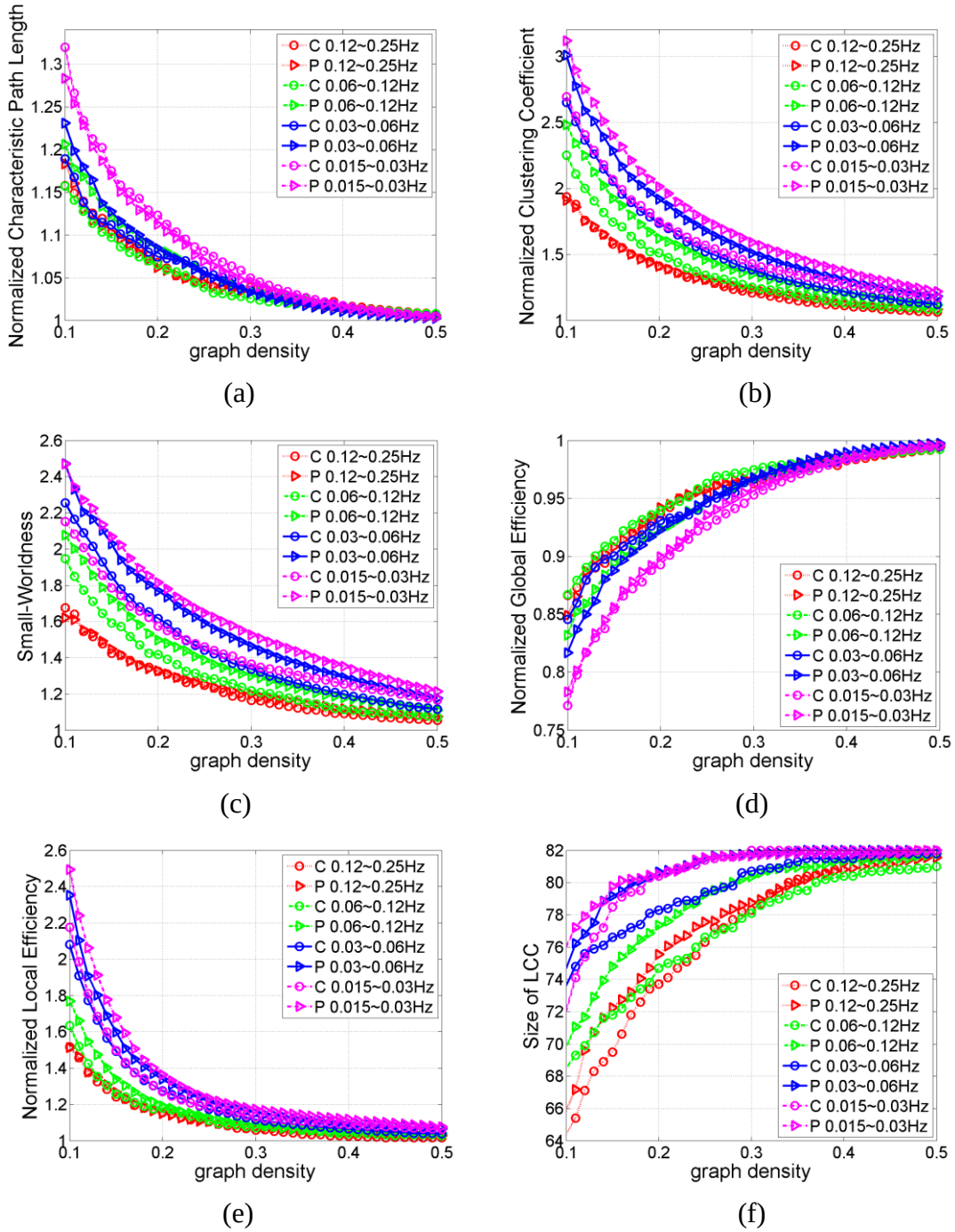

Figure 6.2: Mean global network measures across graph densities in 4 frequency bands for control group (C) and BPD group (P): (a) normalized characteristic path length, (b) normalized clustering coefficient, (c) small-worldness, (d) normalized global efficiency, (e) normalized local efficiency, (f) size of largest connected component.

We next analyzed the between-group difference of the graph measures by non-parametric permutation test of the AUC, as described in Section 6.2.4. Although all graph measures defined in this study can deal with disconnected nodes, the AUC for group comparison was computed within density range 0.2 to 0.5, instead of the whole small-world regime 0.1 to 0.5. This density range was chosen so that the network was connected with just a few disconnected nodes. Permutation test results showed that the between-group difference of network topology are most significant in the 0.03~0.06Hz frequency range. At this frequency band, BPD patients showed significantly (*p*-value < 0.05) larger size of LCC, C_{norm}, S, and L_{norm}, compared with healthy controls. The boxplots of these significant features are shown in Figure 6.3, and the corresponding *p*-value, effect size and power are listed in Table 6.1. BPD patients also showed higher C_{norm} in 0.015~0.03Hz network, and greater size of LCC and C_{norm} in the 0.06~0.12Hz frequency bands. No between-group differences were found in the 0.12~0.25Hz frequency band.

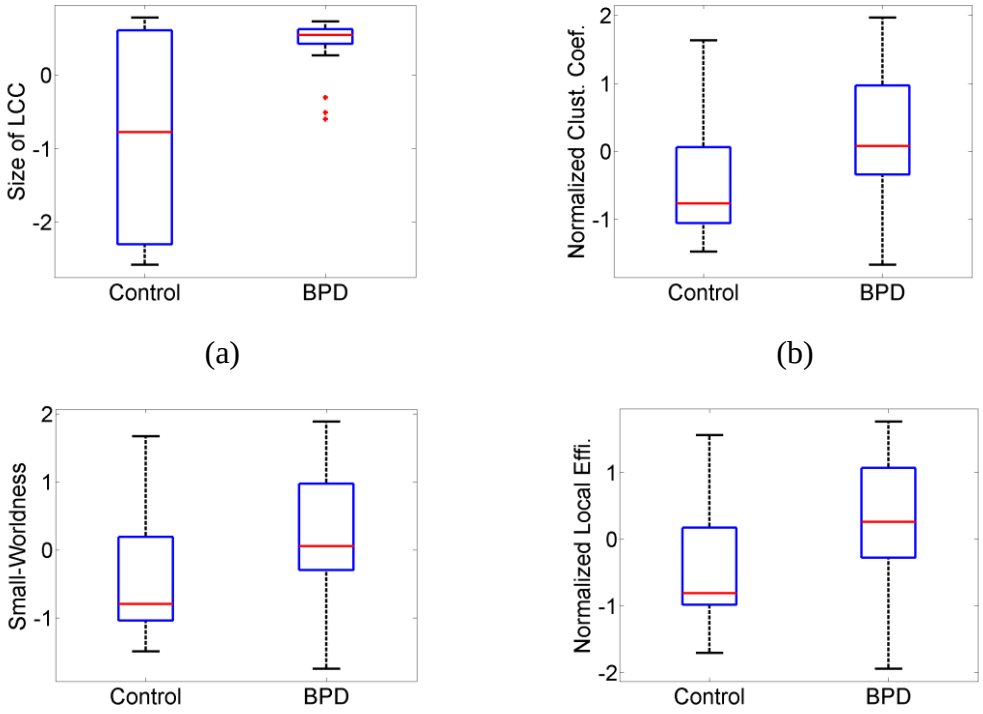

Figure 6.3: Boxplots of global network measures in 0.03~0.06Hz that show significant between-group difference (*p*-value <0.05): (a) size of the largest connected component (LCC), (b) normalized clustering coefficient, (c) small-worldness, (d) normalized local efficiency.

Table 6.1: *P*-value, effect size, and power of global network measures in 0.03~0.06Hz frequency band that show significant between-group difference (*p*-value<0.05)

graph measures	***p*-value**	**effect size**	**power**
size of largest connected component	0.0008	1.2049	0.8295
normalized clustering coefficient	0.0285	0.7550	0.3918
small-worldness	0.0308	0.7263	0.3789
normalized local efficiency	0.0193	0.8155	0.4415

The increased size of LCC, C_{norm}, S and L_{norm} together suggests increased local cliquishness (clustering) in the intrinsic functional brain networks in patients with BPD versus healthy controls. Table 6.2 and Table 6.3 list the brain regions that showed increased nodal clustering coefficient and increased nodal local efficiency in BPD patients, respectively. These regions are mainly located within the limbic system, which is associated with various structural and functional abnormalities in BPD, as reported by previous neuroimaging studies.

Table 6.2: Brain regions that show significantly (permutation *p*-value < 0.05, uncorrected) higher clustering coefficient in patients in 0.03~0.06Hz network

brain regions	***p*-value**	**effect size**	**power**
right temporal pole	0.0004	1.3596	0.8711
left temporal pole	0.0029	1.1129	0.7154
right pallidum	0.0053	1.0349	0.6681
left entorhinal	0.0197	0.7489	0.4612
right amygdala	0.0257	0.7588	0.4356
left amygdala	0.0432	0.6246	0.3525

Table 6.3: Brain regions that show significantly (permutation p-value < 0.05, uncorrected) higher local efficiency in patients in 0.03~0.06Hz network

brain regions	***p*-value**	**effect size**	**power**
right temporal pole	0.0004	1.3161	0.8753
left temporal pole	0.0022	1.0724	0.7329
right pallidum	0.0087	0.9511	0.6102
left entorhinal	0.0161	0.7832	0.5106
right amygdala	0.0137	0.8187	0.5351
left amygdala	0.0251	0.7237	0.4515

It is noteworthy that a simple measure, the size of largest connected component (LCC), showed the most significant between-group difference compared with other discriminating global network measures (Figure 6.3). Previous fMRI study of resting-state functional brain connectivity has suggested that the size of LCC is a non-trivial predictor of a wide variety of other graph metrics, and is sensitive to disease state [130]. In Figure 6.4, we show the scatter plot of the size of LCC against other discriminating graph measures in the 0.03~0.06Hz band network, including the normalized clustering coefficient, normalized local efficiency and small-worldness. Correlation analysis (age and gender partialed out) shows that the size of LCC is positively correlated with all these three significant graph measures.

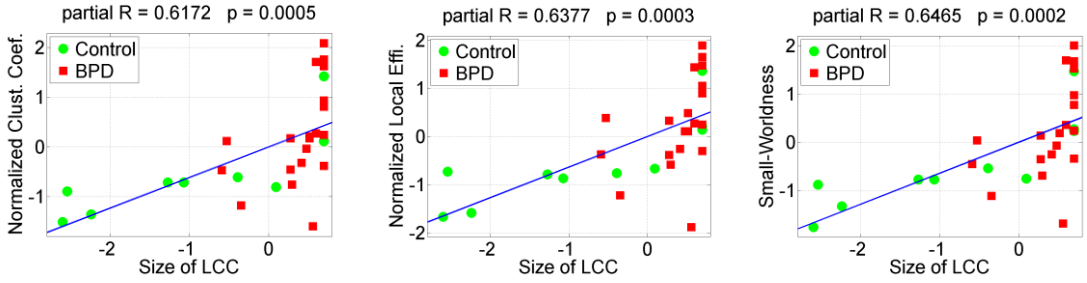

(a) (b) (c)

Figure 6.4: Scatter plot of the size of largest connected component (LCC) in 0.03~0.06Hz band network against other significant graph measures. The size of LCC is positively correlated with (a) the normalized clustering coefficient, r =0.6172, p = 5e-4, (b) normalized local efficiency, r = 0.6377, p = 3e-4 and (c) small-world-ness, r = 0.6465, p = 2e-4.

After identifying the significant network topology patterns, we further investigated the relationship between these topology patterns with the altered functional brain connectivity pattern we identified in chapter 5. Figure 6.5 shows the scatter plot of the mean connectivity in the subnetwork with primary threshold t-score = 2.75, against the size of LCC, normalized clustering coefficient, normalized local efficiency and small-worldness. Mean connectivity of the subnetwork was negatively correlated with all these four graph topology measures (age and gender partialed out).

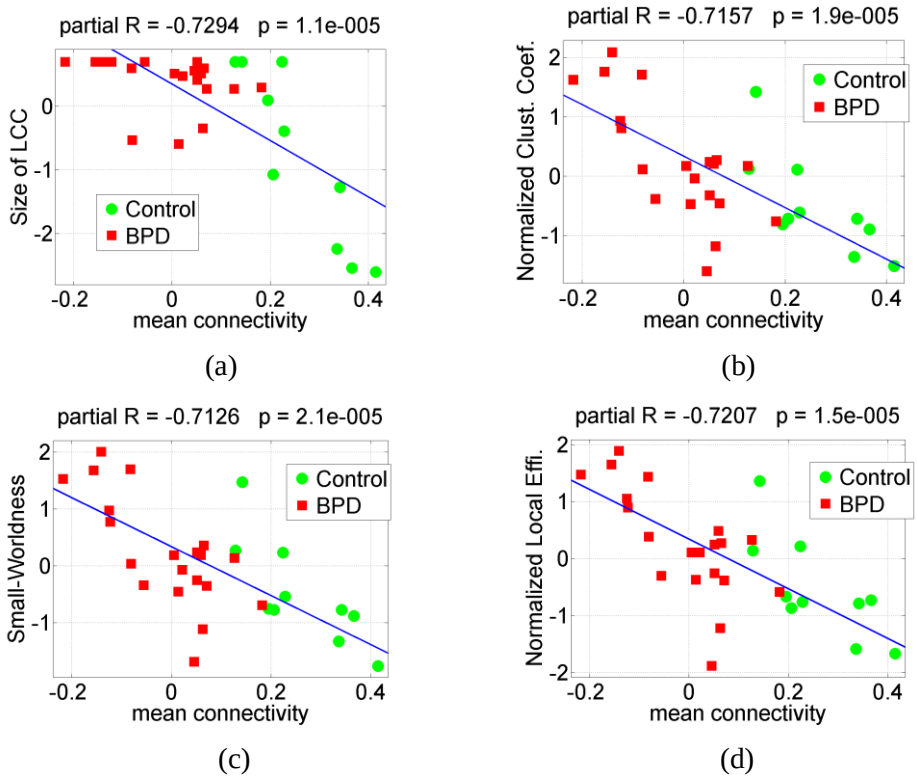

Figure 6.5: Scatter plot of the mean connectivity of the subnetwork that showed lower connectivity strength in BPD identified by NBS method (primary threshold t-score = 2.75), against the four significant graph topology measures. The mean connectivity of the subnetwork shows significant negative correlations with: (a) size of largest connected component, r = -0.7294, p = 1.1e-6, (b) the normalized clustering coefficient, r = -0.7157, p = 1.9e-5, (c) small-worldness, r = -0.7126, p = 2.1e-5, and (d) normalized local efficiency, r = -0.7207, p = 1.5e-5.

6.3.2 Altered Nodal Centrality

Figure 6.6 shows the degree distribution of brain regions in the 0.03~0.06Hz functional brain network, and marks the brain regions with significantly increased or decreased degree (permutation p-value < 0.05, uncorrected) in BPD patients. The permutation p-values of the discriminating regions are listed in Table 6.4 and Table 6.5. BPD patients showed increased degree at several brain regions with low degree, and decreased degree at several brain regions with high degree, indicating reduced number of connections to

hub nodes and increased number of connections to non-hub nodes in the resting-state functional brain network. Furthermore, we observed that brain areas that show increased clustering coefficient and local efficiency (Table 6.2 and Table 6.3), including the bilateral temporal poles, bilateral amygdala, pallidum and entorhinal cortex, are nodes with low degree. This finding suggests that the increased local cliquishness in BPD is located at the non-hub nodes in the functional brain networks.

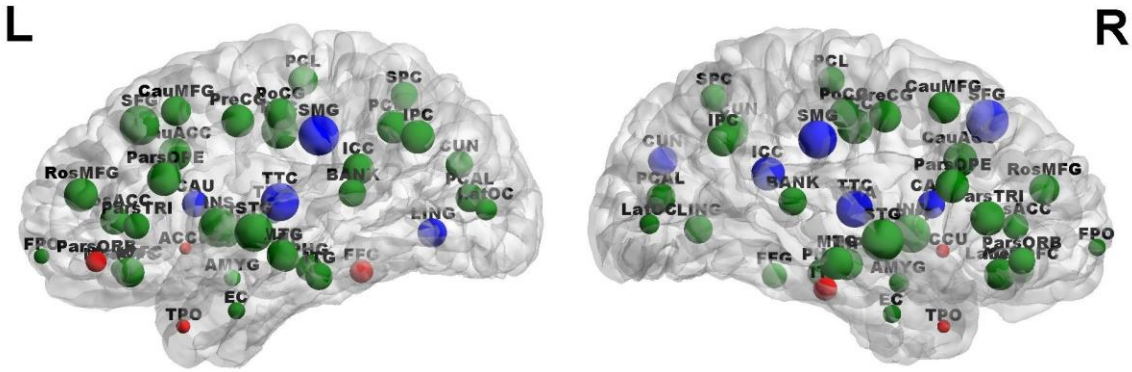

Figure 6.6: Degree distribution in the 0.03~0.06Hz functional brain network. The size of a node reflects the value of degree associated with the node. Nodes with large size represent hub regions with high degree. The red and blue nodes are regions that show significantly higher and lower degree in patients compared with controls, respectively.

Table 6.4: *P*-value, effect size and power of brain regions that showed significantly (permutation p-value < 0.05, uncorrected) higher degree measure in BPD compared with healthy controls.

brain regions	***p*-value**	**effect size**	**power**
left pars orbitalis	0.001	1.176	0.676
left temporal pole	0.007	1.02	0.5996
right temporal pole	0.008	0.97	0.5567
left accumbens	0.014	0.917	0.5143
right accumbens	0.014	0.939	0.5048
right inferior temporal gyrus	0.026	0.778	0.4187

Table 6.5: *P*-value, effect size and power of brain regions that showed significantly (permutation p-value < 0.05, uncorrected) lower degree measure in BPD compared with healthy controls.

brain regions	***p*-value**	**effect size**	**power**
right isthmus– cingulate cortex	0.008	-0.995	0.5533
right supramarginal gyrus	0.008	-1.024	0.5539
right transverse temporal cortex	0.023	-0.84	0.4205
left transverse temporal cortex	0.027	-0.77	0.4015
left lingual gyrus	0.031	-0.722	0.4055
left caudate	0.033	-0.736	0.381
right superior frontal gyrus	0.033	-0.734	0.3707
right caudate	0.034	-0.759	0.3867
right cuneus cortex	0.038	-0.704	0.3695

6.3.3 Clinical Correlates of Network Topology Measures

The normalized clustering coefficient, the small-worldness and the local efficiency are positively (*p*-value < 0.05, uncorrected) correlated with ZANBPD relationship, anger and affect scores (Table 6.6 and Figure 6.7). The higher the values of the topological measures are, the higher these correlated clinical scores. Together with the result in Section 5.4.3, the findings suggest that altered functional brain network topology and connectivity may contribute to specific symptoms of the disease.

Table 6.6: Correlations between clinical symptom scores and global network topology measures (age, gender and MADRS partialed out)

	Normalized Clustering Coefficient		Normalized Local Efficiency		Small-worldness	
	r	*p*-value	*r*	*p*-value	*r*	*p*-value
ZANBPD_SR relationship	0.7175	0.0012	0.6982	0.0018	0.7079	0.0015
ZANBPD_I relationship	0.6683	0.0034	0.6942	0.002	0.6619	0.0038
ZANBPD_I anger	0.5317	0.0281	0.5663	0.0178	0.543	0.0243
ZANBPD_I sum_affect	0.519	0.0328	0.4977	0.0421	0.516	0.034

ZAN-BPD_I: Zanarini Rating Scale for Borderline Personality Disorder interview score;
ZAN-BPD_SR: Zanarini Rating Scale for Borderline Personality Disorder self-rating score

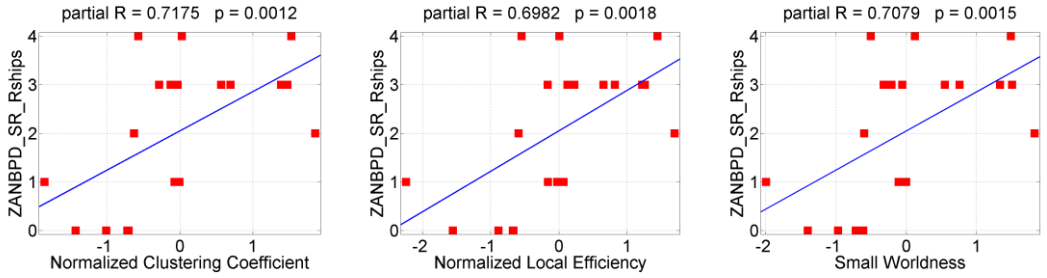

(a) (b) (c)

Figure 6.7: Scatter plots of ZANBPD_SR relationship problem scores against three global network topology measures: (a) normalized clustering coefficient, r = 0.7175, p = 0.0012, (b) normalized local efficiency, r = 0.6982, p = 0.0018, (c) small-worldness, r = 0.7079, p = 0.0015.

6.3.4 Classification Results

Given the significant between-group difference of network topology features, we tested whether these measures could be used as features to distinguish BPD patients from healthy controls using LDA classifier. Table 6.7 lists the leave-one-out classification

results using single global network measures that showed significant between-group difference, including size of largest connected component, normalized clustering coefficient, normalized local efficiency and small-worldness of the whole functional brian network. The best classification result was achieved using the size of largest connected component (85% sensitivity and 60% specificity). Besides the discriminating global network features, the left and right temporal poles showed the most significant between-group difference in nodal topological measures compared with other brain areas (Table 6.2 and Table 6.3). Table 6.8 lists the classification results using nodal network measures of these two regions, including nodal clustering coefficient, local efficiency and degree. The best classification result was achieved using the clustering coefficients of these two regions (90% sensitivity and 70% specificity).

Table 6.7: Classification results using single global network measure: size of largest connected component, normalized clustering coefficient, normalized local efficiency and small-worldness

	Accuracy	**Specificity**	**Sensitivity**
size of largest connected component	0.7667	0.6	0.85
normalized clustering coefficient	0.6667	0.7	0.65
normalized local efficiency	0.6667	0.7	0.65
small-worldness	0.6667	0.7	0.65

Table 6.8: Classification results using pairs of regional network measures of the left and right temporal poles, including clustering coefficient, local efficiency and degree

	Accuracy	**Specificity**	**Sensitivity**
clustering coefficient	0.8333	0.7	0.9
local efficiency	0.8	0.6	0.9
degree	0.7	0.7	0.7

6.4 Discussions

6.4.1 BPD-Related Alterations of Functional Brain Network Topology

Using graph-theory based complex network analysis approach, we examined the topology of resting-state functional brain networks of adults with BPD versus healthy controls. As hypothesized, patients with BPD showed evidence for abnormalities in topological structure in the intrinsic functional brain networks. These abnormalities appear to be related to specific symptoms of BPD and can be used as features to distinguish patients with BPD from healthy controls using a machine learning classifier. These findings add to prior neuroimaging studies that have reported abnormal connections between specific brain regions in BPD, and may provide new, clinically-relevant knowledge about the neurophysiology of the disease.

The emergence of graph-theory based complex network analysis provides an important mathematical framework to characterize the global and regional topology in brain connectivity networks. Our graph analysis identified significant alterations of small-world properties and network efficiency in patients with BPD versus healthy controls at the 0.03~0.06Hz frequency band, including increased *size of largest connected network component* (LCC), *small-worldness*, *clustering coefficient* and *local efficiency*. The increased size of LCC indicates a lower number of disconnected nodes in the network. Previous fMRI study of resting-state functional brain networks has reported increased size of LCC in schizophrenia patients, and suggested that the size of LCC is a predictor of other graph measures in graph analysis [130]. This is consistent with our finding that the size of LCC is positively correlated with other discriminating network topology measures, including the *small-worldness*, *clustering coefficient* and *local efficiency*.

The higher values of *clustering coefficient* and *local efficiency* together suggest greater network cliquishness, i.e., clustered structure, within the resting-state functional brain networks in BPD patients. Brain regions that showed increased local cliquishness in

patients include the bilateral temporal poles, bilateral amygdala, right pallidum, and left entorhinal cortex. These regions are mainly located within the limbic and paralimbic systems. Abnormalities of limbic regions in BPD have been consistently reported by both structural and functional neuroimaging studies [84], [85]. For example, the amygdala, which plays a crucial role in emotion processing and in the initiation of fear and stress responses [142], has been considered to be highly relevant to BPD psychopathology [143]. Neural imaging studies reported volume reduction [144], hyperreactivity in response to emotional stimuli [84], and increased functional connectivity in resting-state [117], at this area in BPD patients. Note that hyperconnectivity of brain regions implicated in emotion processing may reflect clinically well-observed BPD features such as affective hyperarousal and intense emotional reactions [84].

The bilateral temporal poles, i.e., the anterior-most portion of the temporal lobes, are also associated with significantly increased local cliquishness in patients. Temporal pole is often considered part of an extended limbic system, which is lateral to the amygdala and has tight connectivity to limbic and paralimbic regions. Research has suggested that this area binds complex, highly processed perceptual inputs to visceral emotional responses [145]. Structural and functional deficits of this area in patients with BPD have also been reported by previous neuroimaging studies [146]. The finding in this study that in resting-state functional brain networks, patients with BPD show higher levels of local cliquishness at the amygdala and temporal poles, which are responsible for processing negative emotion and visceral responses to negative emotion, could potentially explain the vulnerability in this patient group for a rapid rise to negative affect that is difficult for them to regulate.

In addition to the small-world properties and network efficiency, we also investigated the centrality of brain regions, which characterizes the importance of a node in the whole brain network. On the one hand, BPD patients show higher nodal centrality than controls at several brain regions with low degree, such as temporal poles and the nucleus accumbens. On the other hand, patients with BPD showed lower nodal centrality than controls at several hub nodes in the network, such as the supramarginal gyrus and the

transverse temporal cortex. These findings suggest that BPD might cause an increased number of connections to non-hub nodes and a decreased number of connections to hub nodes in functional brain networks. Furthermore, we also noticed that brain regions where patients with BPD showed increased local cliquishness are associated with low degree, suggesting that the increased local cliquishness in the whole brain network discussed above occurs in non-hub nodes. These alterations in the topological organizations of functional brain networks may add new knowledge to the current understanding of neural dysfunction in BPD.

In this study, we found several important relationships among the network measures and between network and clinical measures, which add strength and validity to the overall findings. First, mean connectivity within the subnetwork differentiating patients with BPD from controls at the 0.03~0.06Hz frequency band was associated with significant alterations of network topology. Interestingly, the mean connectivity of the subnetwork was negatively correlated with all four global network topology measures that had shown significant group differences (higher in patients), including the size of largest graph component, normalized clustering coefficient, small-worldness, and normalized local efficiency. In these relationships, participants with lower mean connectivity showed higher values of the global measures. This finding suggests a possible relationship between the functional connectivity between brain areas and the topological organizations of whole-brain functional networks.

Second, the properties of small-worldness, clustering coefficient and local efficiency all showed positive correlations with several key BPD symptom scores, including problems in relationships, anger and affect problems. The decreased functional connectivity in the NBS subnetwork we discussed in Chapter 5 showed negative correlations with a variety of key BPD symptoms, such as depression, obsessive compulsive symptoms, hostility, affect, impulsivity, and relationship problems. Although these correlation analyses were exploratory and the results were not corrected for multiple comparisons, the preliminary findings suggest that the aberrant topological and connectivity features may have important clinical relevance. BPD is very heterogeneous,

and so treatments will optimally be tailored to each individual's aberrant pattern of neurobiology. By better characterizing the neural underpinnings of specific facets of illness, this type of research will pave the way for conceptualizing and testing more targeted, neuroscientifically-informed treatments.

Last but not least, the significant network topology features showed promising classification accuracy in distinguishing BPD patients from healthy controls with LDA classifier, which further demonstrated the between-group differences of these network properties showed in statistical tests. Together these findings suggest that the network measures derived from graph theory in this study are clinically meaningful, and may shed light on the neurobiological underpinnings of BPD, and could eventually have potential in clinical applications such as diagnosis and treatment selection.

Finally, we wish to highlight that we consider this exploratory study is a first and important step. The preliminary findings of group differences and relationships with clinical measures reported here require replication with larger samples. Once confirmed, these findings could form the basis for longitudinal studies testing important questions such as: (1) how topological network structure and functional connectivity change in patients with BPD across stages of illness; (2) whether these abnormalities present early in development, even before onset of the disorder; (3) which factors contribute to development of network organization abnormalities; and (4) whether and how interventions for BPD impact these aspects of neural network organization and connectivity.

6.4.2 Methodological Considerations

To compute various network topology measures, after obtaining the correlation coefficients between all brain regions, we used thresholding to remove weak and non-significant links, since they may represent spurious connections and may obscure the topology of strong and significant connections in functional brain networks [121]. Negative connections, i.e., functional anti-correlations, and self-connections were ignored in the present study, as suggested in [121]. We applied a set of subject-specific

correlation thresholds to ensure that all networks have the same number of nodes and links at each graph density. To determine the statistical significance of each graph measure, an efficient test is needed to compare the graph-metric-versus-graph-density curves between groups. Instead of performing massive comparisons at each single density, we performed non-parametric permutation test on the AUC of each graph measure, which serves as a scalar summary of the curve values across densities. This approach offers a comprehensive examination of the entire topological structure of the original weighted connectivity graph over specific density range of interest. In addition, a machine learning classifier was applied to classify BPD patients from healthy controls based on the discriminating network measures. The significant network features and the machine learning based classification scheme may have potential to be used in a computer-aided objective test to assist in clinical diagnosis of BPD.

6.4.3 Limitations

The limitation of the study is the small sample size (20 patients vs. 10 controls), which leads to low statistical power: 0.38~0.83 (mean 0.51, std. 0.214) for global measures and 0.35~0.875 (mean 0.518, std. 0.15) for nodal measures. Low statistical power not only reduces the probability of detecting a true effect, but also reduces the probability that a statistically significant results reflects a true effect [147]. The effect sizes (Cohen's *d*) for the four global topology measures are 0.726~1.205 (mean 0.875, std. 0.222), indicating medium to large effects [140]. The absolute values of effect size for nodal topology measures are 0.625~1.36 (mean 0.888, std. 0.193), also indicating medium to large effects [140]. These effect sizes are comparable with previous effect sizes reported in neuroimaging studies that have compared BPD subjects and healthy volunteers [144], [148]–[150]. However, they might be overestimated due to low statistical power [147]. Besides the power issue, small number of subjects does not allow us to assess the relative differences between subtypes of the disease, or design more complex classification models which might cause data overfitting. Therefore, the findings of this study should be viewed as exploratory, and need to be validated and extended on large samples with high statistical power.

Some other limitations of the current work need to be further addressed. First, 82 cortical and subcortical regions were chosen as nodes in the functional brain networks. Brain networks derived using different parcellation schemes may show different topological structures. In addition, Pearson correlation coefficients were used to measure the functional connectivity in the network, which could only measure the linear relationship between two time series. There are other types of connectivity measures like coherence, and mutual information, which could account for time lags and measure non-linear correlations between two time series. Further studies are needed to compare the topology and connectivity of functional brain networks constructed with different node sets and connectivity measures. Lastly, it is important to note that the current study considers a single static network structure as an average representation of the overall resting-state functional connectivity over 6 minute time duration. This method is consistent with other similar studies on topological organization of functional brain networks [110], [130], [134]. However, recent fMRI research has shown that resting-state functional brain connectivity is not static [151]. Therefore, future work is needed to explore the dynamic network topology changes across longer time durations.

6.5 Conclusions

In this chapter, we applied graph-theory based complex network analysis to investigate BPD-related alterations of topological organizations in resting-state functional brain networks. In the 0.03~0.06Hz functional brain networks, BPD patients showed increased local cliquishness characterized by increased size of largest connected component, clustering coefficient, local efficiency, and small-worldness, particularly at the limbic areas. Patients also showed decreased nodal centrality at several hub nodes, but increased nodal centrality at several non-hub nodes in the network. In addition, the significant network measures were positively correlated with several clinical symptom scores for BPD diagnosis, and showed high predictive power in patient vs. control classification

using a machine learning classifier. The findings of this work may help in gaining new knowledge into the neural underpinnings of BPD.

However, due to limitation of small sample sizes, the reported results should be viewed as exploratory and need to be validated on large samples in future works. Future efforts will be directed towards studying functional brain networks constructed with different node sets and connectivity measures, exploring the dynamic network structure across time, and testing the results on a larger sample size. Future work will also be directed towards comparing the topological properties of functional brain networks in different psychiatric disorders, including BPD, obsessive compulsive disorder, and major depressive disorder.

Chapter 7

Conclusions and Future Work

7.1 Conclusions

In this research, we explore quantitative, discriminative and interpretable neuroimaging biomarkers for two common mental disorders: schizophrenia and borderline personality disorder (BPD). We have presented an interdisciplinary research framework that combines domain knowledge, neuroimaging techniques, signal processing, graph theory, machine learning and statistical analysis approaches to address four key problems related to biomarker discovery: feature extraction, feature selection, feature validation and classification. The identified neuroimaging patterns contain meaningful space, frequency and time information in brain activity, connectivity and network structure, which may add new knowledge to the current understanding of the underlying mechanisms of the illnesses. Furthermore, based on the discriminating patterns, a computer-aided screening system can be build that uses machine learning classifiers to distinguish psychiatric patients from healthy people. Such system may enable quantitative assessment of mental disorders, which would benefit a large number of psychiatric patients.

In the first part of the dissertation, we present our work on biomarker discovery for schizophrenia using MEG data recorded during language processing tasks. MEG captures ongoing brain activity from whole-head locations with very high temporal resolution. This motivates us to explore spatial-temporal-spectral features in neural oscillatory activity. We first identified several Event-Related Desynchronization/Synchronization (ERDS) features that showed high discriminating power in schizophrenia classification. Then, we proposed two novel Spectral Power Ratio (SPR) feature sets: the Band Power Ratio (BPR) and the Window Power Ratio (WPR), which reflect the inter-relationships of

spectral power between different frequency bands, and between different time periods of neural oscillatory activity. We identified 3 BPR and 3 WPR clusters that showed significant between-group difference using rigorous statistical tests. Based on only two WPR and one BPR feature combined, over 95% cross validation classification accuracies were achieved using three different linear classifiers separately, which demonstrated strong discriminating power of the key SPR features. These features may bring new insight about the neural mechanisms of language processing impairments in patients with schizophrenia.

In the second part of the dissertation, we explore biomarkers in BPD using resting-state fMRI data. Considering the high spatial resolution of fMRI, we focus on investigating the connectivity and topological structure patterns of the functional brain networks. Using graph-theory based analysis and Network-based Statistics (NBS), we identified an interconnected subnetwork in 0.03–0.06 Hz frequency band that showed significantly lower connectivity strength in patient group. We also identified several network topology features that showed increased network cliquishness and altered centrality in BPD. These significant network measures were correlated with several clinical symptom scores for BPD diagnosis, and showed high predictive power in patient vs. control classification using a machine learning classifier. These novel findings may add new knowledge to the current understanding of functional brain networks in BPD.

7.2 Future Work

The limitation of this research is the small sample size for both schizophrenia (22 subjects) and BPD (30 subjects) studies. Small sample size leads to low statistical power, which not only reduces the probability of detecting a true effect, but also reduces the probability that a statistically significant results reflect a true effect [147] . The effect size of the identified features might be overestimated due to low statistical power [147]. Besides the power issue, small number of subjects does not allow us to assess the relative difference between subtypes of the illnesses. The biomarkers are assumed to be valid

across all the patients in the study, i.e., assume disease is homogenous. However, this assumption does not always hold true due to disease and population heterogeneity. Different subsets of patients tend to have different factors that drive the phenotype of interest. Furthermore, small sample size does not allow us to design complex classification models which might cause data overfitting. Therefore, the findings of this study should be viewed as exploratory, and need to be validated and extended on larger samples in future research before clinical applications.

For the schizophrenia study, a future research direction would be to improve the spatial resolution of the MEG features. MEG is a non-invasive neuroimaging modality that assesses brain activity using sensors outside the head. The signal collected at each MEG sensor is a weighted sum of electric activity from multiple brain sources. Therefore, the challenge posed by MEG is to determine the location of electric activity within the brain from the induced magnetic fields outside the head. Future work will be directed towards solving the source localization problem using advanced signal processing techniques such as beamforming and independent component analysis (ICA).

For the BPD study, there are several problems that can be further investigated in future works. First, 82 cortical and subcortical regions were chosen as nodes in the functional brain networks. Brain networks derived using different parcellation schemes may show different connectivity and topological structures. In addition, linear correlation coefficients were used to measure the functional connectivity in the network, which could only measure the linear relationship between two time series. There are other types of connectivity measures like spectrum coherence and mutual information, which could account for time lags and measure non-linear correlations. Further studies are needed to compare the topology and connectivity of functional brain networks constructed with different node sets and connectivity measures. Lastly, it is important to note that the current study considers a single static network structure as an average representation of the overall resting-state functional connectivity over 6-minute time duration. Recent fMRI research has shown that resting-state functional brain connectivity is not static

[151]. Therefore, future work can be directed to exploring the dynamic network topology changes across longer time durations.

References

[1] D. J. Stein, K. A. Phillips, D. Bolton, K. W. M. Fulford, J. Z. Sadler, and K. S. Kendler, "What is a mental / psychiatric disorder ? From DSM-IV to DSM-V," *Psychol. Med.*, vol. 40, pp. 1759–1765, 2010.

[2] "Mental illness - Mayo Clinic." [Online]. Available: http://www.mayoclinic.org/diseases-conditions/mental-illness/basics/definition/con-20033813?DSECTION=all&p=1.

[3] "NIMH » Any Mental Illness (AMI) Among U.S. Adults." [Online]. Available: https://www.nimh.nih.gov/health/statistics/prevalence/any-mental-illness-ami-among-us-adults.shtml.

[4] "NIMH » Any Disorder Among Children." [Online]. Available: https://www.nimh.nih.gov/health/statistics/prevalence/any-disorder-among-children.shtml.

[5] D. Bloom, E. Cafiero, E. Jan é-Llopis, S. Abrahams-Gessel, L. Bloom, S. Fathima, A. Feigl, T. Gaziano, M. Mowafi, A. Pandya, K. Prettner, L. Rosenberg, B. Seligman, A. Stein, and C. Weinstein, "The global economic burden of non-communicable diseases," *World Econ. Forum*, no. September, pp. 1–48, 2011.

[6] "Causes of Mental Illness." [Online]. Available: http://www.webmd.com/mental-health/mental-health-causes-mental-illness.

[7] "Mental illness Tests and diagnosis - Mayo Clinic." [Online]. Available: http://www.mayoclinic.org/diseases-conditions/mental-illness/basics/tests-diagnosis/con-20033813.

[8] A. Abi-Dargham and G. Horga, "The search for imaging biomarkers in psychiatric disorders," *Nat Med*, vol. advance on, Oct. 2016.

[9] "Functional Magnetic Resonance Imaging - Wiki." [Online]. Available: https://en.wikipedia.org/wiki/Functional_magnetic_resonance_imaging.

[10] “Magnetoencephalography - Wiki.” [Online]. Available: https://en.wikipedia.org/wiki/Magnetoencephalography.

[11] “NIMH » Schizophrenia.” [Online]. Available: https://www.nimh.nih.gov/health/statistics/prevalence/schizophrenia.shtml.

[12] “NIMH » Borderline Personality Disorder.” [Online]. Available: https://www.nimh.nih.gov/health/statistics/prevalence/borderline-personality-disorder.shtml.

[13] I. Guyon and A. Elisseeff, “An Introduction to Variable and Feature Selection,” *J. Mach. Learn. Res.*, vol. 3, no. 3, pp. 1157–1182, 2003.

[14] R. G. Miller, *Simultaneous Statistical Inference*. New York, NY: Springer New York, 1981.

[15] “Bonferroni correction - wiki.” [Online]. Available: https://en.wikipedia.org/wiki/Bonferroni_correction.

[16] E. Maris and R. Oostenveld, “Nonparametric statistical testing of EEG- and MEG-data,” *J. Neurosci. Methods*, vol. 164, no. 1, pp. 177–190, 2007.

[17] A. Zalesky, A. Fornito, and E. T. Bullmore, “Network-based statistic: Identifying differences in brain networks,” *Neuroimage*, vol. 53, no. 4, pp. 1197–1207, 2010.

[18] T. Xu, M. Stephane, and K. K. Parhi, “Multidimensional analysis of the abnormal neural oscillations associated with lexical processing in schizophrenia.,” *Clin. EEG Neurosci.*, vol. 44, pp. 135–43, 2013.

[19] T. Xu, M. Stephane, and K. K. Parhi, “Abnormal Neural Oscillations in Schizophrenia Assessed by Spectral Power Ratio of MEG During Word Processing,” *IEEE Trans. Neural Syst. Rehabil. Eng.*, vol. 24, no. 11, pp. 1148–1158, Nov. 2016.

[20] T. Xu, M. Stephane, and K. K. Parhi, “Classification of single-trial MEG during sentence processing for automated schizophrenia screening,” in *International IEEE/EMBS Conference on Neural Engineering, NER*, 2013, pp. 363–366.

[21] T. Xu, K. R. Cullen, B. Mueller, M. W. Schreiner, K. O. Lim, S. C. Schulz, and K. K. Parhi, "Network analysis of functional brain connectivity in borderline personality disorder using resting-state fMRI," *NeuroImage Clin.*, vol. 11, pp. 302–315, 2016.

[22] G. Pfurtscheller and F. H. Lopes da Silva, "Functional meaning of even-related desynchronization (ERD) and synchronization (ERS)," in *Event-Related Desynchronization: Handbook of Electroencephalography and Clinical Neurophysiology*, 1999, pp. 51–65.

[23] Y. Chen and C. Lin, "Combining SVMs with Various Feature Selection Strategies," in *Feature Extraction*, vol. 324, no. 1, 2006, pp. 315–324.

[24] I. Guyon, J. Weston, S. Barnhill, and V. Vapnik, "Gene selection for cancer classification using support vector machines," *Mach. Learn.*, vol. 46, no. 1–3, pp. 389–422, 2002.

[25] B. E. Boser, I. M. Guyon, and V. N. Vapnik, "A Training Algorithm for Optimal Margin Classifiers," in *Proceedings of the 5th Annual ACM Workshop on Computational Learning Theory*, 1992, pp. 144–152.

[26] C. Cortes and V. Vapnik, "Support-vector networks," *Mach. Learn.*, vol. 20, no. 3, pp. 273–297, 1995.

[27] F. Cherkassky, Mulier, *Learning from data: Concepts, theory, and methods.*, 2nd ed. Wiley-IEEE Press, 2007.

[28] H. Peng, F. Long, and C. Ding, "Feature selection based on mutual information: Criteria of Max-Dependency, Max-Relevance, and Min-Redundancy," *IEEE Trans. Pattern Anal. Mach. Intell.*, vol. 27, pp. 1226–1238, 2005.

[29] "NIMH · Schizophrenia." [Online]. Available: http://www.nimh.nih.gov/health/topics/schizophrenia/index.shtml. [Accessed: 23-Sep-2014].

[30] W. A. Phillips and S. M. Silverstein, "Convergence of biological and

psychological perspectives on cognitive coordination in schizophrenia.," *Behav. Brain Sci.*, vol. 26, no. 1, pp. 65–82; discussion 82–137, 2003.

[31] K. J. Friston and K. J. Friston, "Schizophrenia and the disconnection hypothesis.," *Acta Psychiatr. Scand. Suppl.*, vol. 395, pp. 68–79, 1999.

[32] P. J. Uhlhaas and W. Singer, "Abnormal neural oscillations and synchrony in schizophrenia.," *Nat. Rev. Neurosci.*, vol. 11, pp. 100–113, 2010.

[33] G. Buzsáki and A. Draguhn, "Neuronal oscillations in cortical networks.," *Science*, vol. 304, no. 5679, pp. 1926–1929, 2004.

[34] G. Buzsáki, *Rhythms of the Brain*, vol. 1. 2006.

[35] T. Harmony, T. Fernández, J. Silva, J. Bosch, P. Valdés, A. Fernández-Bouzas, L. Galán, E. Aubert, and D. Rodríguez, "Do specific EEG frequencies indicate different processes during mental calculation?," *Neurosci. Lett.*, vol. 266, pp. 25–28, 1999.

[36] M. Stephane, a. Leuthold, M. Kuskowski, K. McClannahan, and T. Xu, "The Temporal, Spatial, and Frequency Dimensions of Neural Oscillations Associated With Verbal Working Memory," *Clin. EEG Neurosci.*, vol. 43, pp. 145–153, 2012.

[37] E. Bleuler, *Dementia Praecox or the Group of Schizophrenias*. New York: International Universities Press, 1950.

[38] M. Stephane, G. Pellizzer, C. R. Fletcher, and K. McClannahan, "Empirical evaluation of language disorder in schizophrenia.," *J. Psychiatry Neurosci.*, vol. 32, no. 4, pp. 250–258, 2007.

[39] M. Stephane, M. Kuskowski, and J. Gundel, "Abnormal dynamics of language in schizophrenia," *Psychiatry Res.*, vol. 216, no. 3, pp. 320–324, 2014.

[40] G. Pfurtscheller and F. H. Lopes Da Silva, "Event-related EEG/MEG synchronization and desynchronization: basic principles."

[41] G. Pfurtscheller, "Functional brain imaging based on ERD/ERS," *Vision Res.*, vol. 41, no. 10, pp. 1257–1260, 2001.

[42] R. C. Oldfield, “The assessment and analysis of handedness: The Edinburgh inventory,” *Neuropsychologia*, vol. 9, no. 1, pp. 97–113, 1971.

[43] American Psychiatric Association, *Diagnostic and Statistical Manual of Mental Disorders, Fourth Edition, Text Revision*, vol. Washington. 2000.

[44] J. R. Blair and O. Spreen, “Predicting premorbid IQ: A revision of the national adult reading test,” *Clinical Neuropsychologist*, vol. 3. pp. 129–136, 1989.

[45] J. Overall and D. Gorham, “The Brief Psychiatric Rating Scale,” *Psychol. Rep.*, vol. 10, pp. 799–812, 1962.

[46] S. R. Kay, A. Fiszbein, and L. a Opler, “【Ba-22】The positive and negative syndrome scale (PANSS) for schizophrenia.,” *Schizophr. Bull.*, vol. 13, pp. 261–76, 1987.

[47] M. A. Gernsbacher, *Handbook of psycholinguistics*. San Diego: Academic Press, 1994.

[48] N. Ille, P. Berg, and M. Scherg, “Artifact correction of the ongoing EEG using spatial filters based on artifact and brain signal topographies.,” *J. Clin. Neurophysiol.*, vol. 19, pp. 113–124, 2002.

[49] Y. Chen and C. Lin, “Combining SVMs with Various Feature Selection Strategies,” *Strategies*, vol. 324, pp. 1–10, 2006.

[50] A. Delorme and S. Makeig, “EEGLAB: An open source toolbox for analysis of single-trial EEG dynamics including independent component analysis,” *J. Neurosci. Methods*, vol. 134, no. 1, pp. 9–21, 2004.

[51] M. Stephane, N. F. Ince, A. Leuthold, G. Pellizzer, A. H. Tewfik, C. Surerus, M. Kuskowski, and K. McClannahan, “Temporospatial characterization of brain oscillations (TSCBO) associated with subprocesses of verbal working memory in schizophrenia.,” *Clin. EEG Neurosci.*, vol. 39, no. 4, pp. 194–202, 2008.

[52] N. F. Ince, G. Pellizzer, A. H. Tewfik, K. Nelson, A. Leuthold, K. McClannahan, and M. Stephane, “Classification of schizophrenia with spectro-temporo-spatial

MEG patterns in working memory," *Clin. Neurophysiol.*, vol. 120, pp. 1123–1134, 2009.

[53] L. V. Moran and L. E. Hong, "High vs low frequency neural oscillations in schizophrenia," *Schizophrenia Bulletin*, vol. 37, no. 4. pp. 659–663, 2011.

[54] C. M. Krause, P. Grönholm, A. Leinonen, M. Laine, A. L. Sääkkinen, and C. Söderholm, "Modality matters: The effects of stimulus modality on the 4- to 30-Hz brain electric oscillations during a lexical decision task," *Brain Res.*, vol. 1110, pp. 182–192, 2006.

[55] C. M. Krause, "Auditorily elicited event-related desynchronization (ERD) and synchronization (ERS) as a method of studying cortical correlates of cognitive processes," *Rev. Esp. Neuropsicol.*, vol. 2, no. 1–2, pp. 77–91, 2000.

[56] K. Tavabi, D. Embick, and T. P. L. Roberts, "Spectral-temporal analysis of cortical oscillations during lexical processing.," *Neuroreport*, vol. 22, no. 10, pp. 474–8, 2011.

[57] P. J. Uhlhaas, C. Haenschel, D. Nikolić, and W. Singer, "The role of oscillations and synchrony in cortical networks and their putative relevance for the pathophysiology of schizophrenia," *Schizophrenia Bulletin*, vol. 34, no. 5. pp. 927–943, 2008.

[58] S. Williams and P. Boksa, "Gamma oscillations and schizophrenia," *Journal of Psychiatry and Neuroscience*, vol. 35, no. 2, pp. 75–77, 2010.

[59] P. Fries, "A mechanism for cognitive dynamics: Neuronal communication through neuronal coherence," *Trends in Cognitive Sciences*, vol. 9, no. 10. pp. 474–480, 2005.

[60] R. Hannemann, J. Obleser, and C. Eulitz, "Top-down knowledge supports the retrieval of lexical information from degraded speech," *Brain Res.*, vol. 1153, no. 1, pp. 134–143, 2007.

[61] H. Tiitinen, J. Sinkkonen, K. Reinikainen, K. Alho, J. Lavikainen, and R.

Naatanen, “Selective attention enhances the auditory 40-Hz transient response in humans,” *Nature*, vol. 364, no. 6432, pp. 59–60, 1993.

[62] R. Boostani, K. Sadatnezhad, and M. Sabeti, “An efficient classifier to diagnose of schizophrenia based on the EEG signals,” *Expert Syst. Appl.*, vol. 36, pp. 6492–6499, 2009.

[63] J. Escudero, E. Ifeachor, A. Fernández, J. J. López-Ibor, and R. Hornero, “Changes in the MEG background activity in patients with positive symptoms of schizophrenia: spectral analysis and impact of age.,” *Physiol. Meas.*, vol. 34, pp. 265–79, 2013.

[64] T. Xu, M. Stephane, and K. K. Parhi, “Selection of abnormal neural oscillation patterns associated with sentence-level language disorder in Schizophrenia,” in *Proceedings of the Annual International Conference of the IEEE Engineering in Medicine and Biology Society, EMBS*, 2012, pp. 4923–4926.

[65] M. Sabeti, S. D. Katebi, R. Boostani, and G. W. Price, “A new approach for EEG signal classification of schizophrenic and control participants,” *Expert Syst. Appl.*, vol. 38, no. 3, pp. 2063–2071, 2011.

[66] R. Wix-Ramos, X. Moreno, E. Capote, G. González, E. Uribe, and A. Eblen-Zajjur, “Drug Treated Schizophrenia, Schizoaffective and Bipolar Disorder Patients Evaluated by qEEG Absolute Spectral Power and Mean Frequency Analysis.,” *Clin. Psychopharmacol. Neurosci.*, vol. 12, no. 1, pp. 48–53, 2014.

[67] J. S. Kim, K. S. Shin, W. H. Jung, S. N. Kim, J. S. Kwon, and C. K. Chung, “Power spectral aspects of the default mode network in schizophrenia: an MEG study.,” *BMC Neurosci.*, vol. 15, p. 104, 2014.

[68] J. K. Johannesen, B. F. O’Donnell, A. Shekhar, J. H. McGrew, and W. P. Hetrick, “Diagnostic specificity of neurophysiological endophenotypes in schizophrenia and bipolar disorder.,” *Schizophr. Bull.*, vol. 39, no. 6, pp. 1219–29, 2013.

[69] A. Bachiller, A. Díez, V. Suazo, C. Domínguez, M. Ayuso, R. Hornero, J. Poza, and V. Molina, “Decreased spectral entropy modulation in patients with

schizophrenia during a P300 task," *Eur. Arch. Psychiatry Clin. Neurosci.*, pp. 1–11, 2014.

[70] Z. Zhang and K. K. Parhi, "Low-Complexity Seizure Prediction From iEEG/sEEG Using Spectral Power and Ratios of Spectral Power," *IEEE Trans. Biomed. Circuits Syst.*, vol. 10, no. 3, pp. 693–706, 2016.

[71] Z. Zhang and K. K. Parhi, "Seizure Prediction using Polynomial SVM Classification," in *Proc. of 2015 IEEE Engineering in Medicine and Biology Society Conference (EMBC)*, 2015, pp. 5748–5751.

[72] Z. Zhang and K. K. Parhi, "Seizure Detection using Regression Tree Based Feature Selection and Polynomial SVM Classification," in *Proc. of 2015 IEEE Engineering in Medicine and Biology Society Conference (EMBC)*, 2015, pp. 6578–6581.

[73] R. V. A. Sheorajpanday, G. Nagels, A. J. T. M. Weeren, D. De Surgeloose, and P. P. De Deyn, "Additional value of quantitative EEG in acute anterior circulation syndrome of presumed ischemic origin," *Clin. Neurophysiol.*, vol. 121, no. 10, pp. 1719–1725, 2010.

[74] P. D. Welch, "The Use of Fast Fourier Transform for the Estimation of Power Spectra: A Method Based on Time Aver. aging Over Short, Modified Periodograms," *IEEE Trans. AUDIO Electroacoust.*, vol. AU-15, pp. 70–73, 1967.

[75] K. K. Parhi and M. Ayinala, "Low-Complexity Welch Power Spectral Density Computation," *IEEE Trans. Circuits Syst. Regul. Pap.*, vol. 61, no. 1, pp. 172–182, 2014.

[76] S. Mika, G. Ratsch, J. Weston, and B. Scholkopf, "Fisher discriminant analysis with kernels," *Neural Networks Signal Process. IX, 1999. Proc. 1999 IEEE Signal Process. Soc. Work.*, pp. 41–48, 1999.

[77] Y. Freund and R. E. Schapire, "Large margin classification using the perceptron algorithm," *Mach. Learn.*, vol. 37, no. 3, pp. 277–296, 1999.

[78] J. P. Roiser, R. Wigton, J. M. Kilner, M. A. Mendez, N. Hon, K. J. Friston, and E. M. Joyce, “Dysconnectivity in the frontoparietal attention network in schizophrenia,” *Front. Psychiatry*, vol. 4, 2013.

[79] O. Demirci, V. P. Clark, and V. D. Calhoun, “A projection pursuit algorithm to classify individuals using fMRI data: Application to schizophrenia,” *Neuroimage*, vol. 39, no. 4, pp. 1774–1782, 2008.

[80] Y.-J. Li and F.-Y. Fan, “Classification of Schizophrenia and Depression by EEG with ANNs*.,” *Conf. Proc. IEEE Eng. Med. Biol. Soc.*, vol. 3, pp. 2679–2682, 2005.

[81] A. P. Georgopoulos, E. Karageorgiou, A. C. Leuthold, S. M. Lewis, J. K. Lynch, A. A. Alonso, Z. Aslam, A. F. Carpenter, A. Georgopoulos, L. S. Hemmy, I. G. Koutlas, F. J. P. Langheim, J. R. McCarten, S. E. McPherson, J. V Pardo, P. J. Pardo, G. J. Parry, S. J. Rottunda, B. M. Segal, S. R. Sponheim, J. J. Stanwyck, M. Stephane, and J. J. Westermeyer, “Synchronous neural interactions assessed by magnetoencephalography: a functional biomarker for brain disorders.,” *J. Neural Eng.*, vol. 4, pp. 349–355, 2007.

[82] Y. Freund and R. R. E. Schapire, “Experiments with a New Boosting Algorithm,” in *International Conference on Machine Learning*, 1996, pp. 148–156.

[83] “NIMH · Borderline Personality Disorder.” [Online]. Available: http://www.nimh.nih.gov/health/topics/borderline-personality-disorder/index.shtml. [Accessed: 11-Apr-2015].

[84] A. Krause-Utz, D. Winter, I. Niedtfeld, and C. Schmahl, “The latest neuroimaging findings in borderline personality disorder.,” *Curr. Psychiatry Rep.*, vol. 16, p. 438, 2014.

[85] A. S. New, M. M. Perez-Rodriguez, and L. H. Ripoll, “Neuroimaging and Borderline Personality Disorder,” *Psychiatr. Ann.*, vol. 42, no. 2, pp. 65–71, Feb. 2012.

[86] M. Goodman, E. A. Hazlett, J. B. Avedon, D. R. Siever, K. W. Chu, and A. S.

New, “Anterior cingulate volume reduction in adolescents with borderline personality disorder and co-morbid major depression,” *J. Psychiatr. Res.*, vol. 45, no. 6, pp. 803–807, 2011.

[87] P. M. Nunes, A. Wenzel, K. T. Borges, C. R. Porto, R. M. Caminha, and I. R. de Oliveira, “Volumes of the hippocampus and amygdala in patients with borderline personality disorder: a meta-analysis.,” *J. Pers. Disord.*, vol. 23, no. 4, pp. 333–45, 2009.

[88] M. Sala, E. Caverzasi, M. Lazzaretti, N. Morandotti, G. De Vidovich, E. Marraffini, F. Gambini, M. Isola, M. De Bona, G. Rambaldelli, G. D'Allio, F. Barale, F. Zappoli, and P. Brambilla, “Dorsolateral prefrontal cortex and hippocampus sustain impulsivity and aggressiveness in borderline personality disorder,” *J. Affect. Disord.*, vol. 131, no. 1–3, pp. 417–421, 2011.

[89] P. H. Soloff, P. Pruitt, M. Sharma, J. Radwan, R. White, and V. A. Diwadkar, “Structural brain abnormalities and suicidal behavior in borderline personality disorder,” *J. Psychiatr. Res.*, vol. 46, no. 4, pp. 516–525, 2012.

[90] P. Soloff, J. Nutche, D. Goradia, and V. Diwadkar, “Structural brain abnormalities in borderline personality disorder: a voxel-based morphometry study.,” *Psychiatry Res.*, vol. 164, no. 3, pp. 223–236, 2008.

[91] J. Mauchnik and C. Schmahl, “The latest neuroimaging findings in borderline personality disorder,” *Current Psychiatry Reports*, vol. 12, no. 1. pp. 46–55, 2010.

[92] B. Biswal, F. Z. Yetkin, V. M. Haughton, and J. S. Hyde, “Functional connectivity in the motor cortex of resting human brain using echo-planar MRI.,” *Magn. Reson. Med.*, vol. 34, no. 4, pp. 537–541, 1995.

[93] M. D. Fox, A. Z. Snyder, J. L. Vincent, M. Corbetta, D. C. Van Essen, and M. E. Raichle, “The human brain is intrinsically organized into dynamic, anticorrelated functional networks.,” *Proc. Natl. Acad. Sci. U. S. A.*, vol. 102, no. 27, pp. 9673–8, 2005.

[94] V. D. Calhoun, T. Adali, G. D. Pearlson, and J. J. Pekar, “A method for making

group inferences from functional MRI data using independent component analysis.," *Hum. Brain Mapp.*, vol. 14, no. 3, pp. 140–51, 2001.

[95] V. G. Van De Ven, E. Formisano, D. Prvulovic, C. H. Roeder, and D. E. J. Linden, "Functional connectivity as revealed by spatial independent component analysis of fMRI measurements during rest," *Hum. Brain Mapp.*, vol. 22, no. 3, pp. 165–178, 2004.

[96] S. Kamphausen, P. SchrÖder, S. Maier, K. Bader, B. Feige, C. P. Kaller, V. Glauche, S. Ohlendorf, L. T. Van Elst, S. KlÖppel, G. A. Jacob, D. Silbersweig, K. Lieb, and O. TÜscher, "Medial prefrontal dysfunction and prolonged amygdala response during instructed fear processing in borderline personality disorder," *World Journal of Biological Psychiatry*. pp. 1–12, 2012.

[97] K. R. Cullen, N. Vizueta, K. M. Thomas, G. J. Han, K. O. Lim, J. Camchong, B. A. Mueller, C. H. Bell, M. D. Heller, and S. C. Schulz, "Amygdala Functional Connectivity in Young Women with Borderline Personality Disorder," *Brain Connectivity*, vol. 1, no. 1. pp. 61–71, 2011.

[98] R. C. Wolf, F. Sambataro, N. Vasic, M. Schmid, P. A. Thomann, S. D. Bienentreu, and N. D. Wolf, "Aberrant connectivity of resting-state networks in borderline personality disorder," *J. Psychiatry Neurosci.*, vol. 36, pp. 402–411, 2011.

[99] A. Doll, C. Sorg, A. Manoliu, A. Wöller, C. Meng, H. Förstl, C. Zimmer, A. M. Wohlschläger, and V. Riedl, "Shifted intrinsic connectivity of central executive and salience network in borderline personality disorder.," *Front. Hum. Neurosci.*, vol. 7, p. 727, 2013.

[100] D. W. Black, M. C. Zanarini, A. Romine, M. Shaw, J. Allen, and S. C. Schulz, "Comparison of Low and Moderate Dosages of Extended-Release Quetiapine in Borderline Personality Disorder: A Randomized, Double-Blind, Placebo-Controlled Trial.," *Am. J. Psychiatry*, no. March, pp. 1–9, 2014.

[101] M. C. Zanarini, J. G. Gunderson, F. R. Frankenburg, and D. L. Chauncey, "The Revised Diagnostic Interview for Borderlines: Discriminating BPD from other

Axis II Disorders," *Journal of Personality Disorders*, vol. 3, no. 1. pp. 10–18, 1989.

[102] M. C. Zanarini, A. A. Vujanovic, E. A. Parachini, J. L. Boulanger, F. R. Frankenburg, and J. Hennen, "Zanarini Rating Scale for Borderline Personality Disorder (ZAN-BPD): a continuous measure of DSM-IV borderline psychopathology.," *J. Pers. Disord.*, vol. 17, no. 3, pp. 233–42, Jun. 2003.

[103] R. L. Spitzer, J. Williams, and M. Gibbon, *Structured clinical interview for DSM-IV*. Biometrics Research: New York, 1994.

[104] L. Derogatis and R. Unger, "Symptom Checklist-90-Revised," *Corsini Encycl. Psychol.*, pp. 18–19, 2010.

[105] "FreeSurfer." [Online]. Available: https://surfer.nmr.mgh.harvard.edu/.

[106] G. H. Glover, T. Q. Li, and D. Ress, "Image-based method for retrospective correction of physiological motion effects in fMRI: RETROICOR," *Magn. Reson. Med.*, vol. 44, pp. 162–167, 2000.

[107] "FSL." [Online]. Available: http://fsl.fmrib.ox.ac.uk/fsl/fslwiki/. [Accessed: 12-Apr-2015].

[108] J. D. Power, K. A. Barnes, A. Z. Snyder, B. L. Schlaggar, and S. E. Petersen, "Spurious but systematic correlations in functional connectivity MRI networks arise from subject motion," *Neuroimage*, vol. 59, pp. 2142–2154, 2012.

[109] S. Achard, R. Salvador, B. Whitcher, J. Suckling, and E. Bullmore, "A resilient, low-frequency, small-world human brain functional network with highly connected association cortical hubs.," *J. Neurosci.*, vol. 26, pp. 63–72, 2006.

[110] K. Supekar, V. Menon, D. Rubin, M. Musen, and M. D. Greicius, "Network analysis of intrinsic functional brain connectivity in Alzheimer's disease," *PLoS Comput Biol*, vol. 4, no. 6, p. e1000100, 2008.

[111] F. Skidmore, D. Korenkevych, Y. Liu, G. He, E. Bullmore, and P. M. Pardalos, "Connectivity brain networks based on wavelet correlation analysis in Parkinson

fMRI data," *Neurosci. Lett.*, vol. 499, no. 1, pp. 47–51, 2011.

[112] M. J. Shensa, "The discrete wavelet transform: wedding the a trous and Mallatalgorithms," *IEEE Trans. Signal Process.*, vol. 40, no. 10, 1992.

[113] G. Nason and B. Silverman, "The stationary wavelet transform and some statistical applications," *Wavelets Stat.*, pp. 281–299, 1995.

[114] S. A. Montgomery and M. Asberg, "A new depression scale designed to be sensitive to change," *Br. J. Psychiatry*, vol. 134, no. 4, pp. 382–389, 1979.

[115] R. L. Buckner, J. R. Andrews-Hanna, and D. L. Schacter, "The brain's default network: anatomy, function, and relevance to disease.," *Ann. N. Y. Acad. Sci.*, vol. 1124, pp. 1–38, 2008.

[116] S. Sreenivas, S. G. Boehm, and D. E. J. Linden, "Emotional faces and the default mode network," *Neurosci. Lett.*, vol. 506, no. 2, pp. 229–234, 2012.

[117] A. Krause-Utz, I. M. Veer, S. A. R. B. Rombouts, M. Bohus, C. Schmahl, and B. M. Elzinga, "Amygdala and anterior cingulate resting-state functional connectivity in borderline personality disorder patients with a history of interpersonal trauma.," *Psychol. Med.*, vol. 44, no. 13, pp. 2889–901, Oct. 2014.

[118] C. R. Genovese, N. A. Lazar, and T. Nichols, "Thresholding of statistical maps in functional neuroimaging using the false discovery rate," *Neuroimage*, vol. 15, pp. 870–878, 2002.

[119] D. S. Bassett and E. T. Bullmore, "Human brain networks in health and disease.," *Curr. Opin. Neurol.*, vol. 22, no. 4, pp. 340–347, 2009.

[120] E. Bullmore, E. Bullmore, O. Sporns, and O. Sporns, "Complex brain networks: graph theoretical analysis of structural and functional systems.," *Nat. Rev. Neurosci.*, vol. 10, no. 3, pp. 186–98, 2009.

[121] M. Rubinov and O. Sporns, "Complex network measures of brain connectivity: Uses and interpretations," *Neuroimage*, vol. 52, no. 3, pp. 1059–1069, 2010.

[122] C. J. Stam, "Characterization of anatomical and functional connectivity in the

brain: A complex networks perspective," *Int. J. Psychophysiol.*, vol. 77, no. 3, pp. 186–194, 2010.

[123] S. H. Strogatz, "Exploring complex networks.," *Nature*, vol. 410, no. 6825, pp. 268–276, 2001.

[124] Y. He, Z. J. Chen, and A. C. Evans, "Small-world anatomical networks in the human brain revealed by cortical thickness from MRI," *Cereb. Cortex*, vol. 17, no. 10, pp. 2407–2419, 2007.

[125] R. Salvador, J. Suckling, M. R. Coleman, J. D. Pickard, D. Menon, and E. Bullmore, "Neurophysiological architecture of functional magnetic resonance images of human brain.," *Cereb. Cortex*, vol. 15, no. 9, pp. 1332–1342, 2005.

[126] C. J. Stam, "Functional connectivity patterns of human magnetoencephalographic recordings: a 'small-world' network?," *Neuroscience Letters*, vol. 355, no. 1–2. pp. 25–28, 2004.

[127] Y. Liu, M. Liang, Y. Zhou, Y. He, Y. Hao, M. Song, C. Yu, H. Liu, Z. Liu, and T. Jiang, "Disrupted small-world networks in schizophrenia," *Brain*, vol. 131, no. 4, pp. 945–961, 2008.

[128] M. P. van den Heuvel, R. C. W. Mandl, C. J. Stam, R. S. Kahn, and H. E. Hulshoff Pol, "Aberrant frontal and temporal complex network structure in schizophrenia: a graph theoretical analysis.," *J. Neurosci.*, vol. 30, pp. 15915–15926, 2010.

[129] M.-E. Lynall, D. S. Bassett, R. Kerwin, P. J. McKenna, M. Kitzbichler, U. Muller, and E. Bullmore, "Functional connectivity and brain networks in schizophrenia.," *J. Neurosci.*, vol. 30, no. 28, pp. 9477–9487, 2010.

[130] D. S. Bassett, B. G. Nelson, B. A. Mueller, J. Camchong, and K. O. Lim, "Altered resting state complexity in schizophrenia," *Neuroimage*, vol. 59, no. 3, pp. 2196–2207, 2012.

[131] E. J. Sanz-Arigita, M. M. Schoonheim, J. S. Damoiseaux, S. a Rombouts, E. Maris, F. Barkhof, P. Scheltens, and C. J. Stam, "Loss of 'small-world' networks

in Alzheimer's disease: graph analysis of FMRI resting-state functional connectivity," *PLoS One*, vol. 5, no. 11, p. e13788, 2010.

[132] C. J. Stam, W. de Haan, A. Daffertshofer, B. F. Jones, I. Manshanden, A. M. van Cappellen van Walsum, T. Montez, J. P. A. Verbunt, J. C. de Munck, B. W. van Dijk, H. W. Berendse, and P. Scheltens, "Graph theoretical analysis of magnetoencephalographic functional connectivity in Alzheimer's disease.," *Brain*, vol. 132, no. Pt 1, pp. 213–224, 2009.

[133] Y. He, Z. Chen, and A. Evans, "Structural insights into aberrant topological patterns of large-scale cortical networks in Alzheimer's disease.," *J. Neurosci.*, vol. 28, no. 18, pp. 4756–4766, 2008.

[134] J. Zhang, J. Wang, Q. Wu, W. Kuang, X. Huang, Y. He, and Q. Gong, "Disrupted brain connectivity networks in drug-naive, first-episode major depressive disorder," *Biol. Psychiatry*, vol. 70, no. 4, pp. 334–342, 2011.

[135] S. J. J. Leistedt, N. Coumans, M. Dumont, J. P. Lanquart, C. J. Stam, and P. Linkowski, "Altered sleep brain functional connectivity in acutely depressed patients," *Hum. Brain Mapp.*, vol. 30, no. 7, pp. 2207–2219, 2009.

[136] D. J. Watts and S. H. Strogatz, "Collective dynamics of 'small-world' networks.," *Nature*, vol. 393, no. 6684, pp. 440–442, 1998.

[137] V. Latora and M. Marchiori, "Efficient behavior of small-world networks.," *Phys. Rev. Lett.*, vol. 87, no. 19, p. 198701, 2001.

[138] M. E. J. Newman, "The Structure and Function of Complex Networks," *SIAM Review*, vol. 45, no. 2. pp. 167–256, 2003.

[139] M. D. Humphries and K. Gurney, "Network 'small-world-ness': A quantitative method for determining canonical network equivalence," *PLoS One*, vol. 3, no. 4, 2008.

[140] J. Cohen, "Statistical power analysis for the behavioral sciences," *Statistical Power Analysis for the Behavioral Sciences*, vol. 2nd. p. 567, 1988.

[141] “Power and Sample Size | Free Online Calculators.” [Online]. Available: http://powerandsamplesize.com/. [Accessed: 03-Feb-2016].

[142] K. N. Ochsner and J. J. Gross, “The neural architecture of emotion regulation,” *Handb. Emot. Regul.*, pp. 87–109, 2007.

[143] F. Leichsenring, E. Leibing, J. Kruse, A. S. New, and F. Leweke, “Borderline personality disorder.,” *Lancet*, vol. 377, no. 9759, pp. 74–84, 2011.

[144] P. M. Nunes, A. Wenzel, K. T. Borges, C. R. Porto, R. M. Caminha, and I. R. de Oliveira, “Volumes of the hippocampus and amygdala in patients with borderline personality disorder: a meta-analysis.,” *J. Pers. Disord.*, vol. 23, no. 4, pp. 333–345, 2009.

[145] I. R. Olson, A. Plotzker, and Y. Ezzyat, “The Enigmatic temporal pole: A review of findings on social and emotional processing,” *Brain*, vol. 130, no. 7, pp. 1718–1731, 2007.

[146] A. Buchheim, G. Roth, G. Schiepek, O. Pogarell, and S. Karch, “Neurobiology of borderline personality disorder (BPD) and antisocial personality disorder (APD),” *Schweizer Arch. fur Neurol. und Psychiatr.*, vol. 164, no. 4, pp. 115–122, 2013.

[147] K. S. Button, J. P. a Ioannidis, C. Mokrysz, B. a Nosek, J. Flint, E. S. J. Robinson, and M. R. Munafò, “Power failure: why small sample size undermines the reliability of neuroscience.,” *Nat. Rev. Neurosci.*, vol. 14, no. 5, pp. 365–76, 2013.

[148] A. Buchheim, S. Erk, C. George, H. Kächele, T. Kircher, P. Martius, D. Pokorny, M. Ruchsow, M. Spitzer, and H. Walter, “Neural correlates of attachment trauma in borderline personality disorder: a functional magnetic resonance imaging study.,” *Psychiatry Res.*, vol. 163, no. 3, pp. 223–235, 2008.

[149] S. Reitz, R. Kluetsch, I. Niedtfeld, T. Knorz, S. Lis, C. Paret, P. Kirsch, A. Meyer-Lindenberg, R.-D. Treede, U. Baumgärtner, M. Bohus, and C. Schmahl, “Incision and stress regulation in borderline personality disorder: neurobiological mechanisms of self-injurious behaviour.,” *Br. J. Psychiatry*, pp. 1–9, 2015.

[150] E. Bøen, L. T. Westlye, T. Elvsåshagen, B. Hummelen, P. K. Hol, B. Boye, S. Andersson, S. Karterud, and U. F. Malt, "Smaller stress-sensitive hippocampal subfields in women with borderline personality disorder without posttraumatic stress disorder.," *J. Psychiatry Neurosci.*, vol. 39, no. 2, pp. 127–34, 2014.

[151] C. Chang and G. H. Glover, "Time-frequency dynamics of resting-state brain connectivity measured with fMRI," *Neuroimage*, vol. 50, no. 1, pp. 81–98, 2010.

[152] M. Sabeti, S. Katebi, and R. Boostani, "Entropy and complexity measures for EEG signal classification of schizophrenic and control participants," *Artif. Intell. Med.*, vol. 47, pp. 263–274, 2009.